Paleoceanographic dynamics of the Southern Indian Ocean reconstructed from geochemical and sedimentological proxies across the last glacial cycle

Inauguraldissertation
der Philosophisch-naturwissenschaftlichen Fakultät
der Universität Bern

vorgelegt von

Helen Eri Amsler
von Bözen, Aargau

Leiter der Arbeit:
Prof. Dr. Samuel L. Jaccard
Institut für Geologie und Oeschger Centre for Climate Change Research
Universität Bern

Paleoceanographic dynamics of the Southern Indian Ocean reconstructed from geochemical and sedimentological proxies across the last glacial cycle

Inauguraldissertation
der Philosophisch-naturwissenschaftlichen Fakultät
der Universität Bern

vorgelegt von

Helen Eri Amsler
von Bözen, Aargau

Leiter der Arbeit:
Prof. Dr. Samuel L. Jaccard
Institut für Geologie und Oeschger Centre for Climate Change Research
Universität Bern

Von der Philosophisch-naturwissenschaftlichen Fakultät angenommen.

Bern, 16. Oktober 2020 Der Dekan:
Prof. Dr. Zoltan Balogh

Abstract

The Southern Ocean is believed to play an important role in Earth's climate system as a region where a large part of the exchange between the deep ocean and the atmosphere occurs. Several processes have been identified to impact Southern Ocean dynamics and to contribute to the glacial-interglacial redistribution of CO_2 between the ocean and atmosphere and therefore substantially influencing climate. The aim of this study is to further investigate the interplay of these processes during the last glacial cycle, focusing on the Indian sector of the Southern Ocean.

Our geochemical and sedimentological reconstructions based on five marine sediment cores retrieved from the Southern Indian Ocean, increase the spatial and temporal resolution of available paleoceanographic records, and thereby advance our understanding towards a more complete representation of Southern Ocean dynamics.

The studied cores span a meridional transect across the Subantarctic Zone (SAZ) to the Antarctic Zone (AZ) of the Southern Ocean. The results show consistently lower bottom water oxygenation during glacial compared to interglacial periods. We propose these oxygenation changes to be primarily controlled by ocean circulation dynamics and by a general reorganization of deep-water masses. The impact of local organic carbon respiration is only observed in the SAZ, as biogenic opal export increased as a result of iron fertilization.

The input of lithogenic material increased during glacial periods in both the SAZ and AZ, similar to existing records from the Southeast Atlantic and the Eastern Indian Ocean. This may have fuelled export production in the SAZ to some extent, but co-limitation by macronutrients inhibited a continued increase throughout MIS 2. We ascribe the lithogenic material to originate from multiple sources including southern America, southern Africa and more local volcanogenic sources, and possibly from Antarctica for the southernmost core.

Furthermore, changes in near-bottom water flow, reconstructed based on sortable silt records, imply a highly dynamic Antarctic Circumpolar Current (ACC) through time. The flow path is strongly directed by bathymetry.

However, the ACC can overcome these structural constraints as fronts migrate, possibly impacting upwelling patterns.

The results of this dissertation highlight the importance of the Southern Indian Ocean as an active player in the evolution of the climate system. The paleoceanographic records generated as part of this thesis may contribute to build a more complete picture of the driving mechanisms in the Southern Ocean dynamics and improve predictions of future climate scenarios and adaptation studies.

Table of Contents

List of Figures

List of Tables

CHAPTER 1

Introduction

Introduction

1.1 The role of the ocean in Earth's climate

The current and projected continuation of anthropogenically induced increase in atmospheric concentrations of carbon dioxide (CO_2) and other greenhouse gases (e.g. methane (CH_4), nitrous oxide (N_2O), chlorofluorocarbons (CFCs)) may change the climate system in ways that are difficult to predict (IPCC, 2014). Climate models are used to assess potential future behavior of the Earth's system under different forcing scenarios. Yet, climate models need to be validated by comparison with direct measurements and observations. To gain insight beyond the timescales of a few hundred years of human observation we rely on proxy data to reconstruct past climates and test the models under different climate background states. Geological archives allowing for past climate reconstructions include, among others, marine and lacustrine sediments and ice cores. Studying and understanding these archives and the climate system in the past, is key to improve predictions of the responses under future conditions of global climate change.

Antarctic ice core records have highlighted multiple cycles of glacial and interglacial periods, with variations in atmospheric CO_2 concentrations and air temperature being strongly correlated over the past 800,000 years (Figure 1.1) (Bereiter et al., 2015; Jouzel et al., 2007; Lüthi et al., 2008), suggesting that atmospheric CO_2 is an important driver for the climate system (Shakun et al., 2012). Ice ages were globally 3–4°C colder than interglacials, such as the Holocene, with large regional differences, and the partial pressure of atmospheric CO_2 ($pCO_{2,atm}$) was around 80–100 ppmv lower during cold climate intervals (Hain et al., 2014; Shakun et al., 2012; Siegenthaler et al., 2005). Today, annually-averaged global atmospheric CO_2 concentrations exceed 409 ppmv, which is the highest value of the last 800 ka (thousand years) and likely of the entire Quaternary period since 2.6 Ma (Da et al., 2019; Dlugokencky and Tans, 2020).

About a third of the combined anthropogenic CO_2 emissions since preindustrial times (fossil fuel and land use) has been taken up by the ocean, significantly buffering the rate of increase in atmospheric CO_2 concentration (Gruber et al., 2009; Khatiwala et al., 2013; Sabine et al., 2004). The continuing increase in

atmospheric pCO_2 will have societal and environmental consequences as well as implications for atmospheric and oceanic circulation. Enhanced acidification (Hönisch et al., 2012; Raven et al., 2005), more widespread de-oxygenation (Jaccard et al., 2014), and sea-level rise (Church and White, 2011) are amongst the far-reaching impacts the oceans are facing. Furthermore, the capacity of the ocean to take up anthropogenic CO_2 and thus moderate global climate effects, might be impacted as well (DeVries et al., 2017; Gruber et al., 2009; Le Quéré et al., 2007; Sabine et al., 2004).

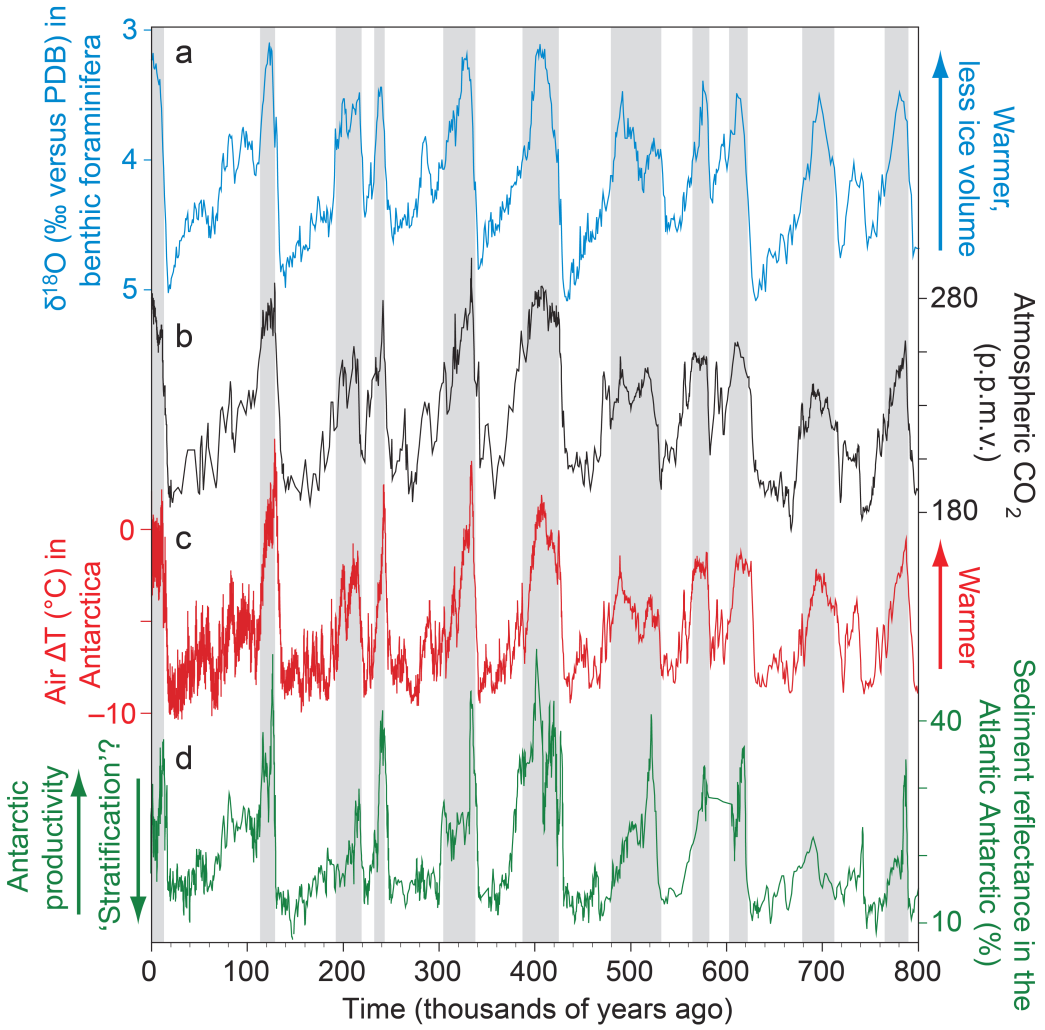

Figure 1.1: Records of changing climate over the last 800 ka showing the characteristic glacial-interglacial see-saw pattern with gradual cooling into full glacial conditions and contrasting rapid temperature increases during deglacials (Sigman et al., 2010). a) Benthic foraminiferal $\delta^{18}O$ (high values indicating colder deep-sea temperatures and increase in continental ice), b) partial pressure of atmospheric CO_2, c) Antarctic air temperatures, d) Southern Ocean marine biological productivity inferred from sediment reflectance data.

On glacial-interglacial timescales, the ocean's capacity to store carbon is an important regulating factor in the climate system (Rahmstorf, 2002). The carbon reservoir of the deep ocean is sufficiently voluminous and dynamic to have leverage on the air-sea partitioning of CO_2 and by inference on climate (Broecker, 1982; Sigman et al., 2010; Sigman and Boyle, 2000).

The Southern Ocean in particular, plays a major role in modulating the atmospheric carbon inventory, as carbon- and nutrient-rich deep waters are upwelled along tilted density surfaces (isopycnals), enabling gas exchange with the atmosphere (Marshall and Speer, 2012; Talley, 2013). The Southern Ocean accounts for about 40% of the oceanic anthropogenic CO_2 uptake and for about 75% of the excess heat uptake since the preindustrial times (Frölicher et al., 2015). The ocean however, has a limited uptake capacity and it has been suggested that it may become a less efficient sink for anthropogenic CO_2 in the future (Le Quéré et al., 2007; Sabine et al., 2004).

It becomes clear that changes in ocean dynamics could have a substantial impact on the global carbon cycle. A number of synergistic processes related to ocean circulation, polar ocean (micro)nutrient biogeochemistry, sea-ice dynamics, and ocean-atmosphere interaction have been proposed to modulate glacial-interglacial climate oscillations (e.g. Adkins, 2013; Ferrari et al., 2014; Hain et al., 2014; Jaccard et al., 2013; Kohfeld and Ridgwell, 2009; Sigman et al., 2010; Sigman and Boyle, 2000). This PhD thesis focuses on better constraining the interplay between these aspects across the last glacial cycle, using sedimentological and geochemical tools in marine sedimentary archives retrieved from the deep Southern Indian Ocean.

1.2 Marine carbon cycle and the carbon pumps

Carbon is constantly exchanged between the Earth's carbon reservoirs. The size and residence times of the different reservoirs vary greatly. The ocean can be subdivided in a surface and a deep reservoir with sizes of 700 Pg C and 38,000 Pg C, respectively (preindustrial values, Sigman and Boyle, 2000). The atmosphere (600 Pg C) is comparable to the surface ocean. These two combined with the terrestrial reservoir (2100 Pg C) represent less than 10% of the voluminous deep ocean carbon reservoir. The Earth's sediments and crust however, are by far the largest carbon reservoir (48,000,000 Pg C), yet the

residence time is in the range of hundreds of Ma (million years), bearing little impact on the exogenic carbon cycle on quaternary glacial-interglacial timescales.

Variations in oceanic CO_2 levels are controlled by several parameters such as temperature, salinity and carbonate chemistry, thus influencing the air-sea exchange of carbon. The direction of gas flow depends on the partial pressure of CO_2 in the atmosphere ($pCO_{2,atm}$) and in the surface ocean ($pCO_{2,aq}$). The partial pressure of CO_2 in seawater in turn, is a function of temperature and salinity; CO_2 is comparatively more soluble in cold and fresh than in warm and salty water (Sigman and Boyle, 2000; Zeebe, 2012). If all other factors were kept equal, low latitude oceans would thus be regions of CO_2 outgassing, while high latitude oceans would represent regions of CO_2 uptake (Kohfeld and Ridgwell, 2009). In addition to this temperature- and salinity-dependent mechanism that is referred to as solubility pump, aqueous carbon chemistry largely controls pCO_2 in the ocean waters and has a greater impact on glacial-interglacial $pCO_{2,atm}$ changes (Volk and Hoffert, 1985).

As CO_2 dissolves in seawater, it reacts with water (H_2O) to form carbonic acid (H_2CO_3), which dissociates to form bicarbonate (HCO_3^-) and carbonate (CO_3^{2-}), referred to collectively as dissolved inorganic carbon (DIC) (Hain et al., 2014):

$$CO_2 + H_2O \leftrightarrow H_2CO_3 \leftrightarrow HCO_3^- + H^+ \leftrightarrow CO_3^{2-} + 2H^+ \qquad \text{Eq. (1.1)}$$

Today the largest part of DIC in the ocean is present in the form of HCO_3^- (~90%) and to a lesser extent of CO_3^{2-} (~10%), and H_2CO_3 and CO_2 account only for ~0.5% (Sarmiento and Gruber, 2006). Alkalinity (ALK) defined as the excess of bases over acids in a solution, determines the ocean's buffer capacity, that is the ability to let H_2CO_3 dissociate to the other DIC species. The ocean's alkalinity can be approximated by the sum of HCO_3^- and two times CO_3^{2-}. This reaction (Eq. 1.1) is reversible and the relative abundance of each species depends on the pH of the water; under lower pH conditions, the reaction is shifted towards the left, causing an increase in H_2CO_3 and thus $pCO_{2,aq}$ (Sarmiento and Gruber, 2006). Also, an overall increase in DIC content would lead to higher $pCO_{2,aq}$. In contrast, an overall increase in ALK would lead to a lowering of $pCO_{2,aq}$.

These chemical reactions cause the exchange rate of CO_2 between the atmosphere and surface ocean to amount to several months, an order of magnitude slower than for other gases (Sarmiento and Gruber, 2006).

The overall global ocean concentration of DIC and ALK and their (re)distribution in the surface and the deep ocean are mainly controlled by the production and remineralization of organic matter and calcium carbonate by marine organisms and circulation dynamics (Hain et al., 2014; Kohfeld and Ridgwell, 2009). These mechanisms are commonly referred to as the biological carbon pump (Figure 1.2), which can further be distinguished as the soft-tissue pump (C_{org}) and the carbonate pump ($CaCO_3$) (Kohfeld and Ridgwell, 2009; Volk and Hoffert, 1985). It is generally believed that the soft-tissue pump has greater implications for $pCO_{2,atm}$ than the carbonate pump (Hain et al., 2014).

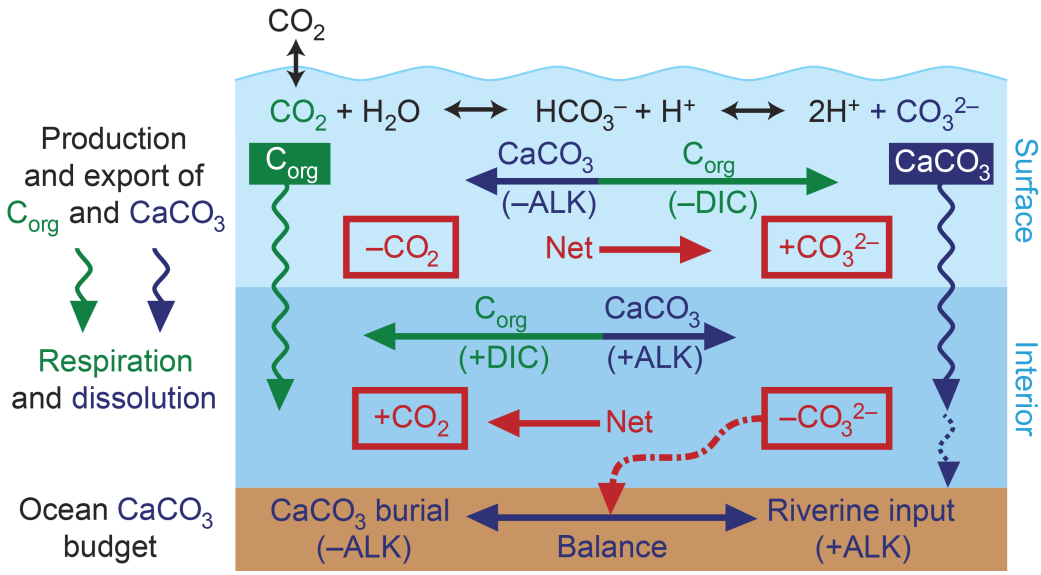

Figure 1.2: Schematic view of the ocean's biological pump (Sigman et al., 2010). On one side, the soft-tissue pump removes DIC from the surface waters by export of C_{org}. The carbonate pump on the other side removes ALK and DIC in a 2:1 ratio from surface waters by export of $CaCO_3$ shells. In the ocean interior, C_{org} and carbonate are remineralized, increasing DIC and ALK in the deep.

The soft-tissue pump (Figure 1.2 left) removes DIC from surface waters through photosynthetic CO_2 fixation and export of organic carbon (C_{org}) into deeper waters (Kohfeld and Ridgwell, 2009). Only around 1% of the exported C_{org} accumulates on the seafloor, whereas the remainder is remineralized back into DIC in the water column, consuming dissolved O_2 (Hain et al., 2014). This

process lowers DIC concentrations in surface waters and increases DIC and nutrient concentrations at depth. Photosynthesis does not only require CO_2 and light, but also macronutrients (nitrate, phosphate and silicate) and micronutrients, such as iron (Fe). A lack of any of these building blocks can act as a limiting factor for phytoplankton growth. As a result, the general scarcity of bioavailable Fe and light in today's Southern Ocean restricts photosynthesis, leaving an excess of unused nutrients at the ocean surface (Kohfeld and Ridgwell, 2009; Studer et al., 2015).

If the soft-tissue pump solely acted as a net export of organic matter, it would reduce $pCO_{2,atm}$. However, it is the balance between the net export of C_{org} and the counteracting upwelling of DIC- and nutrient-rich subsurface waters that controls CO_2 exchange with the atmosphere. This balance is often referred to as the efficiency of the soft-tissue pump (Hain et al., 2014; Sigman and Boyle, 2000). The balance can be influenced by a number of mechanisms, such as changes in ocean circulation (e.g. Marshall and Speer, 2012; Sigman and Boyle, 2000), water-column stratification (e.g. Adkins, 2013; Sigman et al., 2004), sea-ice extent (Watson and Naveira Garabato, 2006; Wolff et al., 2010), as well as changes in biological productivity (e.g. Martínez-García et al., 2014). Therefore, the more complete the utilization of upwelled nutrients by phytoplankton, the more efficient the pump works, thereby reducing $pCO_{2,atm}$ (Hain et al., 2014). The efficiency of the biological pump can also be described as the ratio between regenerated (related to the remineralization of C_{org} in the water-column) and preformed nutrients (biologically unused excess surface nutrients supplied to the ocean interior by newly formed deep water) (Hain et al., 2014). The biological carbon pump acts to decrease the proportion of preformed nutrients by incorporating them in exported organic matter and converting them to remineralized nutrients. The more efficient this conversion process functions, the more effective the biological pump is in sequestering carbon in the deep ocean (Ito and Follows, 2005; Sigman et al., 2010).

Some species of phytoplankton and zooplankton (e.g. coccolithophores and foraminifera) form carbonate ($CaCO_3$) shells. The sinking of these shells to the ocean subsurface removes ALK and DIC from the surface ocean in a 2:1 ratio (Zeebe, 2012). This process is referred to as the carbonate pump (Figure 1.2

right) and acts in the opposite direction with regard to CO_2 concentration in the surface ocean, when compared to the soft-tissue pump:

$$Ca^{2+} + 2HCO_3^- \leftrightarrow CaCO_3 + CO_2 + H_2O \qquad \text{Eq. (1.2)}$$

Around 25% of the exported $CaCO_3$ accumulates on the seafloor (Hain et al., 2014). The remainder dissolves back to ALK and DIC in a 2:1 ratio. The carbonate pump depends on ocean chemistry, mostly on surface ocean pH, impacting the capacity of calcifying plankton to build their shells (Kohfeld and Ridgwell, 2009).

On glacial-interglacial timescales, carbonate compensation has to be taken into account. ALK is largely balanced by the riverine supply of dissolved chemical species from weathering on one hand and output by carbonate burial in marine sediments on the other hand (Sarmiento and Gruber, 2006). The depth of the lysocline, below which most $CaCO_3$ is dissolved, depends on the concentration of CO_3^{2-} and thus determines the $CaCO_3$ burial rate (Sigman et al., 2010). When CO_3^{2-} concentration is below $CaCO_3$ saturation, marine carbonates dissolve and the lysocline shoals. Changes in the lysocline depth are affected by redistribution of ALK and DIC by the soft-tissue and carbonate pumps (Sigman and Boyle, 2000). As discussed above, a more efficient soft-tissue pump contributes to lower $pCO_{2,aq}$ in the surface ocean. This leads to an increase of $pCO_{2,aq}$ at depth, lowering pH and thereby decreasing CO_3^{2-} concentration. This results in the shoaling of the lysocline, which reduces the area of $CaCO_3$ burial, increasing total ocean ALK. This in turn, increases CO_3^{2-} at depth and deepens the lysocline until $CaCO_3$ balance is restored. As such, overall higher ocean ALK lowers $pCO_{2,aq}$ and thus promotes drawdown of $pCO_{2,atm}$ (Sigman et al., 2010).

1.3 Global and Southern Ocean circulation

Global ocean circulation is essential for the uptake, storage and redistribution of heat, freshwater, (micro)nutrients, and carbon around the globe (Rahmstorf, 2002) and is driven by a combination of buoyancy forcing, atmospheric dynamics, and internal mixing (Broecker, 1991; Lumpkin and Speer, 2007; Munk and Wunsch, 1998; Rahmstorf, 2002).

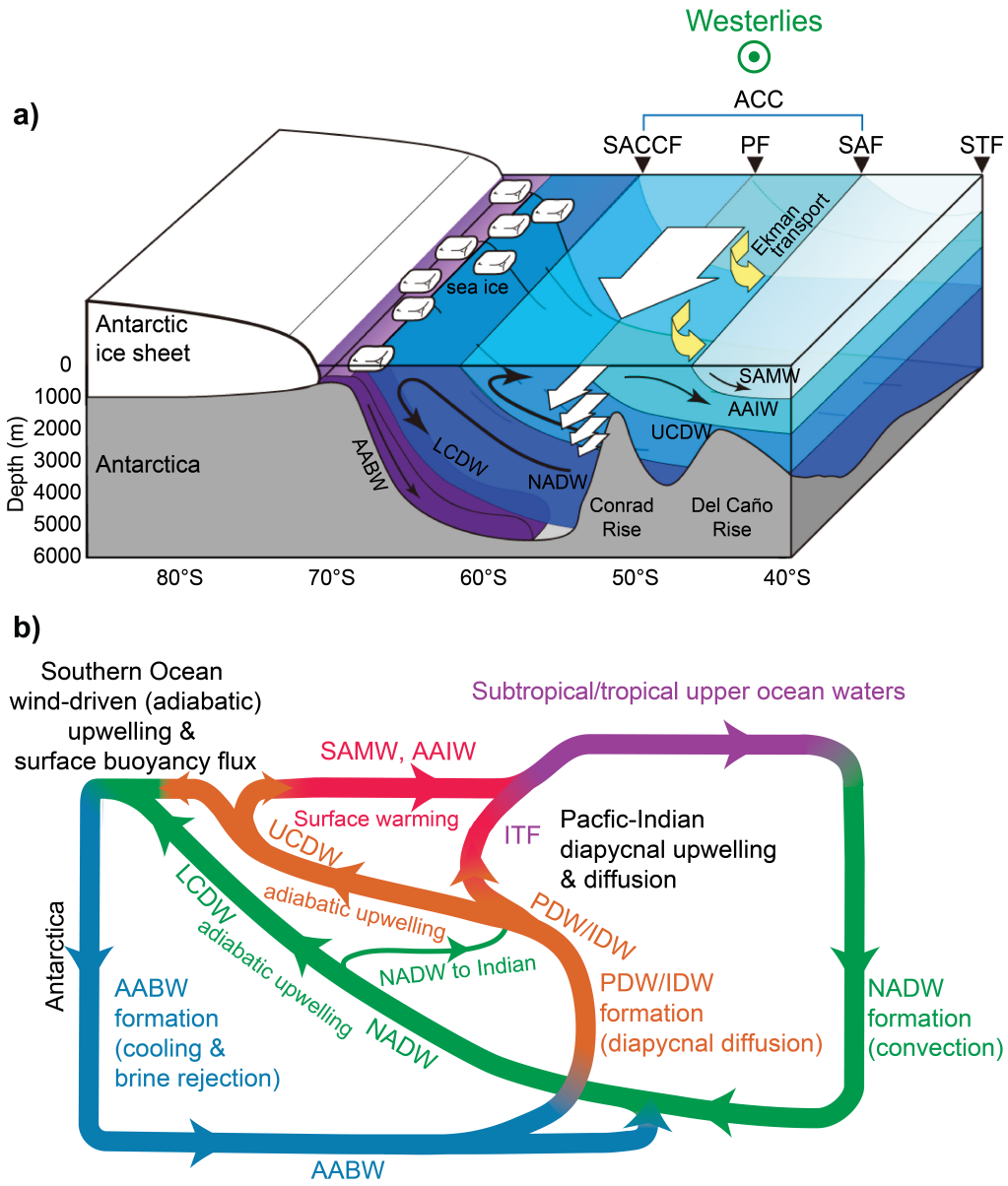

Figure 1.3: Schematic view of the Southern Ocean. a) Block diagram of hydrographic fronts and interaction with the southern hemisphere westerlies driving northward Ekman transport across the ACC (STF = Subtropical Front, SAF = Subantarctic Front, PF = Polar Front, SACCF = Southern ACC Front). b) Circulation paths of water masses (NADW = North Atlantic Deep Water, LCDW = Lower Circumpolar Deep Water, UCDW = Upper Circumpolar Deep Water, AABW = Antarctic Bottom Water, PDW/IDW = Pacific/Indian Deep Water, SAMW = Subantarctic Mode Water, AAIW = Antarctic Mode Water, ITF = Indonesian Throughflow) (Talley, 2013).

Surface ocean currents are mainly influenced by wind forcing. The general pattern of winds includes the trade winds in the (sub)tropics, westerlies at mid-latitudes and polar easterlies at high latitudes (Sarmiento and Gruber, 2006). The surface ocean is subjected to the effect of Earth's rotation, meaning that the resulting wind-induced, so called Ekman transport is deflected 90° towards

the right of the wind direction in the northern hemisphere and 90° towards the left in the southern hemisphere. The water experiencing direct Ekman transport is confined to the upper 10–100 m of the water column. Ekman transport causes upwelling (Ekman suction) in regions of divergence and downwelling (Ekman pumping) in regions of convergence. Upwelling regions are thus important for biological activity, since nutrients from the ocean subsurface are brought up to the sunlit surface waters, as it is the case, for example in the Southern Ocean (Sarmiento and Gruber, 2006).

The wind driven surface ocean currents are linked to the meridional overturning circulation (Figure 1.3). Circumpolar Deep Water (CDW) accounts for much of the Southern Ocean subsurface waters and is composed of an upper (UCDW) and a lower (LCDW) component. LCDW is mostly composed of salty North Atlantic Deep Water (NADW), characterized by higher oxygen content than UCDW, which is formed from older Indian and Pacific Deep Waters (IDW and PDW) (Talley, 2013). Both UCDW and LCDW upwell along tilted isopycnals to the surface south of the Polar Front (PF). Ekman transport directs part of this upwelled waters northward across the ACC, where they are downwelled to form Subantarctic Mode Water (SAMW) and Antarctic Intermediate Water (AAIW). Near the equator they resurface as (sub)tropical upper ocean waters and become northward travelling precursors of NADW (Talley, 2013). The denser part of the upwelled CDW diverges polewards close to the Antarctic continent, where sea-ice formation and associated brine-rejection enables the formation of cold Antarctic Bottom Water (AABW) (Ohshima et al., 2013). Being the densest deep water mass, AABW flows northward in the abyss and spreads into all ocean basins. In the subtropical and tropical Indian and Pacific Oceans, part of the AABW is upwelled by turbulent mixing along rough seabed topography and forms IDW and PDW, closing the global meridional overturning cycle (Ferrari et al., 2014; Talley, 2013).

1.4 Changes of the ocean in the past and implications for climate

The marine carbon cycle and ocean circulation may have operated differently in the past, potentially affecting atmospheric CO_2 concentrations.

1.4.1 Changes in the solubility pump

During peak glacial periods such as the Last Glacial Maximum (LGM), the mean global ocean temperature was colder, with estimates ranging around 2–5°C (Bereiter et al., 2018; Elderfield et al., 2012), depending on the region (high latitudes experienced greater cooling than low latitudes) (Kohfeld and Ridgwell, 2009; Sigman and Boyle, 2000). As CO_2 is more soluble in colder water, this would have led to a temperature-driven CO_2 uptake, reducing $pCO_{2,atm}$ by 30 ppmv.

Glacial cooling has led to a buildup of ice sheets on continents, causing sea-level to drop by approximately 120 m, resulting in ~3% saltier oceans (Kohfeld and Ridgwell, 2009; Sigman and Boyle, 2000). Such a rise in salinity reduces CO_2 solubility, increasing $pCO_{2,atm}$ by 6 ppmv. Storing fresh water away from the ocean also leads to a change in DIC and ALK that increases $pCO_{2,atm}$ by another 7 ppmv (Kohfeld and Ridgwell, 2009). Thus, the salinity and DIC/ALK effects combined, partly cancel out the temperature-driven effect on CO_2 solubility (Kohfeld and Ridgwell, 2009). Therefore, other mechanisms have to come into play to account for the observed glacial CO_2 drawdown, namely changes in the efficiency of the biological carbon pump and changes in ocean circulation (Sigman and Boyle, 2000).

1.4.2 Changes in the biological pump

As described above, $pCO_{2,atm}$ is particularly sensitive to changes in the Southern Ocean circulation and biogeochemistry, hence we focus on the biological carbon pump in this region. The Southern Ocean can be divided into the Subantarctic Zone (SAZ) in the north and the Antarctic Zone (AZ) in the south (Marinov et al., 2006), with clearly distinct characteristics. These two zones are separated by the Polar Front and the Polar Frontal Zone (Marinov et al., 2006; Toggweiler et al., 2006).

Today, the SAZ is described as a region rich in surface nutrients with biological export production limited mainly by the scarcity of bioavailable Fe and silicic acid (Kumar et al., 1995; Martin, 1990; Martínez-García et al., 2014). The AZ is characterized by generally colder waters (<2°C) and high surface nutrient concentrations supplied to the surface by regional upwelling. Biological export production is largely dominated by opal producing organisms such as diatoms

(Cortese et al., 2004; Geibert et al., 2005), and phytoplankton growth is modulated by the availability of dissolved Fe and light.

For glacial periods, a consistent picture characterized by higher C_{org} export in the SAZ and generally lower C_{org} export in the AZ has emerged (Jaccard et al., 2013; Kohfeld et al., 2005; Marinov et al., 2006). Increased export production in the SAZ during glacial times, has been ascribed to Fe-fertilization by enhanced input of iron-bearing dust, resulting in more complete nutrient utilization (Anderson et al., 2014; Chase et al., 2001; Kohfeld et al., 2005; Martínez-García et al., 2014, 2009). However, the degree to which Fe can be solubilized from dust particles is not fully constrained (Fischer et al., 2010; Parekh et al., 2008).

The glacial AZ behaves differently, with lower export production than today, partly limited by expanded sea-ice (e.g. Chase et al., 2003). However, the combination of more complete nutrient utilization during glacial periods together with lower export production, is consistent with generally reduced upwelling intensities and thus decreased nutrient supply to the surface (Anderson et al., 2014; Robinson and Sigman, 2008; Studer et al., 2015).

Higher glacial Fe-availability in the Southern Ocean may also have lowered the stoichiometric $Si(OH)_4$:NO_3^- demand by diatoms (Brzezinski et al., 2002), causing a shift from silicic acid depletion towards nitrate depletion. As such, more silicic acid could have been transported to the north, possibly fueling diatom productivity in the tropics (Bradtmiller et al., 2007; Brzezinski et al., 2002), although the hypothesis remains debated (Kienast et al., 2006; Dumont et al., 2020).

In both SAZ and AZ, proxy reconstructions suggest that dissolved nitrate has been more completely utilized during glacial periods (Martínez-García et al., 2014; Studer et al., 2015); in the SAZ by alleviating the limitation of Fe-scarcity on phytoplankton growth and in the AZ by a more complete nutrient uptake by phytoplankton due to reduced upwelling. In combination, these processes result in an overall enhanced efficiency of the biological carbon pump, contributing to sequester CO_2 in the ocean interior and away from the atmosphere.

1.4.3 Changes in circulation

A potential slowdown or even shutdown of NADW formation during glacial periods had been postulated (e.g. McManus et al., 2004), yet recent proxy reconstructions report little change in the strength of NADW formation (Böhm et al., 2015; Lippold et al., 2016; 2012). However, water-mass tracers suggest that the general ocean circulation pattern was different during past ice-ages (Adkins, 2013; Curry and Oppo, 2005; Lynch-Stieglitz et al., 2007). During peak glacials, a shoaling of the NADW has been reported, often referred to as Glacial North Atlantic Intermediate Water (GNAIW) (Adkins, 2013; Curry and Oppo, 2005; Sigman et al., 2010). This would have led to a generally shallower Atlantic Meridional Overturning Circulation (AMOC), allowing for AABW to expand further to the north (Adkins, 2013; Curry and Oppo, 2005). Today at the surface, NADW is saltier and denser than AABW, but in the deep ocean, the coldness of AABW makes it denser than NADW (Adkins, 2013). This means that in today's oceans, some of the isopycnals are shared by both water masses, allowing for relatively efficient mixing, facilitated by interaction with bathymetry (Adkins, 2013; Ferrari et al., 2014).

During the transition into ice ages, cooling of NADW will eventually form colder CDW that is upwelled around Antarctica. This allows for the production of saltier AABW without pre-freshening during sea-ice formation (Adkins, 2013). These processes result in a glacial ocean characterized by i) greater salinity stratification at depth, which reduces the exchange between the shallower northern sourced GNAIW and deep southern-sourced water masses, ii) AABW filling up large parts of the deep ocean and expanding northwards, and iii) reduced mixing between the different subsurface water masses, slowing circulation and causing deep waters to become gradually enriched in remineralized DIC and ALK (Adkins, 2013; Lynch-Stieglitz et al., 2007; Sigman et al., 2010). Older ventilation ages implied by radiocarbon measurements on benthic foraminifera support this glacial deep-water mass distribution (Gottschalk et al., 2016; Skinner et al., 2010; 2017).

Moreover, Southern Ocean dynamics may have been altered by changes in wind forcing and its potential impact on ACC flow and associated Ekman transport (e.g. Rintoul, 2018). Yet, there seems to be no consistent agreement between climate model outputs and observations as to how the southern hemisphere

westerly winds (SHW) might have changed in the past (Chavaillaz et al., 2013; Kohfeld et al., 2013). Similarly, the response of the ACC is still debated (e.g. Franzese et al., 2006; Lamy et al., 2015; Manoj and Thamban, 2015; Mazaud et al., 2010; McCave et al., 2014; Molyneux et al., 2007). A recent study compiling numerical model results, reports that simulations forced by stronger SHW consistently result in a rise in atmospheric pCO_2 due to enhanced Ekman suction (Gottschalk et al., 2019 *and references therein*). Yet, simulations forced by meridionally shifting the mean trajectory of the SHW, result in no coherent climatic response; a northward shift of the mean westerly wind belt leads to a weak positive change in $pCO_{2,atm}$ and also results in an increase in the outcrop area, so that carbon stemming primarily from intermediate water-depth is released. These effects are however, partly compensated by enhanced marine export production and changes in the terrestrial carbon cycle, resulting in muted changes in the global carbon cycle in response to SHW shifts.

As an additional important factor, glacial sea-ice expansion might have interfered with circulation and stratification changes (Ferrari et al., 2014). Besides its albedo effect on the Earth's heat budget (Rahmstorf, 2002), larger sea-ice extent could have acted as a barrier mechanism, inhibiting air-sea gas exchange (Stephens and Keeling, 2000; Watson and Naveira Garabato, 2006; Wolff et al., 2010) and seasonal sea-ice melting could have contributed to stronger salinity stratification (Stephens and Keeling, 2000).

A combination of these circulation-related processes could have worked synergetically and may have substantially decreased gas exchange between deep water and the surface ocean, with consequences for climate.

1.4.4 Implications for atmospheric CO_2

None of the mechanisms described above can solely be responsible for lowering atmospheric CO_2 to the observed glacial levels, and it has become clear that glacial-interglacial variability must be caused by a combination of processes (Kohfeld and Ridgwell, 2009).

The sensitivity of the soft-tissue pump was estimated to be around -13–20 ppmv and that of the carbonate pump around +5 ppmv (Hain et al., 2014). Integrating the respective contributions of the biological carbon pump fueled by Fe-fertilization in the SAZ, would equate to a reduction of up to 35–40 ppmv

(Hain et al., 2014; Jaccard et al., 2013; Sigman et al., 2010). A glacial reorganization with stronger stratification, reduced upwelling, extended sea-ice, and more complete nutrient utilization in the AZ of the Southern Ocean could have reduced $pCO_{2,atm}$ by another 40 ppmv (Jaccard et al., 2013; Sigman et al., 2010). The combination of processes outlined above, thus has the potential to account for a large portion of the observed decrease in glacial atmospheric CO_2 concentrations (Hain et al., 2010; Jaccard et al., 2013).

1.5 Objectives of the PhD thesis

Despite a large community effort, key processes of the Southern Ocean and their interactions are still not fully understood, even with their potential importance for the global carbon cycle. One reason is the unbalanced data availability, as most studies have been carried out in the Atlantic and to a lesser extent Pacific sectors of the Southern Ocean. In order to integrate the different results and ideas and provide a robust interpretation of past Southern Ocean dynamics, increasing the temporal as well as the spatial resolution of sediment records is necessary.

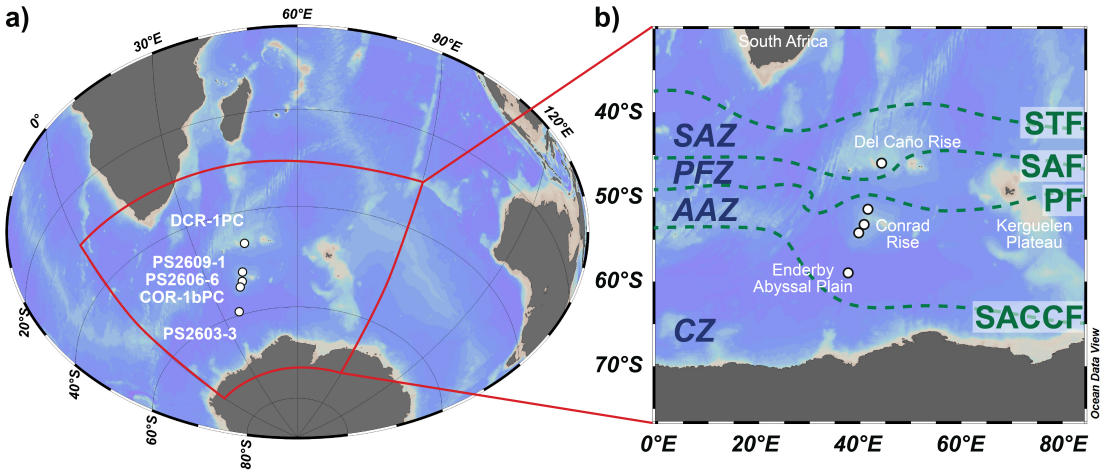

Figure 1.4: Study site with core locations (white circles). a) Broad view of southern hemisphere bathymetry and core locations. b) Study site with today's position of the fronts, from north to south: Subtropical Front (STF), Subantarctic Front (SAF), Polar Front (PF), and the Southern ACC Front (SACCF), and with the hydrographic zonation, from north to south: Subantarctic Zone (SAZ), Polar Frontal Zone (PFZ), Antarctic Zone (AZ), and Continental Zone (CZ) (Orsi et al., 1995) (plotted with the ODV-software, Schlitzer, 2018).

Originally designed in the framework of IODP pre-proposal 918 'Southern Ocean Climate Evolution', this thesis focuses on reconstructing paleoceanographic dynamics from the sedimentary archives of the Southern Indian Ocean, using geochemical and sedimentological proxies. In this project we address some of the above mentioned issues by investigating five marine sediment cores retrieved along a meridional transect covering ~15° in the SW Indian sector of the Southern Ocean (Figure 1.4 and Table 1.1). The cores are located in different oceanographic zones spanning the Subantarctic Zone (SAZ) just north of the Subantarctic Front (SAF), the Polar Frontal Zone (PFZ) and the Antarctic Zone (AZ) south of the Polar Front (PF) as far south as the Enderby Abyssal Plain close to the Southern ACC Front (SACCF) (Orsi et al., 1995). Thus, the cores have the potential to record paleoceanographic changes across the major zones of the Southern Ocean and to increase the spatio-temporal resolution of available marine records in a region that remains underrepresented. The sedimentary archives cover time intervals varying from 45 ka to 180 ka, allowing for a better understanding of key processes across the past glacial cycle.

Table 1.1: Core location, recovery and approximate analyzed age interval.

Ship	Core	Latitude	Longitute	Depth (mbsl)	Recovery (m)	Age (~ka)
Hakuho-maru	**DCR-1PC**	46°01.34'S	44°15.24'E	2'632	10.1	180
	COR-1bPC	54°16.04'S	39°45.98'E	2'828	10.475	45
Polarstern	**PS2609-1**	51°29.9'S	41°35.8'E	3'113	17.5	120
	PS2606-6	53°13.9'S	40°48.1'E	2'545	12.19	110
	PS2603-3	58°59.2'S	37°37.7'E	5'289	9.41	300

The main objectives of this PhD thesis are:

1) Investigating glacial-interglacial changes in bottom water oxygenation and assessing their relation to Southern Ocean circulation dynamics and export production, with the implications for remineralized carbon storage.

2) Reconstructing past lithogenic fluxes in different zones of the Southern Ocean and exploring the potential fertilization effect on marine export production.
3) Determining changes in near-bottom current speed to gain insight into ACC dynamics and their possible impact on atmospheric CO_2 concentrations.
4) Comparing the results to existing records from the Indian and Atlantic sectors of the Southern Ocean as well as to Antarctic ice core records to better constrain common patterns and explain regional differences.

The results will potentially help developing a more complete understanding of the evolution of Southern Ocean dynamics and thus contribute to better assess its role in modulating Earth's climate system in the past, present and future.

1.6 Approach and proxies

1.6.1 Vertical particle flux (^{230}Th-normalization)

The normalization approach with thorium-230 (^{230}Th) is used to quantify the vertical flux of particles as they settle from the ocean surface to the seafloor (Costa et al., 2020; Francois et al., 2004; Henderson and Anderson, 2003). Bottom currents can redistribute sediments while the particles are settling on the seafloor, leading to biases in interpretations of vertical flux. As a result, sedimentary mass accumulation rates cannot correctly infer the downward settling of particles as the approach does not account for syndepositional sediment redistribution. The vertical flux of sedimentary constituents can be robustly constrained by the ^{230}Th-normalization approach, which relies on the fact that ^{230}Th, a very particle reactive radionuclide, is readily scavenged by sinking particles and thus rapidly removed from the water column. Unlike ^{230}Th, its mother nuclide ^{234}U is highly soluble and is uniformly distributed within the oceans due to its long residence time of several 100 ka, largely exceeding the ocean mixing time (Dunk et al., 2002). ^{230}Th, characterized by an oceanic residence time of less than 4 (surface water) to 40 years (deep water) (Anderson et al., 1983), thus does not experience much lateral advection before settling (Yu et al., 2001). Hence, the basic assumption is that the flux of this scavenged

^{230}Th ($F^{230}Th$) reaching the seafloor corresponds to its production rate (β_{230} = 2.67E^{-5} dpm/cm^3/ka) within the overlying water column. With uranium being uniformly distributed in the ocean, the ^{230}Th production ($P^{230}Th$) is a function of the water depth z:

$$F^{230}Th \approx P^{230}Th = \beta_{230} \times z \qquad \text{Eq. (1.3)}$$

Therefore, the ^{230}Th concentration associated with particle scavenging (A_{Th230}^{scav}) should be inversely correlated to the sediment flux. As a result of its high particle affinity, ^{230}Th remains in the sediments even after the particles that originally transported it, dissolve during early diagenesis. Using the initial concentration of scavenged ^{230}Th ($A_{Th230,(0)}^{scav}$) in the sediment (corrected for radioactive decay of ^{230}Th), the preserved vertical flux ($^{pr}F_v$) of material can be estimated:

$$prF_v = \frac{\beta_{230} \times z}{A_{Th230,(0)}^{scav}} \qquad \text{Eq. (1.4)}$$

Normalizing the concentration of any sedimentary component (j) with the ^{230}Th-approach provides a quantitative estimate of its preserved vertical flux ($^{pr}F_v^j$) through time, with f_j being the weight fraction of constituent j in the sediment:

$$prF_v^j = prF_v \times f_j \qquad \text{Eq. (1.5)}$$

$A_{Th230,(0)}^{scav}$ is determined according to the corrections described by Francois et al. (2004), summarized as follows.

The total of sedimentary ^{230}Th consists of three distinct pools and the concentration of the scavenged fraction (A_{Th230}^{scav}) has to be inferred from the total ^{230}Th concentration, by subtracting the detrital and the authigenic fractions:

$$A_{Th230}^{scav} = A_{Th230}^{total} - A_{Th230}^{det} - A_{Th230}^{auth} \quad \text{Eq. (1.6)}$$

For the detrital fraction, it is generally assumed that detrital ^{230}Th is in secular equilibrium with detrital ^{238}U. The latter can be derived from the activity of ^{232}Th, an isotope exclusively found in the detrital mineral fraction, and based on the assumption of a constant regionally-informed crustal activity ratio $(A_{U238}/A_{Th232})^{det}$. We considered a ratio of 0.5 for cores DCR-1PC, COR-1bPC, PS2909-1, and PS2909-6 (Francois et al., 2004; Henderson and Anderson, 2003). For PS2603-3, the core located farthest south and potentially influenced by lithogenic material derived from Antarctic continental crust, the minimum ^{238}U/^{232}Th activity ratio observed is 0.27 $\pm$ 0.01. We therefore set the lithogenic end-member conservatively to 0.27.

$$A_{U238}^{det} \approx A_{Th230}^{det} = A_{Th232}^{total} \times \left(\frac{A_{U238}}{A_{Th232}}\right)^{det} \times \alpha \quad \text{Eq. (1.7)}$$

with $\alpha = 0.96 \pm 0.04$ as a correction factor for the loss of ^{234}U due to alpha-recoiling, taking into account a slight disequilibrium of the resulting $(A_{U238}/A_{Th232})^{det}$ (Bourne et al., 2012).

The authigenic fraction of ^{230}Th comes from the decay chain of ^{238}U — ^{234}U — ^{230}Th. Since ^{234}U/^{238}U in seawater is constant at 1.147, authigenic ^{230}Th can be calculated as follows:

$$A_{Th230}^{auth} = 1.147 \times A_{U238}^{auth} \left(1 - e^{-\lambda t}\right) \quad \text{Eq. (1.8)}$$

with $A_{U238}^{auth} = A_{U238}^{tot} - A_{U238}^{det}$, and t is the time elapsed since deposition, and $\lambda = \frac{\ln 2}{\tau_{1/2}}$ with $\tau_{1/2}$ being the half-life of ^{230}Th.

^{230}Th itself is radioactive and to get the original scavenged ^{230}Th at time of deposition ($t = 0$), its decay has to be accounted for:

$$A_{Th230,(0)}^{scav} = A_{Th230}^{scav} \times e^{\lambda t} \quad \text{Eq. (1.9)}$$

This method relies on several assumptions that introduce some uncertainties (Bourne et al., 2012). These include the estimation of the detrital ratio between ^{238}U and ^{232}Th, errors in the age model, grain size effects on the sedimentary ^{230}Th inventory, and the assumption of ^{230}Th being immediately scavenged (Bourne et al., 2012; Francois et al., 2004; Kretschmer et al., 2010; Yu et al., 2001). Furthermore, the time of authigenic U emplacement in the sediment might deviate from the time of sedimentation, since U often diffuses and precipitates below the sediment-water interface (Francois et al., 2004). However, we consider this ^{230}Th-normalization method as a valid tool to correct for sediment redistribution (Costa et al., 2020; Bourne et al., 2012; Kretschmer et al., 2010).

1.6.2 Bottom water oxygenation (authigenic uranium and manganese)

The sedimentary accumulation (and post-depositional dissolution) of redox-sensitive trace-metals such as uranium (U) and manganese (Mn) depend on the redox-conditions of the sedimentary environment and indirectly reflect changes in bottom water oxygenation states (e.g. Calvert and Pedersen, 1996; Jaccard et al., 2016; Langmuir, 1978). Sedimentary redox conditions depend on multiple factors including bacterial organic-matter respiration, sedimentation rates and bottom water oxygenation (e.g. Jaccard et al., 2016).

Uranium is soluble in oxygenated seawater, occurring as a stable U(VI) carbonate complex and precipitates as insoluble U(IV) in the form of uraninite in oxygen-depleted environments (Langmuir, 1978; Morford and Emerson, 1999). One of the main removal mechanisms from seawater is the diffusion of dissolved U into reducing sediments where it is precipitated as authigenic uranium (aU) phases (Klinkhammer and Palmer, 1991; Langmuir, 1978). Sedimentary aU enrichments imply intervals of more reducing conditions, resulting from enhanced organic carbon respiration and/or lower bottom water oxygenation (Bradtmiller et al., 2010; Jaccard et al., 2009; McManus et al., 2005). If oxygenating conditions recur, aU can be redissolved (burn-down), especially in low sedimentation rate regimes (<2 cm/ka) (Colley et al., 1989; Jacobel et al., 2017; Mangini et al., 2001). While a part of the re-dissolved uranium is lost to the seawater, the other part diffuses deeper down into the sediment where reducing conditions still prevail, and reprecipitates.

^{238}U in the sediment has a detrital and an authigenic origin. The authigenic fraction can be calculated by the excess of ^{238}U over ^{232}Th, which has only a detrital source and by assuming a constant detrital ratio between the two elements (Francois et al., 2004):

$$aU(ppm) = A_{U238}^{total} - \left(\frac{A_{U238}}{A_{Th232}}\right)^{det} \times A_{Th232}^{total} \times 1/\eta \qquad \text{Eq. (1.10)}$$

with η being the ^{238}U conversion factor, 1 ppm = 0.746 dpm/g (Chase et al., 2003).

Manganese on the other hand, precipitates as oxyhydroxides (Mn(III) and(IV)) under well-oxygenated conditions (Calvert and Pedersen, 1996). In sedimentary environments in which the accumulation of organic matter (and by inference bacterial respiration) is low and oxic conditions prevail, authigenic Mn enrichments can be expected (e.g. Calvert and Pedersen, 1996; Jaccard et al., 2009). In more reducing environments, there is no accumulation of authigenic Mn-oxides, and the downcore Mn distribution is controlled solely by its insoluble detrital fraction (Jaccard et al., 2009). To assess authigenic enrichments of Mn in oxic bottom waters, we use the ratio between Mn and titanium (Ti), an element assumed to be exclusively associated with detrital sources (Jaccard et al., 2009). Any sedimentary Mn fraction in excess relative to the detrital background is assumed to have authigenically precipitated under oxic conditions.

1.6.3 Lithogenic flux (detrital ^{232}Th)

Reconstructing lithogenic fluxes using common thorium (^{232}Th) is a robust way to determine detrital input to the open ocean (e.g. Anderson et al., 2014; Kienast et al., 2016; Martínez-García et al., 2009; McGee et al., 2016; Sayles et al., 2001; Thöle et al., 2019; Winckler et al., 2008). ^{232}Th is nearly exclusively found in the lithogenic fraction and is enriched in the continental crust and comparatively low in mid-ocean ridge basalt (MORB)-like material (Kienast et al., 2016; McGee et al., 2016; Winckler et al., 2008). Its concentration has been relatively well constrained in upper continental crust from around the world to 10.7 ± 2 ppm (Kienast et al., 2016; McGee et al., 2007; Taylor and McLennan, 1995). In open ocean environments, away from fluvial, hemipelagic, or

glaciogenic inputs of continental material, ^{232}Th is thought to be primarily delivered by dust (Kienast et al., 2016; Winckler et al., 2008). Recently, a slightly higher Th concentration of 14 ± 1 ppm has been proposed for sediments finer than 5 µm and excluding Patagonian sourced material (McGee et al., 2016). In our sediment cores, the detrital material was predominantly in the silt fraction (2–63 µm) likely stemming from South America (Li et al., 2008; Mahowald et al., 2006). As such, our calculations of lithogenic fluxes are based on the traditional value of 10.7 ppm. Furthermore, calculation using the traditional value allows for a quantitative comparison with other cores from the region.

We can use the ^{230}Th-normalization method (described above) to determine lithogenic fluxes as follows:

$$lith.\,flux = \frac{A_{Th232}^{total}}{10.7 \times \gamma} \times prF_v \qquad \text{Eq. (1.11)}$$

with γ being the conversion factor for ^{232}Th, 1 ppm = 0.243 dpm/g (Chase et al., 2003).

1.6.4 Bottom water flow velocity (sortable silt mean size)

The mean grain-size of the sortable silt fraction ($\overline{\text{SS}}$) can be used to quantify the flow velocity in the sedimentation regime. At flow speeds below 10–15 cm/s fluctuations in the mean size of terrigenous non-cohesive sortable silt range (10–63 µm) were found to reflect changes in the intensity of the near-bottom currents (e.g. Bianchi et al., 1999; McCave et al., 2017, 1995; McCave and Hall, 2006). Grains that are finer than 10 µm behave cohesively as in the clay fraction (<2 µm). Such grains often exist in the natural environment as aggregates and cannot be used as paleocurrent proxy, since the analysis is conducted on disaggregated grains (McCave et al., 1995; McCave and Hall, 2006). Grains larger than 63 µm, are rarely transported by bottom currents, thus defining the upper grain size limit of the proxy (McCave et al., 1995). Within the sortable silt fraction, more vigorous flow regime leads to higher $\overline{\text{SS}}$ values due to reduced deposition of finer components. Conversely, slower flow velocities allow finer grains to settle, leading to lower $\overline{\text{SS}}$ values. If deposition of

finer grains (<10 µm) is reduced with increasing flow speed, it can be expected that the ratio of grains between 10–63 µm to the total fine fraction (all grains <63 µm) increases with flow speed. Thus, in current-sorted sediments, changes in sortable silt mean size ($\overline{SS}$) correlate linearly with sortable silt percentage (SS%) within the fine fraction, and thus the degree of this correlation provides an index for sorting (McCave and Andrews, 2019).

1.6.5 Export production (preserved biogenic opal)

Diatoms dominate the export of carbon in the Southern Ocean and have been widely used to reconstruct past changes in marine export production (e.g. Anderson et al., 2009; Bradtmiller et al., 2007; Chase et al., 2003). However, accumulation of sedimentary opal is not only controlled by opal production in the ocean surface, but is also affected by dissolution in the water column and at the seefloor (Dezileau et al., 2003; Pondaven et al., 2000; Ragueneau et al., 2000). Therefore, the link between opal and carbon export is not straightforward, as additional factors play a role, such as Fe-availability affecting the carbon (C) and nitrogen (N) uptake in diatoms relative to silicate (Boutorh et al., 2016; Meyerink et al., 2017; Pichevin et al., 2014). Empirical studies of modern opal export patterns however, suggest that the spatial distribution of opal burial predominantly reflects diatom productivity and opal export (e.g. Bradtmiller et al., 2007; Chase et al., 2003; Nelson et al., 2002; Pondaven et al., 2000; Sayles et al., 2001). Also, approaches with different paleoproductivity proxies show similar glacial-interglacial patterns for the different proxies in the region (Manoj and Thamban, 2015; Thöle et al., 2019). Therefore, we assume that changes in preserved biogenic opal fluxes provide a robust, first-order approximation for past changes in organic carbon export to the sediment.

1.7 Thesis outline

In order to address the set of objectives described above, the main body of this thesis (Chapters 2–4) consists of three manuscripts that will be submitted to scientific journals.

In Chapter 2 we present the evolution of bottom water oxygenation, and associated with this, contrasting productivity patterns in the Subantarctic and

Antarctic zones of the Southern Ocean are discussed with their implications on ocean circulation and upwelling intensities.

In Chapter 3 lithogenic flux records are combined with previously published records for a regional comparison, with regard to a possible impact on surface ocean fertilization.

In Chapter 4 sortable silt reconstructions are discussed and possible changes of the Antarctic Circumpolar Current flow regime are investigated.

Finally, the main conclusions are summarized in Chapter 5 with an outlook and possible future research. Detailed method descriptions can be found in the appendix in Chapter 6.

References

Adkins, J.F., 2013. The role of deep ocean circulation in setting glacial climates. Paleoceanography 28, 539–561. doi: 10.1002/palo.20046

Anderson, R.F., Ali, S., Bradtmiller, L.I., Nielsen, S.H.H., Fleisher, M.Q., Anderson, B.E., Burckle, L.H., 2009. Wind-driven Upwelling in the Southern Ocean and the Deglacial Rise in Atmospheric CO_2. Science 323, 1443–1448. doi: 10.1126/science.1167441

Anderson, R.F., Bacon, M.P., Brewer, P.G., 1983. Removal of ^{230}Th and ^{231}Pa from the open ocean. Earth Planet. Sci. Lett. 62, 7–23

Anderson, R.F., Barker, S., Fleisher, M., Gersonde, R., Goldstein, S.L., Kuhn, G., Mortyn, P.G., Pahnke, K., Sachs, J.P., 2014. Biological response to millennial variability of dust and nutrient supply in the Subantarctic South Atlantic Ocean. Philos. Trans. R. Soc. A 372, 20130054. doi: 10.1098/rsta.2013.0054

Bereiter, B., Eggleston, S., Schmitt, J., Nehrbass-Ahles, C., Stocker, T.F., Fischer, H., Kipfstuhl, S., Chappellaz, J., 2015. Revision of the EPICA Dome C CO_2 record from 800 to 600 kyr before present. Geophys. Res. Lett. 42, 542–549. doi: 10.1002/2014GL061957

Bereiter, B., Shackleton, S., Baggenstos, D., Kawamura, K., Severinghaus, J., 2018. Mean global ocean temperatures during the last glacial transition. Nature 553, 39–44. doi: 10.1038/nature25152

Bianchi, G.G., Hall, I.R., McCave, I.N., Joseph, L., 1999. Measurement of the sortable silt current speed proxy using the Sedigraph 5100 and Coulter Multisizer Ile: Precision and accuracy. Sedimentology 46, 1001–1014. doi: 10.1046/j.1365-3091.1999.00256.x

Böhm, E., Lippold, J., Gutjahr, M., Frank, M., Blaser, P., Antz, B., Fohlmeister, J., Frank, N., Andersen, M.B., Deininger, M., 2015. Strong and deep Atlantic meridional overturning circulation during the last glacial cycle. Nature 517, 73–76. doi: 10.1038/nature14059

Bourne, M.D., Thomas, A.L., Niocaill, C. Mac, Henderson, G.M., 2012. Improved determination of marine sedimentation rates using $^{230}Th_{xs}$. Geochemistry, Geophys. Geosystems 13, 1. doi: 10.1029/2012GC004295

Boutorh, J., Moriceau, B., Gallinari, M., Ragueneau, O., Bucciarelli, E., 2016. Effect of trace metal-limited growth on the postmortem dissolution of the marine diatom *Pseudo-nitzschia delicatissima*. Global Biogeochem. Cycles 30, 57–69. doi: 10.1002/2015GB005088

Bradtmiller, L.I., Anderson, R.F., Fleisher, M.Q., Burckle, L.H., 2007. Opal burial in the equatorial Atlantic Ocean over the last 30 ka: Implications for glacial-interglacial changes in the ocean silicon cycle. Paleoceanography 22, PA4216, 1–15. doi: 10.1029/2007PA001443

Bradtmiller, L.I., Anderson, R.F., Sachs, J.P., Fleisher, M.Q., 2010. A deeper respired

carbon pool in the glacial equatorial Pacific Ocean. Earth Planet. Sci. Lett. 299, 417–425. doi: 10.1016/j.epsl.2010.09.022

Broecker, W.S., 1991. The Great Ocean Conveyor. Oceanography 4, 79–89. doi: 10.5670/oceanog.1991.07

Broecker, W.S., 1982. Glacial to interglacial changes in ocean chemistry. Prog. Oceanogr. 11, 151–197. doi: 10.1016/0079-6611(82)90007-6

Brzezinski, M.A., Pride, C.J., Franck, V.M., Sigman, D.M., Matsumoto, K., Gruber, N., Rau, G.H., Coale, K.H., 2002. A switch from $Si(OH)_4$ to NO_3^- depletion in the glacial Southern Ocean. Geophys. Res. Lett. 29, 12, 1564. doi: 10.1029/2001GL014349

Calvert, S.E., Pedersen, T.F., 1996. Sedimentary geochemistry of manganese: Implications for the environment of formation of manganiferous black shales. Econ. Geol. 91, 36–47. doi: 10.2113/gsecongeo.91.1.36

Chase, Z., Anderson, R.F., Fleisher, M.Q., 2001. Evidence from authigenic uranium for increased productivity of the glacial Subantarctic Ocean. Paleoceanography 16, 5, 468–478. doi: 10.1029/2000PA000542

Chase, Z., Anderson, R.F., Fleisher, M.Q., Kubik, P.W., 2003. Accumulation of biogenic and lithogenic material in the Pacific sector of the Southern Ocean during the past 40,000 years. Deep. Res. Part II Top. Stud. Oceanogr. 50, 799–832. doi: 10.1016/S0967-0645(02)00595-7

Chavaillaz, Y., Codron, F., Kageyama, M., 2013. Southern westerlies in LGM and future (RCP4.5) climates. Clim. Past 9, 517–524. doi: 10.5194/cp-9-517-2013

Church, J.A., White, N.J., 2011. Sea-Level Rise from the Late 19th to the Early 21st Century. Surv. Geophys. 32, 585–602. doi: 10.1007/s10712-011-9119-1

Colley, S., Thomson, J., Toole, J., 1989. Uranium relocations and derivation of quasi-isochrons for a turbidite/pelagic sequence in the Northeast Atlantic. Geochim. Cosmochim. Acta 53, 1223–1234. doi: 10.1016/0016-7037(89)90058-6

Cortese, G., Gersonde, R., Hillenbrand, C.D., Kuhn, G., 2004. Opal sedimentation shifts in the World Ocean over the last 15 Myr. Earth Planet. Sci. Lett. 224, 509–527. doi: 10.1016/j.epsl.2004.05.035

Costa, K.M., Hayes, C.T., Anderson, R.F., Pavia, F.J., Bausch, A., Deng, F., Dutay, J.C., Geibert, W., Heinze, C., Henderson, G., Hillaire-Marcel, C., Hoffmann, S., Jaccard, S.L., Jacobel, A.W., Kienast, S.S., Kipp, L., Lerner, P., Lippold, J., Lund, D., Marcantonio, F., McGee, D., McManus, J.F., Mekik, F., Middleton, J.L., Missiaen, L., Not, C., Pichat, S., Robinson, L.F., Rowland, G.H., Roy-Barman, M., Tagliabue, A., Torfstein, A., Winckler, G., Zhou, Y., 2020. ^{230}Th normalization: New insights on an essential tool for quantifying sedimentary fluxes in the modern and Quaternary ocean. Paleoceanogr. Paleoclimatology 35, e2019PA003820, 1–36. doi: 10.1029/2019PA003820

Curry, W.B., Oppo, D.W., 2005. Glacial water mass geometry and the distribution of $\delta^{13}C$ of ΣCO_2 in the western Atlantic Ocean. Paleoceanography 20, 1–12. doi:

10.1029/2004PA001021

Da, J., Zhang, Y.G., Li, G., Meng, X., Ji, J., 2019. Low CO_2 levels of the entire Pleistocene epoch. Nat. Commun. 10, 1–9. doi: 10.1038/s41467-019-12357-5

DeVries, T., Holzer, M., Primeau, F., 2017. Recent increase in oceanic carbon uptake driven by weaker upper-ocean overturning. Nature 542, 215–218. doi: 10.1038/nature21068

Dezileau, L., Reyss, J.L., Lemoine, F., 2003. Late Quaternary changes in biogenic opal fluxes in the Southern Indian Ocean. Mar. Geol. 202, 143–158. doi: 10.1016/S0025-3227(03)00283-4

Dlugokencky, E., Tans, P., 2020. Trends in Atmospheric Carbon Dioxide. NOAA/GML, available from www.esrl.noaa.gov/gmd/ccgg/trends/ (Accessed June 28th, 2020)

Dumont, M., Pichevin, L., Geibert, W., Crosta, X., Michel, E., Moreton, S., Dobby, K., Ganeshram, R., 2020. The nature of deep overturning and reconfigurations of the silicon cycle across the last deglaciation, Nat. Commun. 11, 1534, doi: 10.1038/s41467-020-15101-6

Dunk, R.M., Mills, R.A., Jenkins, W.J., 2002. A reevaluation of the oceanic uranium budget for the Holocene. Chem. Geol. 190, 45–67. doi: 10.1016/S0009-2541(02)00110-9

Elderfield, H., Ferretti, P., Greaves, M., Crowhurst, S.J., McCave, I.N., Hodell, D., Piotrowski, A.M., 2012. Evolution of Ocean Temperature and Ice Volume Through the Mid-Pleistocene Climate Transition. Science 337, 704–709. doi: 10.1594/PANGAEA.786205

Ferrari, R., Jansen, M.F., Adkins, J.F., Burke, A., Stewart, A.L., Thompson, A.F., 2014. Antarctic sea ice control on ocean circulation in present and glacial climates. Proc. Natl. Acad. Sci. U. S. A. 111, 24, 8753–8758. doi: 10.1073/pnas.1323922111

Fischer, H., Schmitt, J., Lüthi, D., Stocker, T.F., Tschumi, T., Parekh, P., Joos, F., Köhler, P., Völker, C., Gersonde, R., Barbante, C., Le Floch, M., Raynaud, D., Wolff, E., 2010. The role of Southern Ocean processes in orbital and millennial CO_2 variations - A synthesis. Quat. Sci. Rev. 29, 193–205. doi: 10.1016/j.quascirev.2009.06.007

Francois, R., Frank, M., Rutgers van der Loeff, M.M., Bacon, M.P., 2004. ^{230}Th normalization: An essential tool for interpreting sedimentary fluxes during the late Quaternary. Paleoceanography 19, PA1018. doi: 10.1029/2003pa000939

Franzese, A.M., Hemming, S.R., Goldstein, S.L., Anderson, R.F., 2006. Reduced Agulhas Leakage during the Last Glacial Maximum inferred from an integrated provenance and flux study. Earth Planet. Sci. Lett. 250, 72–88. doi: 10.1016/j.epsl.2006.07.002

Frölicher, T.L., Sarmiento, J.L., Paynter, D.J., Dunne, J.P., Krasting, J.P., Winton, M., 2015. Dominance of the Southern Ocean in Anthropogenic Carbon and Heat Uptake in CMIP5 Models. J. Clim. 28, 862–886. doi: 10.1175/JCLI-D-14-00117.1

Geibert, W., Rutgers van der Loeff, M.M., Usbeck, R., Gersonde, R., Kuhn, G., Seeberg-Elverfeldt, J., 2005. Quantifying the opal belt in the Atlantic and southeast Pacific sector of the Southern Ocean by means of ^{230}Th normalization. Global Biogeochem. Cycles 19, 1–39. doi: 10.1029/2005GB002465

Gottschalk, J., Battaglia, G., Fischer, H., Frölicher, T.L., Jaccard, S.L., Jeltsch-Thömmes, A., Joos, F., Köhler, P., Meissner, K.J., Menviel, L., Nehrbass-Ahles, C., Schmitt, J., Schmittner, A., Skinner, L.C., Stocker, T.F., 2019. Mechanisms of millennial-scale atmospheric CO_2 change in numerical model simulations. Quat. Sci. Rev. 220, 30–74. doi: 10.1016/j.quascirev.2019.05.013

Gottschalk, J., Skinner, L.C., Lippold, J., Vogel, H., Frank, N., Jaccard, S.L., Waelbroeck, C., 2016. Biological and physical controls in the Southern Ocean on past millennial-scale atmospheric CO_2 changes. Nat. Commun. 7. doi: 10.1038/ncomms11539

Gruber, N., Gloor, M., Mikaloff Fletcher, S.E., Doney, S.C., Dutkiewicz, S., Follows, M.J., Gerber, M., Jacobson, A.R., Joos, F., Lindsay, K., Menemenlis, D., Mouchet, A., Müller, S.A., Sarmiento, J.L., Takahashi, T., 2009. Oceanic sources, sinks, and transport of atmospheric CO_2. Global Biogeochem. Cycles 23, 1–21. doi: 10.1029/2008GB003349

Hain, M.P., Sigman, D.M., Haug, G.H., 2010. Carbon dioxide effects of Antarctic stratification, North Atlantic Intermediate Water formation, and subantarctic nutrient drawdown during the last ice age: Diagnosis and synthesis in a geochemical box model. Global Biogeochem. Cycles 24, GB4023, 1–19. doi: 10.1029/2010GB003790

Hain, M.P., Sigman, D.M., Haug, G.H., 2014. The Biological Pump in the Past, in: Treatise on Geochemistry (Second Edition). Elsevier, 485–517. doi: 10.1016/B978-0-08-095975-7.00618-5

Henderson, G.M., Anderson, R.F., 2003. The U-series toolbox for paleoceanography. Rev. Mineral. Geochemistry 52, 493–531. doi: 10.2113/0520493

Hönisch, B., Ridgwell, A., Schmidt, D.N., Thomas, E., Gibbs, S.J., Sluijs, A., Zeebe, R., Kump, L., Martindale, R.C., Greene, S.E., Kiessling, W., Ries, J., Zachos, J.C., Royer, D.L., Barker, S., Marchitto, T.M., Moyer, R., Pelejero, C., Ziveri, P., Foster, G.L., Williams, B., 2012. The geological record of ocean acidification. Science 335, 1058–1063. doi: 10.1126/science.1208277

Intergovernmental Panel on Climate Change (IPCC), 2014. Climate Change 2013 – The Physical Science Basis: Working Group I Contribution to the Fifth Assessment Report of the Intergovernmental Panel on Climate Change. Cambridge: Cambridge University Press. doi: 10.1017/CBO9781107415324

Ito, T., Follows, M.J., 2005. Preformed phosphate, soft tissue pump and atmospheric CO_2. J. Mar. Res. 63, 813–839. doi: 10.1357/0022240054663231

Jaccard, S.L., Galbraith, E.D., Frölicher, T.L., Gruber, N., 2014. Ocean (de)oxygenation across the last deglaciation: Insights for the future. Oceanography

27, 26–35. doi: 10.5670/oceanog.2014.05

Jaccard, S.L., Galbraith, E.D., Martínez-García, A., Anderson, R.F., 2016. Covariation of deep Southern Ocean oxygenation and atmospheric CO_2 through the last ice age. Nature 530, 207–210. doi: 10.1038/nature16514

Jaccard, S.L., Galbraith, E.D., Sigman, D.M., Haug, G.H., Francois, R., Pedersen, T.F., Dulski, P., Thierstein, H.R., 2009. Subarctic Pacific evidence for a glacial deepening of the oceanic respired carbon pool. Earth Planet. Sci. Lett. 277, 156–165. doi: 10.1016/j.epsl.2008.10.017

Jaccard, S.L., Hayes, C.T., Hodell, D.A., Anderson, R.F., Sigman, D.M., Haug, G.H., 2013. Two modes of change in SO Productivity. Science 339, 6126, 1419–1423. doi: 10.1126/science.1227545

Jacobel, A.W., McManus, J.F., Anderson, R.F., Winckler, G., 2017. Repeated storage of respired carbon in the equatorial Pacific Ocean over the last three glacial cycles. Nat. Commun. 8. doi: 10.1038/s41467-017-01938-x

Jouzel, J., Masson-Delmotte, V., Cattani, O., Dreyfus, G., Falourd, S., Hoffmann, G., Minster, B., Nouet, J., Barnola, J.M., Chappellaz, J., Fischer, H., Gallet, J.C., Johnsen, S., Leuenberger, M., Loulergue, L., Luethi, D., Oerter, H., Parrenin, F., Raisbeck, G., Raynaud, D., Schilt, A., Schwander, J., Selmo, E., Souchez, R., Spahni, R., Stauffer, B., Steffensen, J.P., Stenni, B., Stocker, T.F., Tison, J.L., Werner, M., Wolff, E.W., 2007. Orbital and millennial Antarctic climate variability over the past 800,000 years. Science 317, 793–796. doi: 10.1126/science.1141038

Khatiwala, S., Tanhua, T., Mikaloff Fletcher, S., Gerber, M., Doney, S.C., Graven, H.D., Gruber, N., McKinley, G.A., Murata, A., Ríos, A.F., Sabine, C.L., 2013. Global ocean storage of anthropogenic carbon. Biogeosciences 10, 2169–2191. doi: 10.5194/bg-10-2169-2013

Kienast, S.S., Kienast, M., Jaccard, S., Calvert, S.E., François, R., 2006. Testing the silica leakage hypothesis with sedimentary opal records from the eastern equatorial Pacific over the last 150 kyrs. Geophys. Res. Lett. 33, L15607, http://doi:10.1029/2006GL026651

Kienast, S.S., Winckler, G., Lippold, J., Albani, S., Mahowald, N.M., 2016. Tracing dust input to the global ocean using thorium isotopes in marine sediments: ThoroMap. Global Biogeochem. Cycles 30, 1526–1541. doi: 10.1002/2016GB005408

Klinkhammer, G.P., Palmer, M.R., 1991. Uranium in the oceans: Where it goes and why. Geochim. Cosmochim. Acta 55, 1799–1806. doi: 10.1016/0016-7037(91)90024-Y

Kohfeld, K.E., Graham, R.M., de Boer, A.M., Sime, L.C., Wolff, E.W., Le Quéré, C., Bopp, L., 2013. Southern Hemisphere westerly wind changes during the Last Glacial Maximum: Paleo-data synthesis. Quat. Sci. Rev. 68, 76–95. doi: 10.1016/j.quascirev.2013.01.017

Kohfeld, K.E., Le Quéré, C., Harrison, S.P., Anderson, R.F., 2005. Role of marine biology in glacial-interglacial CO_2 cycles. Science 308, 74–78. doi:

10.1126/science.1105375

Kohfeld, K.E., Ridgwell, A., 2009. Glacial-Interglacial Variability in Atmospheric CO_2. Surface Ocean–Lower Atmosphere Processes, Geophys. Res. Series 187, 251–286. doi: 10.1029/2008GM000845

Kretschmer, S., Geibert, W., Rutgers van der Loeff, M.M., Mollenhauer, G., 2010. Grain size effects on $^{230}Th_{xs}$ inventories in opal-rich and carbonate-rich marine sediments. Earth Planet. Sci. Lett. 294, 131–142. doi: 10.1016/j.epsl.2010.03.021

Kumar, N., Anderson, R.F., Mortlock, R.A., Froelich, P.N., Kubik, P., Dittrich-Hannen, B., Suter, M., 1995. Increased biological production and export in the glacial Southern Ocean. Nature 378, 675–680. doi: 10.1038/378675a0

Lamy, F., Arz, H.W., Kilian, R., Lange, C.B., Lembke-Jene, L., Wengler, M., Kaiser, J., Baeza-Urrea, O., Hall, I.R., Harada, N., Tiedemann, R., 2015. Glacial reduction and millennial-scale variations in Drake Passage throughflow. Proc. Natl. Acad. Sci. U. S. A. 112, 13496–13501. doi: 10.1073/pnas.1509203112

Langmuir, D., 1978. Uranium solution-mineral equilibria at low temperatures with applications to sedimentary ore deposits. Geochim. Cosmochim. Acta 42, 547–569. doi: 10.1016/0016-7037(78)90001-7

Le Quéré, C., Rödenbeck, C., Buitenhuis, E.T., Conway, T.J., Langenfelds, R., Gomez, A., Labuschagne, C., Ramonet, M., Nakazawa, T., Metzl, N., Gillett, N.P., Heimann, M., 2007. Saturation of the Southern Ocean CO_2 Sink Due to Recent Climate Change. Science 316, 1735–1738. doi: 10.1126/science.1136188

Li, F., Ginoux, P., Ramaswamy, V., 2008. Distribution, transport, and deposition of mineral dust in the Southern Ocean and Antarctica: Contribution of major sources. J. Geophys. Res. Atmos. 113, 1–15. doi: 10.1029/2007JD009190

Lippold, J., Gutjahr, M., Blaser, P., Christner, E., de Carvalho Ferreira, M.L., Mulitza, S., Christl, M., Wombacher, F., Böhm, E., Antz, B., Cartapanis, O., Vogel, H., Jaccard, S.L., 2016. Deep water provenance and dynamics of the (de)glacial Atlantic meridional overturning circulation. Earth Planet. Sci. Lett. 445, 68–78. http://dx.doi.org/10.1016/j.epsl.2016.04.013

Lippold, J., Luo, Y., Francois, R., Allen, S.E., Gherardi, J., Pichat, S., Hickey, B., Schulz, H., 2012. Strength and geometry of the glacial Atlantic Meridional Overturning Circulation. Nat. Geosci. 5, 813–816. doi: 10.1038/ngeo1608

Lumpkin, R., Speer, K., 2007. Global ocean meridional overturning. J. Phys. Oceanogr. 37, 2550–2562. doi: 10.1175/JPO3130.1

Lüthi, D., Le Floch, M., Bereiter, B., Blunier, T., Barnola, J.M., Siegenthaler, U., Raynaud, D., Jouzel, J., Fischer, H., Kawamura, K., Stocker, T.F., 2008. High-resolution carbon dioxide concentration record 650,000–800,000 years before present. Nature 453, 379–382. doi: 10.1038/nature06949

Lynch-Stieglitz, J., Adkins, J.F., Curry, W.B., Dokken, T., Hall, I.R., Herguera, J.C., Hirschi, J.J.M., Ivanova, E. V., Kissel, C., Marchal, O., Marchitto, T.M., McCave, I.N., McManus, J.F., Mulitza, S., Ninnemann, U., Peeters, F., Yu, E.F., Zahn, R.,

2007. Atlantic meridional overturning circulation during the last glacial maximum. Science 316, 66–69. doi: 10.1126/science.1137127

Mahowald, N.M., Muhs, D.R., Levis, S., Rasch, P.J., Yoshioka, M., Zender, C.S., Luo, C., 2006. Change in atmospheric mineral aerosols in response to climate: Last glacial period, preindustrial, modern, and doubled carbon dioxide climates. J. Geophys. Res. Atmos. 111. doi: 10.1029/2005JD006653

Mangini, A., Jung, M., Laukenmann, S., 2001. What do we learn from peaks of uranium and of manganese in deep sea sediments? Mar. Geol. 177, 63–78. doi: 10.1016/S0025-3227(01)00124-4

Manoj, M.C., Thamban, M., 2015. Shifting frontal regimes and its influence on bioproductivity variations during the Late Quaternary in the Indian sector of Southern Ocean. Deep. Res. Part II Top. Stud. Oceanogr. 118, 261–274. doi: 10.1016/j.dsr2.2015.03.011

Marinov, I., Gnanadesikan, A., Toggweiler, J.R., Sarmiento, J.L., 2006. The Southern Ocean biogeochemical divide. Nature 441, 964–967. doi: 10.1038/nature04883

Marshall, J., Speer, K., 2012. Closure of the meridional overturning circulation through Southern Ocean upwelling. Nat. Geosci. 5, 171–180. doi: 10.1038/ngeo1391

Martin, J.H., 1990. Glacial-interglacial CO_2 change: The Iron Hypothesis. Paleoceanography 5, 1–13. doi: 10.1029/PA005i001p00001

Martínez-García, A., Rosell-Melé, A., Geibert, W., Gersonde, R., Masqué, P., Gaspari, V., Barbante, C., 2009. Links between iron supply, marine productivity, sea surface temperature, and CO_2 over the last 1.1 Ma. Paleoceanography 24, 1–14. doi: 10.1029/2008PA001657

Martínez-García, A., Sigman, D.M., Ren, H., Anderson, R.F., Straub, M., Hodell, D.A., Jaccard, S.L., Eglinton, T.I., Haug, G.H., 2014. Iron fertilization of the subantarctic ocean during the last ice age. Science 343, 1347–1350. doi: 10.1126/science.1246848

Mazaud, A., Michel, E., Dewilde, F., Turon, J.L., 2010. Variations of the Antarctic Circumpolar Current intensity during the past 500 ka. Geochemistry, Geophys. Geosystems 11, 1–10. doi: 10.1029/2010GC003033

McCave, I.N., Andrews, J.T., 2019. Distinguishing current effects in sediments delivered to the ocean by ice. I. Principles, methods and examples. Quat. Sci. Rev. 212, 92–107. doi: 10.1016/j.quascirev.2019.03.031

McCave, I.N., Crowhurst, S.J., Kuhn, G., Hillenbrand, C.D., Meredith, M.P., 2014. Minimal change in antarctic circumpolar current flow speed between the last glacial and holocene. Nat. Geosci. 7, 113–116. doi: 10.1038/ngeo2037

McCave, I.N., Hall, I.R., 2006. Size sorting in marine muds: Processes, pitfalls, and prospects for paleoflow-speed proxies. Geochemistry, Geophys. Geosystems 7. doi: 10.1029/2006GC001284

McCave, I.N., Manighetti, B., Robinson, S.G., 1995. Sortable silt and fine sediment size/composition slicing: Parameters for palaeocurrent speed and palaeoceanography. Paleoceanography 10, 593–610. doi: 10.1029/94PA03039

McCave, I.N., Thornalley, D.J.R., Hall, I.R., 2017. Relation of sortable silt grain-size to deep-sea current speeds: Calibration of the 'Mud Current Meter.' Deep. Res. Part I Oceanogr. Res. Pap. 127, 1–12. doi: 10.1016/j.dsr.2017.07.003

McGee, D., Marcantonio, F., Lynch-Stieglitz, J., 2007. Deglacial changes in dust flux in the eastern equatorial Pacific. Earth Planet. Sci. Lett. 257, 215–230. doi: 10.1016/j.epsl.2007.02.033

McGee, D., Winckler, G., Borunda, A., Serno, S., Anderson, R.F., Recasens, C., Bory, A., Gaiero, D., Jaccard, S.L., Kaplan, M., McManus, J.F., Revel, M., Sun, Y., 2016. Tracking eolian dust with helium and thorium: Impacts of grain size and provenance, Geochim. Cosmochim. Acta. Elsevier Ltd. doi: 10.1016/j.gca.2015.11.023

McManus, J.F., Berelson, W.M., Klinkhammer, G.P., Hammond, D.E., Holm, C., 2005. Authigenic uranium: Relationship to oxygen penetration depth and organic carbon rain. Geochim. Cosmochim. Acta 69, 95–108. doi: 10.1016/j.gca.2004.06.023

McManus, J.F., Francois, R., Gherardi, J.-M., Keigwin, L.D., Brown-Leger, S., 2004. Collapse and rapid resumption of Atlantic meridional circulation linked to deglacial climate changes. Nature 428, 834–837, http://doi: 10.1038/nature02494

Meyerink, S.W., Ellwood, M.J., Maher, W.A., Dean Price, G., Strzepek, R.F., 2017. Effects of iron limitation on silicon uptake kinetics and elemental stoichiometry in two Southern Ocean diatoms, *Eucampia antarctica* and *Proboscia inermis*, and the temperate diatom *Thalassiosira pseudonana*. Limnol. Oceanogr. 62, 6, 2445–2462. doi: 10.1002/lno.10578

Molyneux, E.G., Hall, I.R., Zahn, R., Diz, P., 2007. Deep water variability on the southern Agulhas Plateau: Interhemispheric links over the past 170 ka. Paleoceanography 22, 1–14. doi: 10.1029/2006PA001407

Morford, J.L., Emerson, S., 1999. The geochemistry of redox sensitive trace metals in sediments. Geochim. Cosmochim. Acta 63, 1735–1750. doi: 10.1016/S0016-7037(99)00126-X

Munk, W., Wunsch, C., 1998. Abyssal recipes II: energetics of tidal and wind mixing. Deep. Res. Part I Oceanogr. Res. Pap. 45, 1977–2010. doi: 10.1016/S0967-0637(98)00070-3

Nelson, D.M., Anderson, R.F., Barber, R.T., Brzezinski, M.A., Buesseler, K.O., Chase, Z., Collier, R.W., Dickson, M.L., François, R., Hiscock, M.R., Honjo, S., Marra, J., Martin, W.R., Sambrotto, R.N., Sayles, F.L., Sigmon, D.E., 2002. Vertical budgets for organic carbon and biogenic silica in the Pacific sector of the Southern Ocean, 1996–1998. Deep. Res. Part II Top. Stud. Oceanogr. 49, 1645–1674. doi: 10.1016/S0967-0645(02)00005-X

Ohshima, K.I., Fukamachi, Y., Williams, G.D., Nihashi, S., Roquet, F., Kitade, Y., Tamura, T., Hirano, D., Herraiz-Borreguero, L., Field, I., Hindell, M., Aoki, S., Wakatsuchi, M., 2013. Antarctic Bottom Water production by intense sea-ice formation in the Cape Darnley polynya. Nat. Geosci. 6, 235–240. doi:

10.1038/ngeo1738

Orsi, H., Whitworth, T., Nowlin Jr, W.D., 1995. On the meridional extent and fronts of the Antarctic Circumpolar Current. Deep. Res. Part I 42, 5, 641–673. doi: 10.1016/0967-0637(95)00021-W

Parekh, P., Joos, F., Müller, S.A., 2008. A modeling assessment of the interplay between aeolian iron fluxes and iron-binding ligands in controlling carbon dioxide fluctuations during Antarctic warm events. Paleoceanography 23, 1–14. doi: 10.1029/2007PA001531

Pichevin, L.E., Ganeshram, R.S., Geibert, W., Thunell, R., Hinton, R., 2014. Silica burial enhanced by iron limitation in oceanic upwelling margins. Nat. Geosci. 7, 541–546. doi: 10.1038/ngeo2181

Pondaven, P., Ragueneau, O., Tréguer, P., Hauvespre, A., Dezileau, L., Reyss, J.L., 2000. Resolving the 'opal paradox' in the Southern Ocean. Nature 405, 168–172. doi: 10.1038/35012046

Ragueneau, O., Tréguer, P., Leynaert, A., Anderson, R.F., Brzezinski, M.A., DeMaster, D.J., Dugdale, R.C., Dymond, J., Fischer, G., François, R., Heinze, C., Maier-Reimer, E., Martin-Jézéquel, V., Nelson, D.M., Quéguiner, B., 2000. A review of the Si cycle in the modern ocean: Recent progress and missing gaps in the application of biogenic opal as a paleoproductivity proxy. Glob. Planet. Change 26, 317–365. doi: 10.1016/S0921-8181(00)00052-7

Rahmstorf, S., 2002. Ocean circulation and climate during the past 120,000 years. Nature 419, 207–214. doi: 10.1038/nature01090

Raven, J., Caldeira, K., Elderfield, H., Hoegh-Guldberg, O., Liss, P., Riebesell, U., Shepherd, J., Turley, C., Watson, A., 2005. Ocean acidification due to increasing carbon dioxide. The Royal Soc. 12/05

Rintoul, S.R., 2018. The global influence of localized dynamics in the Southern Ocean. Nature 558, 209–218. doi: 10.1038/s41586-018-0182-3

Robinson, R.S., Sigman, D.M., 2008. Nitrogen isotopic evidence for a poleward decrease in surface nitrate within the ice age Antarctic. Quat. Sci. Rev. 27, 1076–1090. doi: 10.1016/j.quascirev.2008.02.005

Sabine, C.L., Feely, R.A., Gruber, N., Key, R.M., Lee, K., Bullister, J.L., Wanninkhof, R., Wong, C.S., Wallace, D.W.R., Tilbrook, B., Millero, F.J., Peng, T.-H., Kozyr, A., Ono, T., Rois, A.F., 2004. The Oceanic Sink for Anthropogenic CO_2. Science 305, 367–371

Sarmiento, J. L., and N. Gruber, 2006. Ocean Biogeochemical Dynamics, Princeton University Press, Princeton and Oxford

Sayles, F.L., Martin, W.R., Chase, Z., Anderson, R.F., 2001. Benthic remineralization and burial of biogenic SiO_2, $CaCO_3$, organic carbon, and detrital material in the Southern Ocean along a transect at 170° West. Deep. Res. Part II Top. Stud. Oceanogr. 48, 19–20, 4323–4383. doi: 10.1016/S0967-0645(01)00091-1

Schlitzer, R., 2018. Ocean Data View. Available at http://odv.awi.de

Shakun, J.D., Clark, P.U., He, F., Marcott, S.A., Mix, A.C., Liu, Z., Otto-Bliesner, B., Schmittner, A., Bard, E., 2012. Global warming preceded by increasing carbon dioxide concentrations during the last deglaciation. Nature 484, 49–54. doi: 10.1038/nature10915

Siegenthaler, U., Stocker, T.F., Monnin, E., Lüthi, D., Schwander, J., Stauffer, B., Raynaud, D., Barnola, J.M., Fischer, H., Masson-Delmotte, V., Jouzel, J., 2005. Atmospheric science: Stable carbon cycle-climate relationship during the late pleistocene. Science 310, 1313–1317. doi: 10.1126/science.1120130

Sigman, D.M., Boyle, E.A., 2000. Glacial/interglacial variations in atmospheric carbon dioxide. Nature 407, 859–869. doi: 10.1038/35038000

Sigman, D.M., Hain, M.P., Haug, G.H., 2010. The polar ocean and glacial cycles in atmospheric CO_2 concentration. Nature 466, 7302, 47–55. doi: 10.1038/nature09149

Sigman, D.M., Jaccard, S.L., Haug, G.H., 2004. Polar ocean stratification in a cold climate. Nature 428, 59–63. doi: 10.1038/nature02357

Skinner, L.C., Fallon, S., Waelbroeck, C., Michel, E., Barker, S., 2010. Ventilation of the Deep Southern Ocean and Deglacial CO_2 Rise. Science 328, 5982, 1147–1151. doi: 10.1126/science.1183627

Skinner, L.C., Primeau, F., Freeman, E., de la Fuente, M., Goodwin, P.A., Gottschalk, J., Huang, E., McCave, I.N., Noble, T.L., Scrivner, A.E., 2017. Radiocarbon constraints on the glacial ocean circulation and its impact on atmospheric CO_2. Nat. Commun. 8, 16010, doi: 10.1038/ncomms16010

Stephens, B.B., Keeling, R.F., 2000. The influence of antarctic sea ice on glacial-interglacial CO_2 variations. Nature 404, 171–174. doi: 10.1038/35004556

Studer, A.S., Sigman, D.M., Martínez-García, A., Benz, V., Winckler, G., Kuhn, G., Esper, O., Lamy, F., Jaccard, S.L., Wacker, L., Oleynik, S., Gersonde, R., Haug, G.H., 2015. Antarctic Zone nutrient conditions during the last two glacial cycles. Paleoceanography 30, 845–862. doi: 10.1002/2014PA002745

Talley, L.D., 2013. Closure of the global overturning circulation through the Indian, Pacific, and Southern Oceans: Schematics and transports. Oceanography 26, 80–97. doi: 10.5670/oceanog.2013.07

Taylor, S.R., McLennan, S.M., 1995. The geochemical the continental evolution crust. Rev. Mineral. Geochemistry 33, 241–265

Thöle, L.M., Amsler, H.E., Moretti, S., Auderset, A., Gilgannon, J., Lippold, J., Vogel, H., Crosta, X., Mazaud, A., Michel, E., Martínez-García, A., Jaccard, S.L., 2019. Glacial-interglacial dust and export production records from the Southern Indian Ocean. Earth Planet. Sci. Lett. 525. doi: 10.1016/j.epsl.2019.115716

Toggweiler, J.R., Russell, J.L., Carson, S.R., 2006. Midlatitude westerlies, atmospheric CO_2, and climate change during the ice ages. Paleoceanography 21, 1–15. doi: 10.1029/2005PA001154

Volk, T., Hoffert, M.I., 1985. Ocean carbon pumps: Analysis of relative strengths and efficiencies in ocean-driven atmospheric CO_2 changes. The carbon cycle and

atmospheric CO_2: natural variations Archean to present. Geophys. Monograph Ser. 32, 99–110. doi: 10.1029/GM032p0099

Watson, A.J., Naveira Garabato, A.C., 2006. The role of Southern Ocean mixing and upwelling in glacial-interglacial atmospheric CO_2 change. Tellus, Ser. B Chem. Phys. Meteorol. 58, 1, 73–87. doi: 10.1111/j.1600-0889.2005.00167.x

Winckler, G., Anderson, R.F., Fleisher, M.Q., McGee, D., Mahowald, N., 2008. Covariant Glacial-Interglacial Dust Fluxes. Science 320, 93–96. doi: 10.1126/science.1150595

Wolff, E.W., Barbante, C., Becagli, S., Bigler, M., Boutron, C.F., Castellano, E., de Angelis, M., Federer, U., Fischer, H., Fundel, F., Hansson, M., Hutterli, M., Jonsell, U., Karlin, T., Kaufmann, P., Lambert, F., Littot, G.C., Mulvaney, R., Röthlisberger, R., Ruth, U., Severi, M., Siggaard-Andersen, M.L., Sime, L.C., Steffensen, J.P., Stocker, T.F., Traversi, R., Twarloh, B., Udisti, R., Wagenbach, D., Wegner, A., 2010. Changes in environment over the last 800,000 years from chemical analysis of the EPICA Dome C ice core. Quat. Sci. Rev. 29, 285–295. doi: 10.1016/j.quascirev.2009.06.013

Yu, E.F., Francois, R., Bacon, M.P., Honjo, S., Fleer, A.P., Manganini, S.J., Rutgers Van Der Loeff, M.M., Ittekot, V., 2001. Trapping efficiency of bottom-tethered sediment traps estimated from the intercepted fluxes of ^{230}Th and ^{230}Pa. Deep. Res. Part I Oceanogr. Res. Pap. 48, 865–889. doi: 10.1016/S0967-0637(00)00067-4

Zeebe, R.E., 2012. History of Seawater Carbonate Chemistry, Atmospheric CO_2, and Ocean Acidification. Annu. Rev. Earth Planet. Sci. 40, 141–165. doi: 10.1146/annurev-earth-042711-105521

CHAPTER 2

Bottom water oxygenation changes in the Southwestern Indian Ocean as an indicator for enhanced respired carbon storage since the last glacial inception

H. Eri Amsler[a, b], Lena M. Thöle[a,b,c], Ingrid Stimac[d], Walter Geibert[d], Minoru Ikehara[e], Gerhard Kuhn[d], Oliver Esper[d], Samuel L. Jaccard[a,b]

[a]Institute of Geological Sciences, University of Bern, Switzerland
[b]Oeschger Centre for Climate Change Research, University of Bern, Switzerland
[c]Department of Earth Sciences, Utrecht University, the Netherlands
[d]Alfred-Wegener-Institut Helmholtz-Zentrum für Polar- und Meeresforschung, Bremerhaven, Germany
[e]Center for Advanced Marine Core Research, Kochi University, Japan

in preparation for *Climate of the Past*

ABSTRACT

We present downcore records of redox-sensitive authigenic uranium (U) and authigenic manganese (Mn) based on five marine sediment cores spanning a transect encompassing the Subantarctic to the Antarctic zones in the Southwest Indian Ocean during the last glacial cycle. We report lower bottom water oxygenation states during glacial and higher oxygenation states during warm periods, suggesting ventilation changes as the dominant contributor for enhanced carbon storage in the ocean interior. Changes in the export of siliceous phytoplankton to the deep-sea may have entailed a minor influence on the oxygenation states, especially in the Subantarctic Zone during the MIS 5/4 transition. The rapid oxygenation during the deglaciation is in line with increased ventilation and enhanced upwelling after the LGM.

2.1 Introduction

On glacial-interglacial timescales, the global ocean plays an important role in regulating changes in the exogenic carbon cycle (e.g. Sigman and Boyle, 2000). The deep ocean has a sufficiently voluminous and dynamic carbon reservoir to modulate air-sea partitioning of CO_2, and by inference, climate. In particular, the Southern Ocean acts as a major conduit connecting the vast ocean interior and the atmosphere, as deep CO_2-rich water masses outcrop along tilted density surfaces (isopycnals) promoting gas exchange with the atmosphere (Marshall and Speer, 2012; Talley, 2013).

Accordingly, a number of different, often synergistic mechanisms, focusing on changes in Southern Ocean circulation, nutrient biogeochemistry and sea-ice dynamics have been proposed to have contributed to lower atmospheric CO_2 during past ice ages (e.g. Adkins, 2013; Ferrari et al., 2014; Hain et al., 2010; Sigman et al., 2010). However, the mechanisms accounting for the generally reduced glacial atmospheric CO_2 inventory are still debated and not yet fully understood. Radiocarbon (^{14}C) data suggest that the deep (>1000–1500 m) ocean was generally more poorly ventilated during the last ice age (Sarnthein et al., 2013; Skinner et al., 2017) (although a portion of this signal could be related to decreased air-sea gas exchange (Galbraith et al., 2015)). The formation of saltier (less buoyant) bottom waters around Antarctica due to more dynamic

sea-ice cycling would have strengthened the stratification and isolation of deeper waters during the Last Glacial Maximum (LGM) (Adkins, 2013; Adkins et al., 2002; Bouttes et al., 2010; Ferrari et al., 2014; Stein et al., 2020). Furthermore, a northward shift of the upwelling region might have led to the exposure of shallower waters, resulting in reduced outgassing and enhanced carbon sequestration in the ocean interior (Sigman and Boyle, 2000; Toggweiler, 1999; Watson et al., 2015).

In addition to these physical mechanisms influencing ocean circulation, changes in marine biology and nutrient biogeochemistry contributed to sequester carbon away from the atmosphere (Francois et al., 1997; Galbraith and Jaccard, 2015; Sigman and Boyle, 2000; Sigman et al., 2010). A more efficient biological carbon pump during glacial periods, sustained by increased Fe-bearing dust supply and/or generally more complete nutrient utilization, would have contributed to curb CO_2 outgassing from the Southern Ocean (e.g. Galbraith and Skinner, 2020; Jaccard et al., 2013; Kohfeld et al., 2005; Kumar et al., 1995; Martínez-García et al., 2014; Sigman et al., 2010; Studer et al., 2015).

At the onset of the last glacial termination (TERM I), approximately 17.5 ka ago, Southern Ocean ventilation resumed as the Earth emerged from the last ice age, and previously sequestered, radiocarbon-depleted CO_2 was released to the atmosphere (e.g. Basak et al., 2018; Bauska et al., 2016; Burke and Robinson, 2012; Gottschalk et al., 2016; Jaccard et al., 2016; Rae et al., 2018; Skinner et al., 2010). Coupled with enhanced upwelling, nutrient- and CO_2-rich subsurface waters were supplied to the sunlit surface ocean, supporting high levels of biological production south of the Polar Front (e.g. Anderson et al., 2009; Frank et al., 2000; Jaccard et al., 2013; Kohfeld et al., 2005; Thöle et al., 2019). At the same time, Fe-bearing dust supply started to dwindle, causing biogenic export production to decline in the Subantarctic Zone (Jaccard et al., 2016, 2013; Martínez-García et al., 2014), further decreasing marine carbon storage.

Reconstructing past changes in bottom water oxygenation has the potential to further document some of these processes. Indeed, variations in the storage of respiratory carbon are accompanied by large changes in dissolved oxygen concentration associated with organic matter remineralization (e.g. Anderson et al., 2019; Gottschalk et al., 2016; Hoogakker et al., 2015; Jaccard et al., 2016, 2009; Jacobel et al., 2017). The temporal evolution of bottom water

oxygenation can thus be reconstructed qualitatively using the distribution of redox-sensitive metals in the marine sedimentary record (e.g. Calvert and Pedersen, 1996; Francois et al., 1997; Frank et al., 2000; Nameroff et al., 2002). Here we focus on authigenic uranium (U) and manganese (Mn), which are both sensitive to oxygen concentrations typically encountered in open ocean conditions. The analyses were carried out on a set of five marine sediment cores spanning a meridional transect in the yet underrepresented Indian sector of the Southern Ocean. Combining these observations with preserved opal flux reconstructions allows for deciphering the different processes affecting bottom water oxygenation and inferring their relative contributions in sequestering CO_2 in the ocean interior.

2.2 Study site, materials and methods

2.2.1 Core locations and material

This study was carried out on five marine sediment cores, retrieved along a meridional transect including Del Caño Rise and Conrad Rise and reaching as far south as Enderby Abyssal Plain (Figure 2.1). Cores DCR-1PC (46°01.34'S, 44°15.24'E, 2632 mbsl) and COR-1bPC (54°16.04'S, 39°45.98'E, 2828 mbsl) were collected during expedition KH-10-7 on R/V Hakuho-maru in 2010–2011. The sediment cores were retrieved from the southern flank of Del Caño Rise (DCR-1PC) and Conrad Rise (COR-1bPC), respectively. Cores PS2609-1 (51°29.9'S, 41°35.8'E, 3113 mbsl), PS2606-6 (53°13.9'S, 40°48.1'E, 2545 mbsl) and PS2603-3 (58°59.2'S, 37°37.7'E, 5289 mbsl) were retrieved during ANT-XI/4 expedition on R/V Polarstern in 1994. Cores PS2609-1 and PS2606-6 were retrieved from Conrad Rise as well, the former one on its northern flank and the latter on the rise itself. Core PS2603-3 is located furthest to the south in the Enderby Abyssal Plain and in the greatest water depth of the five cores.

DCR-1PC is the northernmost core and lies in the Subantarctic Zone (SAZ) of the Southern Ocean and is composed of nannofossil and diatom ooze with variable amounts of clay. All other cores predominantly consist of diatom ooze (Kuhn, 2003a, 2003b, 2003c; Oiwane et al., 2014) and lie south of today's position of the Polar Front (PF) in the Antarctic Zone (AZ).

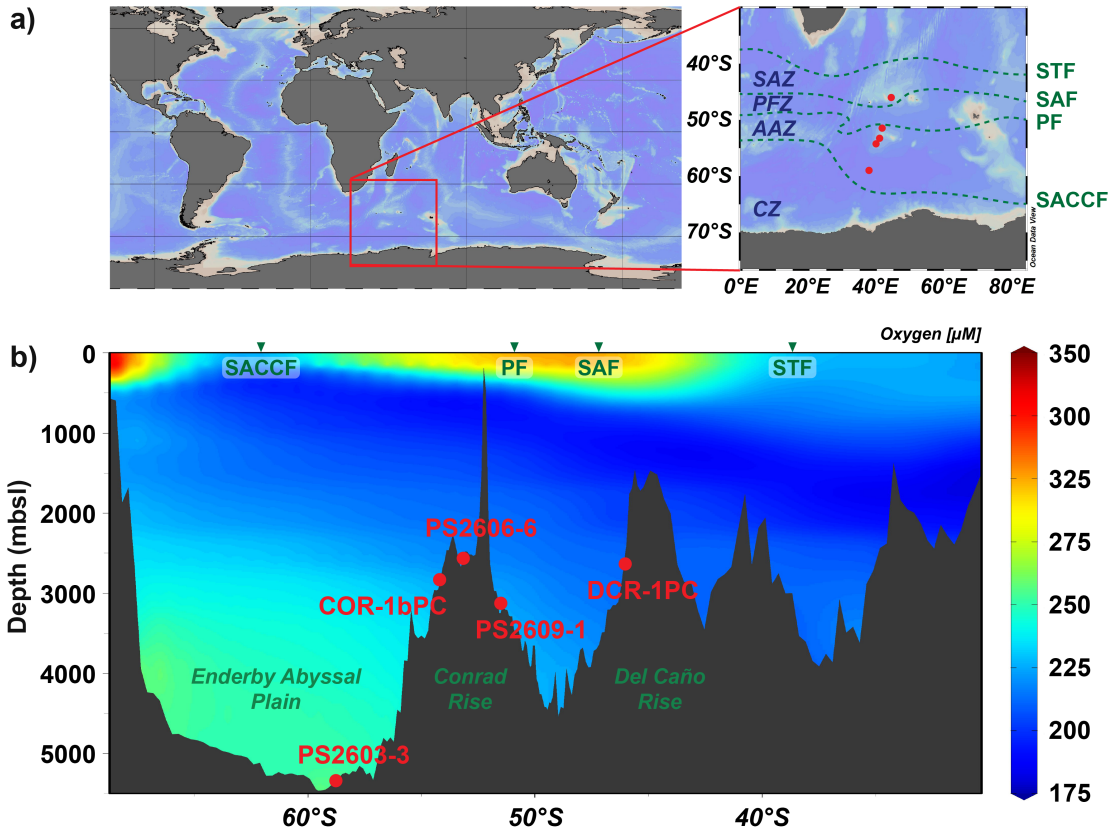

Figure 2.1: a) Core locations in the SW Indian Ocean across the Southern Ocean frontal system. The fronts from north to south are the Subtropical Front (STF), Subantarctic Front (SAF), Polar Front (PF), and the Southern ACC Front (SACCF); the zones between them are defined as the Subantarctic Zone (SAZ), Polar Frontal Zone (PFZ), Antarctic Zone (AZ), and Continental Zone (CZ) (Orsi et al., 1995). b) Cross section of core locations with modern oxygen concentrations (plotted with the ODV-software, Schlitzer, 2018).

2.2.2 Age models

For DCR-1PC, seven ^{14}C-dates were determined and the diatom-based sea surface temperature (SST) record was tuned to the deuterium record of EPICA Dome C, assuming both records are synchronous (Crosta et al., 2020). The stratigraphy for core COR-1bPC is based on 23 calibrated ^{14}C-measurements on planktic foraminifera *neogloboquadrina pachyderma (sinistral)* (Ikehara et al., *in prep.*; Oiwane et al., 2014).

For PS2609-1 and PS2606-6 tie points have been established based on graphical alignment of the magnetic susceptibility (MagSus) record to the global δ^{18}O LR04-stack (Lisiecki and Raymo, 2005). The alignments were fine-tuned with XRF-scanning data of iron (Fe), silicon (Si), titanium (Ti), and calcium (Ca). For PS2606-6 seven ^{14}C-dates were available (Xiao et al., 2016). Additional tie points were added for core PS2609-1 based on graphical alignment of XRF-

scanning titanium (Ti) measurements with the EPICA Dome C dust record (Lambert et al., 2012), assuming synchronous temporal variability. The Ti- and Ca/Ti-records from PS2606-6 were compared to those of PS2609-1 to define a common stratigraphic framework (Table 2.1). Our age model was compared to the recently published ^{14}C-based age model of PS2606-6 (Ronge et al., 2020) and both independently determined age models are consistent with one another.

The age model for core PS2603-3 was determined based on graphical alignment of magnetic susceptibility, XRF-data, and biogenic silica with the LR04-stack (Lisiecki and Raymo, 2005). The extinctions of three diatom species served as biostratigraphic markers: *rouxia leventerae* at 130 ka, *hemidiscus karstenii* at 191 ka and *rouxia constricta* at 300 ka (Zielinski and Gersonde, 2002). There is evidence for a 30-ka long hiatus associated with a sediment disturbance close to the MIS 5/4 boundary. Independent absolute age constraints with the CRS-method (Geibert et al., 2019) yielded similar ages for PS2603-3, except for the interval around the hiatus, where a deviation of around 30 ka is observed.

Table 2.1: Tie points of cores PS2609-1, PS2606-6, and PS2603-3.

Tie points PS2609-1

Depth (cm)	Age pointers (ka)	based on
0	0	
215	10	Ca peak
400	14	MagSus vs LR04; $BSiO_2$ vs LR04; Si/Ti vs LR04
785	28.68	Ti (XRF) vs EDC dust
808	29.88	Ti (XRF) vs EDC dust
1050	58.2	Ti (XRF) vs EDC dust
1145	71	MagSus vs LR04; Fe vs LR04
1157	72.25	Ti (XRF) vs EDC dust
1202	75.87	Ti (XRF) vs EDC dust
1293	83.6	Ti (XRF) vs EDC dust
1340	87	MagSus vs LR04; Fe vs LR04
1595	109	MagSus vs LR04; Fe vs LR04

Tie points PS2603-3

Depth (cm)	Age pointers (ka)	based on
0	0	
90	14	$BSiO_2$ vs LR04; rouxia lenenterae
405	109	$BSiO_2$ vs LR04; hemidiscus karstenii
545	130	$BSiO_2$ vs LR04
640	191	$BSiO_2$ vs LR04; rouxia constricta
690	243	$BSiO_2$ vs LR04
910	300	$BSiO_2$ vs LR04

Tie points PS2606-6

Depth (cm)	Age pointers (ka)	based on
0	0	
14	1.92	^{14}C - Xiao et al. (2016)
128	8.08	^{14}C - Xiao et al. (2016)
198	10.06	^{14}C - Xiao et al. (2016)
228	10.39	^{14}C - Xiao et al. (2016)
266	11.51	Ca/Ti (XRF) vs EDC dust
275	12.12	14C - Xiao et al. (2016)
328	12.79	Ca/Ti (XRF) vs EDC dust
357	14.52	^{14}C - Xiao et al. (2016)
380	15.07	Ca/Ti (XRF) vs EDC dust
427	19.68	^{14}C - Xiao et al. (2016)
478	20.56	Ti (XRF) vs EDC dust
559	24.67	Ti (XRF) vs EDC dust
591	26.20	Ti (XRF) vs EDC dust
639	29.20	Ti (XRF) vs EDC dust
719	44.39	Ti (XRF) vs EDC dust
725	45.44	Ti (XRF) vs EDC dust
786	55.27	Ti (XRF) vs EDC dust
844	67.90	MagSus vs LR04; Ti, Ca (XRF) vs EDC dust
889	71	MagSus vs LR04
905	73.30	Ca/Ti (XRF) vs EDC dust
936	75.87	Ti (XRF) vs EDC dust
968	78.93	Ca/Ti (XRF) vs EDC dust
1013	83.6	Ca/Ti (XRF) vs EDC dust
1036	87	MagSus vs LR04; Ti, Ca (XRF) vs EDC dust
1174	104.69	Ca/Ti (XRF) vs EDC dust
1210	109	MagSus vs LR04

2.2.3 Bottom water oxygenation states

In oxygenated seawater, uranium (U) is present as soluble U(VI). In oxygen-depleted environments however, U is reduced and precipitated as insoluble

U(IV) in the form of uraninite (Langmuir, 1978; Morford and Emerson, 1999). U concentrations in sediment porewaters decreases under reducing conditions, creating a concentration gradient between bottom waters and the uppermost sediment layers. This gradient leads to the diffusion of dissolved U into the sediment and to the precipitation of authigenic uranium (aU) phases (Klinkhammer and Palmer, 1991; Langmuir, 1978).

The authigenic fraction of ^{238}U can be determined by calculating the excess ^{238}U relative to detrital thorium (^{232}Th), an isotope of primarily detrital origin and by assuming a constant, regionally-informed detrital ^{238}U/^{232}Th ratio. This ratio can vary locally, with lower values generally associated with crustal lithogenic sources. We considered a ratio of 0.5 for cores DCR-1PC, COR-1bPC, PS2909-1, and PS2909-6 (Francois et al., 2004; Henderson and Anderson, 2003). For PS2603-3, the core farthest to the south and potentially influenced by lithogenic material originating from the Antarctic continental crust, the minimum ^{238}U/^{232}Th activity ratio observed is 0.27 $\pm$ 0.01. We therefore set the lithogenic end-member conservatively to 0.27.

$$aU = A_{U238}^{total} - A_{Th232}^{total} \times \left(\frac{A_{U238}}{A_{Th232}}\right)^{det} \qquad \text{Eq. (2.1)}$$

The isotopic composition of U and Th were quantified by isotope dilution following Anderson and Fleer (1982), later modified by Choi et al. (2001), Pichat et al. (2004), and Lippold et al. (2009). Freeze-dried marine sediments (150–200 mg) were spiked (^{229}Th, ^{236}U) and completely digested in a pressure-assisted microwave (T_{max} = 180°C), using concentrated HNO_3, HCl and HF. Both elements were separated and purified by anion exchange column chromatography using AG1-X8 resin. Measurements were conducted using a Thermo Fisher Scientific Neptune Plus multi-collector inductively coupled plasma mass spectrometer (MC-ICP-MS) at the University of Bern, and for the PS cores on a single-collector ICP-MS (Thermo Fisher Scientific Element 2) at the Alfred Wegener Institute (AWI) in Bremerhaven. Approximately half of the samples of cores PS2609-1, PS2606-6, and PS2603-3 had been prepared earlier following a similar procedure, albeit with slightly less sediment material (50 mg) and higher temperatures during digestion (T_{max} = 210°C). The

chromatographic separation and subsequent purification of the U and Th fractions was performed using UTEVA resin from Eichrom. The isotope measurements were corrected with a calibrated standard (UREM-11 Sarm 31) and yielded a relative standard deviation of less than 3.8% and 3.5% for ^{238}U and ^{234}U, and less than 5.7% and 4.9% for ^{230}Th and ^{232}Th, respectively. The measurement differences between the two mass spectrometers were within these errors.

In marine sediments, manganese (Mn) precipitates under well-oxygenated conditions as oxyhydroxides (Mn(III) and(IV)) (Calvert and Pedersen, 1996). Mn enrichments in sediments can be observed where the accumulation of organic matter is low and oxic conditions generally prevail (e.g. Calvert and Pedersen, 1993; Jaccard et al., 2009). Under more reducing conditions, the sedimentary distribution of Mn is controlled by the input of insoluble detrital fraction. Any Mn present in the sediment that is in excess relative to the concentration expected from the detrital fraction is assumed to have accumulated authigenically under oxic conditions. Here we use the ratio between Mn and titanium (Ti) to constrain excess Mn, assuming a constant detrital ratio between both elements. Ti is assumed to be associated exclusively with lithogenic sources.

For Mn and Ti analyses in cores PS2609-1 and PS2606-6, the samples were fully digested, evaporated and redissolved in 20 ml 1M HNO_3. An aliquot was then diluted 1:100 and rhodium as internal standard was added. The Mn and Ti concentrations were measured on the single-collector ICP-MS (Thermo Fisher Scientific Element 2) at AWI in Bremerhaven. The reference material NIST 2702 was digested with each batch and measured with the samples.

For cores COR-1bPC and DCR-1PC, the Mn and Ti measurements were acquired by XRF-core logging with a Tatscan-F2 at the Kochi Core Center, Japan (Sakamoto et al., 2006).

2.2.4 Preserved opal export

The sedimentary biogenic opal fraction is predominantly composed of diatom frustules and minor amounts of radiolarians and sponge spicules. Diatoms dominate carbon export in the Southern Ocean, around and mostly south of the PF (Cortese et al., 2004; Ragueneau, 2000). Sedimentary biogenic silica (bSi),

together with other proxies, has been widely used to reconstruct past changes in marine export production (e.g. Anderson et al., 2009; Bradtmiller et al., 2007; Chase et al., 2003). The accumulation of biogenic opal is influenced not only by opal production in the sunlit surface ocean, but also by dissolution in the water column and at the seabed (Dezileau et al., 2003; Pondaven et al., 2000; Ragueneau et al., 2000). Empirical studies of modern opal export patterns suggest that the spatial distribution of opal burial predominantly reflects diatom productivity and opal export (e.g. Chase et al., 2003; Nelson et al., 2002; Pondaven et al., 2000; Sayles et al., 2001). However, the link between opal and carbon export is not straightforward, as other factors such as Fe-availability can affect C and N uptake in diatoms relative to Si (Boutorh et al., 2016; Meyerink et al., 2017; Pichevin et al., 2014). A multi-proxy approach would provide a more unambiguous reconstruction of paleoproductivity in the region. Based on the similar glacial-interglacial patterns of different paleoproductivity proxies in the region (Thöle et al., 2019), we assume that changes in biogenic opal fluxes provide a robust, first-order approximation of past changes in organic carbon delivery to the sediment.

Sedimentary biogenic opal concentrations were determined using Fourier transform infrared spectroscopy (FTIRS) at the University of Bern for cores DCR-1PC and COR-1bPC (Vogel et al., 2016). For the PS cores, the sedimentary opal content was determined by alkaline extraction of silica according to Müller and Schneider (1993) at AWI, Bremerhaven. Both methods provide comparable results.

To reconstruct vertical fluxes of biogenic opal, the ^{230}Th-normalization was used. The vertical particle flux (F) to the sediment was corrected for lateral redistribution following the ^{230}Th-normalization approach (Bourne et al., 2012; Costa et al., 2020; Francois et al., 2004; Henderson and Anderson, 2003). The flux of scavenged ^{230}Th ($F^{230}Th$) settling to the seafloor at a specific water depth z is assumed to be equal to its known production rate (β_{230}) from ^{234}U decay within the water column. The resultant inverse relationship between the scavenged ^{230}Th and the total vertical flux of particulate matter can be used to calculate preserved vertical fluxes ($^{pr}F_v$) from the activity of initial scavenged ^{230}Th in the sediment ($A^{scav}_{Th230,(0)}$).

$$prF_v = \frac{\beta_{230} \times z}{A^{scav}_{Th230,(0)}} \qquad \text{Eq. (2.2)}$$

The calculations to derive the initial scavenged sedimentary ^{230}Th ($A^{scav}_{Th230,(0)}$) take into account i) in situ produced ^{230}Th from the decay of authigenic uranium (^{238}U); ii) in situ produced ^{230}Th from the decay of lithogenic uranium (^{238}U); and iii) radiogenic decay of ^{230}Th after deposition. Normalizing the concentration of a specific sedimentary component (j) with the ^{230}Th-approach (e.g. biogenic opal) provides a quantitative estimate of its preserved vertical flux ($^{pr}F_j$) through time:

$$prF_j = prF_v \times f_j \qquad \text{Eq. (2.3)}$$

where f_j is the weight fraction of constituent j in the sediment.

2.3 Results

2.3.1 Subantarctic Zone of the SW Indian Ocean

Redox-sensitive metal records:

Authigenic uranium concentrations in core DCR-1PC show the highest values of all cores (Figure 2.2). The general pattern is consistent with a climate-related signal, with typically higher concentrations during cold periods and relatively lower concentrations during warmer intervals. More specifically, the highest values occur during MIS 6 and MIS 3–2. During MIS 6 the values decrease gradually, then show a peak around 130 ka, before decreasing steeply to levels well below 1 ppm at the start of MIS 5. The sedimentary aU concentrations are characterized by transient, millennial-scale oscillations during MIS 5 (106–100 ka, 88–85 ka) and then concentrations increase at the end of MIS 5 and stabilize during MIS 4. At the onset of MIS 3, aU levels increase steeply, with values remaining high throughout MIS 3, typically ranging between 5 to almost 8 ppm. Authigenic uranium concentrations start declining after 27 ka and reach the lowest levels of the entire glacial cycle at around 17.5 ka, remaining low throughout the Holocene.

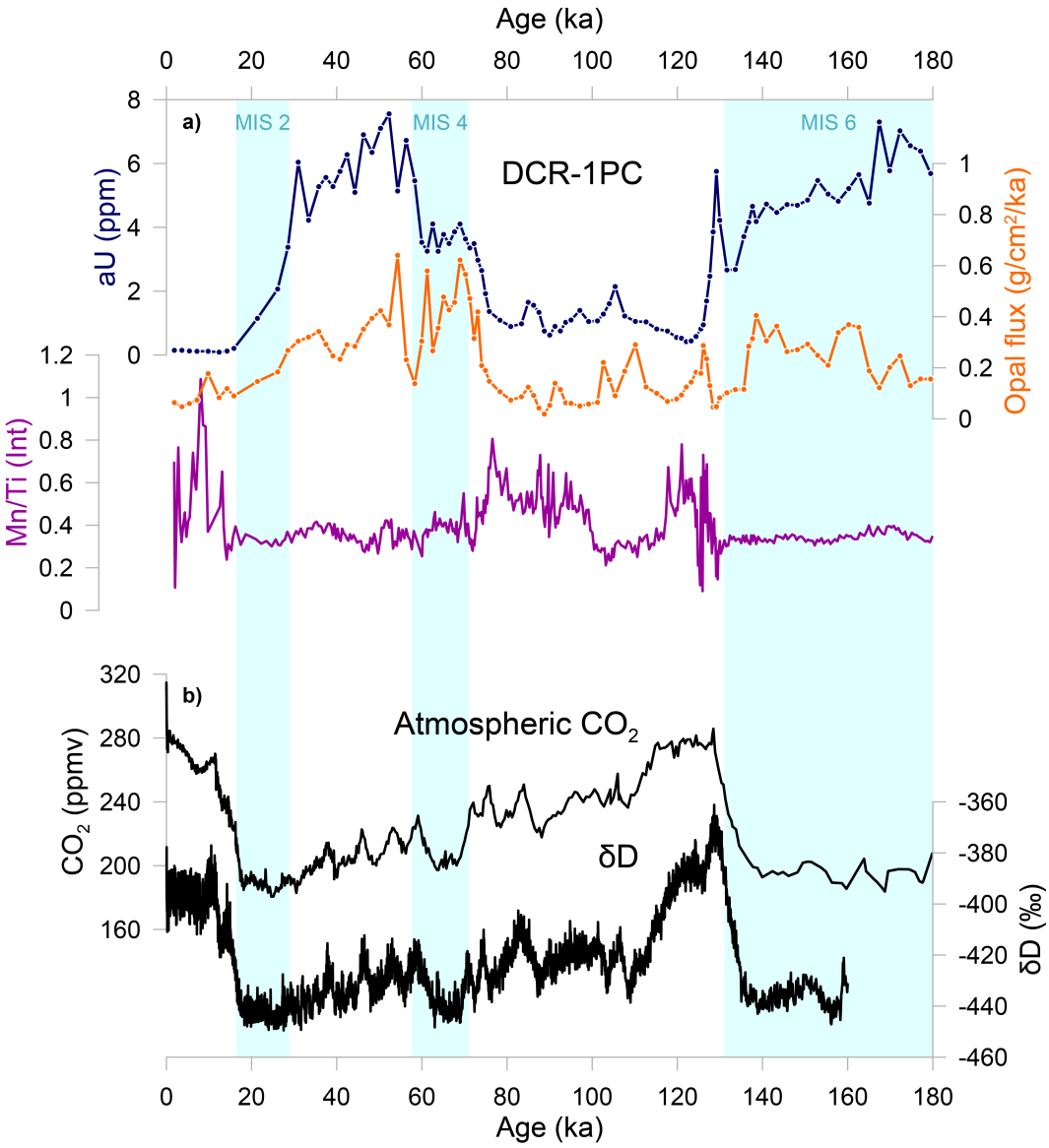

Figure 2.2: a) Authigenic uranium concentrations (in blue), opal fluxes (in orange) and Mn/Ti ratios (in purple) from XRF-scanning in the Subantarctic Zone. b) Atmospheric CO_2 concentrations from EPICA Dome C ice core, composite record (Bereiter et al., 2015 *and references therein*) and δD record from EPICA Dome C ice core reflecting Antarctic air temperatures (Jouzel et al., 2007). Light blue bars show cold periods MIS 2, 4, and 6 (Lisiecki and Raymo, 2005).

Mn is typically enriched above detritic background values during the two major warm climate intervals of MIS 5 and the Holocene, where values are higher and show increased variability, while Mn/Ti ratios hover around detritic values during cold climate intervals, including a period between 115–100 ka where the values are close to background.

Preserved opal export:

Preserved biogenic opal fluxes vary between 0 and 0.7 g/cm^2/ka (Figure 2.2). Opal flux reconstructions show a consistent glacial-interglacial pattern, with typically higher opal fluxes during cold periods and lower fluxes during warm periods. Biogenic opal fluxes decrease about 5 ka before the onset of the glacial terminations, both during MIS 6 and MIS 2.

There are distinct differences between the downcore aU and biogenic opal flux records. During warm intervals and the transition into MIS 4, both aU and biogenic opal flux records appear to be coupled, but at the start of MIS 3 both parameters start decoupling, suggesting a more complex relation between the two proxies. The Mn/Ti ratio shows an opposing behaviour compared to aU, with low and stable values during all the periods where aU is elevated, and with higher and more variable values during warmer climate intervals.

2.3.2 Antarctic Zone of the SW Indian Ocean

Redox-sensitive metal records:

In the following sections the four cores in the Antarctic Zone will be described from north to south wherever possible. The downcore sedimentary aU records vary similarly in all cores south of the PF (Figure 2.3). Concentrations vary between 0 and 3.5 ppm with the southernmost core, PS2603-3, showing overall the lowest values and more subdued variability. The lowest values in all cores are consistently found during MIS 5 and the Holocene. In both PS2609-1 and PS2606-6, there is a pronounced increase of aU during MIS 4. Another increase only clearly visible in PS2609-1 can be found at 85–80 ka. The low values during MIS 3 hover around 1 ppm in PS2609-1 and around 0.5 ppm in PS2606-6, respectively. In COR-1bPC, the core with the shortest sediment record, aU levels start increasing gently from mid MIS 3, before reaching the highest values at peak glacial conditions, as in all four cores.

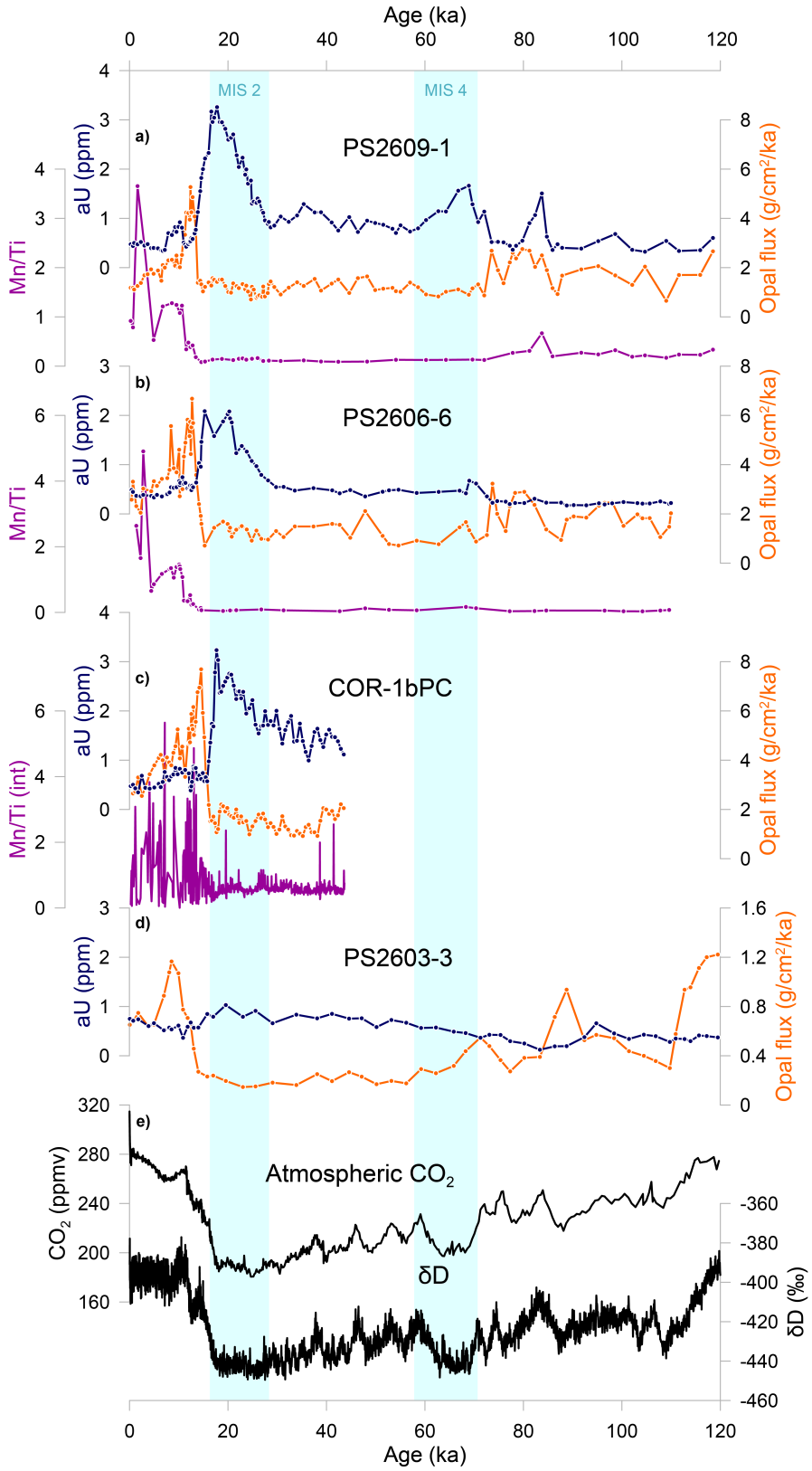

Figure 2.3: a)–d) Authigenic uranium concentrations (in blue), opal fluxes (in orange), and Mn/Ti ratios (in purple) in the Antarctic Zone south of the Polar Front. e) Atmospheric CO_2 from EPICA Dome C ice core, composite record (Bereiter et al., 2015 *and references therein*) and δD record from EPICA Dome C ice core reflecting Antarctic air temperatures (Jouzel et al., 2007). Light blue bars show cold periods MIS 2 and 4 (Lisiecki and Raymo, 2005).

The highest values of aU in all cores occur during MIS 2 with a gradual increase from about 30 ka, peaking during the LGM. Thereafter, aU levels decline sharply to values well below 1 ppm within 2–4 ka, concomitant with the onset of the last glacial termination. After TERM I, a small increase around 11–8 ka is apparent. Throughout the Holocene, aU levels stay below 1 ppm.

Observations within the uranium measurements, which will not further be discussed in the scope of this study, are the remarkably high $^{234}U/^{238}U$ ratios during the Holocene (>1.14) (*data-CD of thesis*). Ratios in the lithogenic end-member are around 1 and can be as low as 0.98 (Henderson, 2002). Seawater uranium has a ratio of 1.14 due to preferential weathering of ^{234}U (François et al., 2004; Henderson, 2002). Ratios between the two end-members can be explained by a mixing of the two. However, during the Holocene the values are consistently above 1.14.

Authigenic Mn levels remain low throughout the entire ice age and increase at the onset of the last glacial termination. The XRF-ratios also show similar trends with low values in MIS 5 and MIS 4 and elevated or more variable values from about 15 ka.

Preserved opal export:

The cores south of the PF show a consistent pattern with relatively low preserved opal fluxes throughout most of MIS 2, 3, and 4, with slight increases and higher variability during MIS 5 and a prominent peak after the LGM. The values reached during this peak are much higher than in the SAZ core, with values up to 4 g/cm^2/ka. PS2603-3 shows the overall lowest values, reaching 1.2 g/cm^2/ka after both TERM I and II.

The variations in the bSi records show a very different pattern from the aU, especially during the LGM and TERM I: simultaneously to the aU decrease, there is a rapid increase in opal fluxes at the onset of the deglaciation. After that, biogenic opal slowly decreases over the course of the Holocene, but not quite to the lowest levels of the LGM. In MIS 5 there is a small increase in opal fluxes around 85–75 ka, which seems to coincide with the slightly higher CO_2 levels during MIS 5. The Mn/Ti ratio stays low throughout the cores and rises

after the LGM, as does the opal flux. The initial increase seems to lag slightly behind the rapid increase in opal fluxes.

2.4 Interpretation and discussion

2.4.1 Dynamics of bottom water oxygenation in the SAZ

The downcore patterns of aU and Mn/Ti are generally coherent (Figure 2.2), and together the records provide a consistent picture, reflecting past changes in oxygenation at the sediment-water interface. Overall the data indicate generally more reducing conditions during cold periods, whereas sediments were more oxidizing during warmer climate intervals. The two redox-sensitive elements however, are not perfectly anti-correlated, consistent with different sensitivities to redox conditions (Tribovillard et al., 2006).

When comparing both redox-sensitive metal records to opal fluxes, the proxies broadly agree, in particular at glacial inceptions. But towards peak glacial conditions the records show some degree of divergence.

The first drop in atmospheric pCO_2 at around 115 ka coincides with a reduction in Mn/Ti values, which could be attributed to a transition towards more reducing conditions associated with a regional increase in carbon export and sequestration (Figure 2.2). At the transition from MIS 5 to MIS 4, both redox proxies show a clear shift towards more reducing conditions, concomitant with a rise in biogenic opal export, coinciding with a substantial increase in dust, lithogenic and iron deposition rates recorded in Antarctic ice cores (e.g. Lambert et al., 2012) and subantarctic marine sediment records (e.g. Anderson et al., 2014; Lamy et al., 2014; Manoj and Thamban, 2015; Martínez-García et al., 2014; Thöle et al., 2019). Kohfeld and Chase (2017) suggest a major change in ocean circulation, contemporaneous with this second drop in CO_2 centered at 72–65 ka. In particular, sedimentary neodymium isotope records and ^{13}C data suggest a major reorganization of deep ocean circulation at that time (e.g. Oliver et al., 2010; Wilson et al., 2015). Indeed, the shoaling of the Atlantic overturning cell may have left the abyssal ocean dominated by dense southern sourced water (e.g. Lynch-Stieglitz, 2016; Matsumoto et al., 2002), which may have increased the density gradient and contributed to isolate the deep ocean,

making it more prone to sequester remineralized carbon (Hain et al., 2010; Skinner, 2009; Yu et al., 2016).

We therefore suggest that both increased export production, and by inference organic matter respiration, as well as a decrease in deep-ocean ventilation (Jaccard et al., 2016) preconditioned the sediments, maintaining sufficiently reducing conditions to allow recording the more subtle ventilation changes of the last ice age (Gottschalk et al., 2020).

The decrease in aU levels and associated re-oxygenation of bottom waters started within MIS 2 and not, as expected, towards the end of the last ice age, when ocean circulation and upwelling began to intensify as the southern hemisphere warmed (Basak et al., 2018; Gottschalk et al., 2016; Jaccard et al., 2016; Rae et al., 2018; Ronge et al., 2020; Skinner et al., 2010). Rather than a regionally disparate initiation of upwelling, the decrease in aU accumulation in core DCR-1PC might be related to diagenetic burn-down. Diagenetic redeposition of sedimentary aU is observed when oxygenated conditions in the uppermost layers of the sediment recur (e.g. Thomson et al., 1990), for example as a result of reinvigorating deep-water ventilation. As oxygen diffuses into pore waters, previously precipitated U will dissolve and will be either lost to the overlying water or diffuse deeper into the sediment, where conditions are still reducing and where it will be reprecipitated (Colley et al., 1989; Jacobel et al., 2017; Mangini et al., 2001). This can likewise affect buried organic carbon (Korff et al., 2016). A high sediment accumulation rate would limit the depth interval over which burn-down would affect the downcore aU record. Core DCR-1PC has the lowest sedimentation rates of the five cores investigated and thus is potentially more prone to be affected by oxidative burn-down. With the lowest sedimentation rate within the core being reported between 17 ka and 25 ka (<1 cm/ka, Figure 2.4), re-dissolution seems the most plausible explanation accounting for the early aU decrease.

During the penultimate glacial termination (TERM II) at around 125 ka, aU appears to have only been marginally affected by remobilization. The sedimentation rate during this interval is higher than during the end of the last ice age (Figure 2.4). The distinct peaks preceding the rapid decrease in aU are a possible indicator for some degree of burn-down at both terminations (Colley et al., 1989).

The early decrease in opal export towards the end of both glacial periods could be related to increasingly complete $Si(OH)_4$ consumption south of the Polar Front (Dumont et al., 2020). Upwelling and thus nutrient supply to the surface water south of the PF were substantially reduced during glacial times (Anderson et al., 2009; Francois et al., 1997). Biological productivity was reduced, but at the same time nitrate consumption was more complete (Studer et al., 2015), stemming CO_2 outgassing from the ocean interior. Part of these surface waters are transported towards the north and when they reach the location of DCR-1PC, they are largely depleted in $Si(OH)_4$. Transitioning towards peak glacial conditions there would have been gradually less $Si(OH)_4$ available for opal production in the SAZ, as reflected by the downcore opal flux records. Relaxed Fe-limitation as a result of enhanced bioavailable Fe-input with dust would have lowered the Si:N uptake ratio in diatoms from >4:1 to 1:1 (Brzezinski et al., 2002). Nitrogen isotope studies show that nitrate utilization was more complete in glacial periods when compared to interglacials (Horn et al., 2011; Martínez-García et al., 2014; Studer et al., 2015), whereas silicon isotopes show an opposite pattern (Brzezinski et al., 2002; Dumont et al., 2020). Despite preferred nitrate uptake and therefore potentially more silicate leakage towards the north, the overall amount of $Si(OH)_4$ upwelled from depth might have been declining, thus limiting diatom growth (Brzezinski et al., 2002; Dumont et al., 2020).

Moreover, a movement of the frontal systems cannot be ruled out as an explanation for the early reduction in opal fluxes. DCR-1PC today is located not only north of the Polar Front, but also north of the Subantarctic Front (Orsi et al., 1995; Pollard et al., 2007). A possible explanation for the opal flux decrease within MIS 2 relates to the northward displacement of the fronts so that the core location lies in the Polar Frontal Zone, where during MIS 2 nutrient availability was likely reduced.

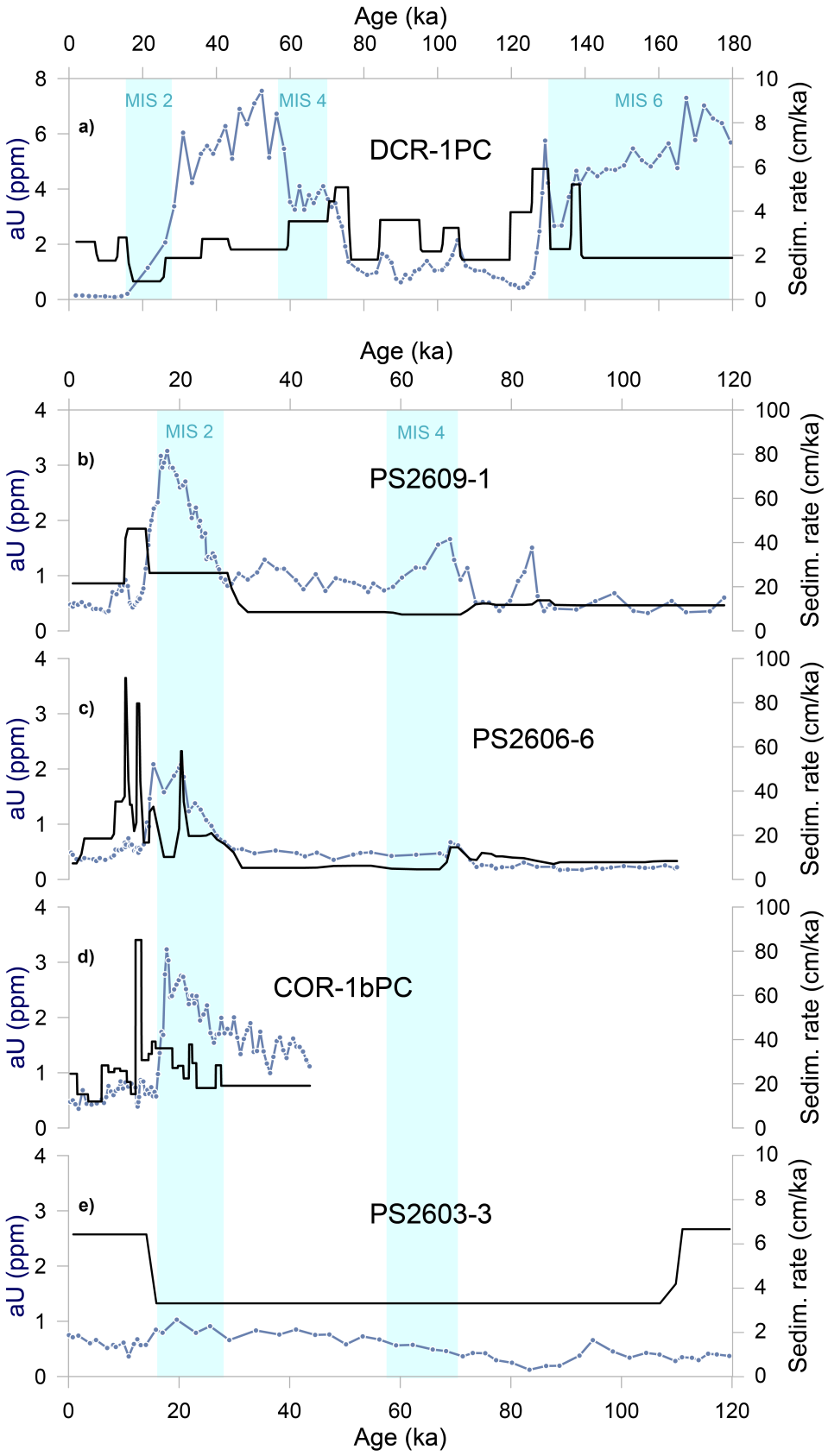

Figure 2.4: a)–e) Sedimentation rates (in black) and authigenic uranium concentrations (in light blue) in all cores from north to south. Light blue bars show cold periods MIS 2, 4, and 6 (Lisiecki and Raymo, 2005).

2.4.2 Dynamics of bottom water oxygenation in the AZ

South of the PF, all of the cores, with the exception of the slowly accumulating core retrieved from Enderby Basin, record similar oceanographic dynamics. The aU and Mn/Ti levels show a consistent downcore pattern with generally more reducing conditions during peak glacial times and rapid oxygenation during glacial terminations, similar to the SAZ record. The noisy Mn/Ti signal from 15 ka onwards, especially in COR-1bPC, suggests a high variability in bottom water oxygenation at levels of Mn-sensitivity. Recorded opal fluxes are persistently low during cold periods, while aU and Mn/Ti values are consistent with increasingly reducing conditions. The rapid increase of preserved opal fluxes coinciding with more oxygenated conditions during TERM I imply that export production and thus the respiratory demand for organic matter remineralization plays a secondary role, whereas ventilation imposes a primary control on sedimentary oxygenation levels.

The rapid increase of biogenic opal fluxes at the onset of both glacial terminations is likely a result of enhanced upwelling of subsurface waters, rich in both (micro)nutrients and CO_2 (Anderson et al., 2009; Jaccard et al., 2016; Skinner et al., 2010). The values of the peak at TERM I suggest that COR-1bPC was closest to the most vigorous upwelling location at the onset of deglaciation.

With the available data of redox-sensitive elements U and Mn and the preserved opal fluxes in these cores, an alternative interpretation needs to be considered. As Fe-scarcity reduces the C and N uptake ratio relative to Si (Boutorh et al., 2016; Meyerink et al., 2017; Pichevin et al., 2014), the opal peak during the deglaciation can at least partly be attributed to Fe-limitation, possibly induced by a reduction of Fe-bearing dust-input. To further constrain this possibility, downcore changes in Si/Fe ratios in diatom shells could be analyzed. However, considering multi-proxy studies of export production in the AZ (e.g. Chase et al., 2003; Thöle et al., 2019) and enhanced upwelling intensities during the deglacial (e.g. Basak et al., 2018; Ronge et al., 2020; Skinner et al., 2010), we suggest the observed opal peak to be the result of increased production due to enhanced nutrient availability from upwelled deep waters, in line with a meridional shift of the Southern Ocean frontal system.

Reinvigorating ventilation in the Southern Ocean associated with the glacial termination would leave a spatially coherent oxygenation pattern in all cores, as it was related to an overall reorganization in ocean circulation. The associated opal signal might slightly differ in time given that the upwelling region shifts along with the frontal system (Anderson et al., 2009). However, the sampling resolution is insufficient to reliably assess the potential time lag between the onset of the aU decrease and the sharp rise of opal production and deposition.

The slight increase in aU concentrations midway through the deglaciation could reflect a transient slowdown in ventilation associated with the Antarctic Cold Reversal (ACR) (Jaccard et al., 2016), notwithstanding age model uncertainties. The concomitant increase in Mn/Ti, which indicates a more oxidizing environment, can be explained by different sensitivities of the two elements to redox changes.

In the southernmost core PS2603-3, aU and preserved opal fluxes suggest similar oceanographic dynamics in the Enderby Abyssal Plain. The opal peak concomitant with the onset of TERM I suggests that the core is similarily recording enhanced upwelling, yet the maximum values of 1.2 g/cm^2/ka are consistent with the core being located further away from the most vigorous upwelling region. The slight increase in the aU record during the glacial maxima suggests that bottom water oxygenation was generally reduced during ice ages. However, the low values compared to the other AZ cores might point to the influence of Antarctic Bottom Water.

2.4.3 Ventilation and circulation changes on glacial-interglacial timescales and their impact on atmospheric pCO_2

Across the sampled transect, the core locations are situated in different water masses. With the exception of the southernmost core, which is currently bathed by Antarctic Bottom Water (AABW), the other four sediment cores are located in Circumpolar Deep Water (CDW), which is formed partly from North Atlantic Deep Water (NADW), mixed with AABW and other deep waters that originate from the Indian and Pacific oceans (Talley, 2013). CDW is upwelled in the Southern Ocean along tilted isopycnals. The lower CDW, which stems mainly from dense, high salinity NADW, then moves towards the south as a precursor for AABW. The less dense upper CDW, which has a more oxygen-

depleted signature from older Indian and Pacific deep waters, is transported to the north by Ekman flow (Talley, 2013). The lower and upper CDW thus have different oxygen concentrations, but the range in oxygen concentration changes is smaller than the ranges reported for the last glacial cycle due to overall increased carbon sequestration as has previously been suggested (Anderson et al., 2019; Galbraith and Skinner, 2020). Therefore, any variations in aU and Mn/Ti values are unlikely to be primarily driven by local variations in oxygenation, but rather represent a coherent regional picture.

As discussed above, export production is unlikely to have played the primary role in modulating past changes in bottom water oxygenation and especially south of the PF, it is of secondary importance. The main factor controlling changes in oxygenation at the sediment-water interface is more likely related to bottom water ventilation changes. This can be argued by the decoupling of aU and opal fluxes in DCR-1PC during the later phase of the glacial periods and by the more pronounced antiphasing in the records south of the PF. This antiphasing at TERM I with invigorated circulation and thus rejuvenation of the deep ocean is linked to enhanced supply of nutrient-rich waters to the surface, which fueled biological production. However, this nutrient-fueled phytoplankton growth was not efficient enough to quantitatively fix dissolved carbon, thus allowing CO_2 to escape to the atmosphere (Sigman et al., 2010; Studer et al., 2015). The increase in opal fluxes in connection with more ventilated bottom waters at the end of the glacial periods fits well with higher atmospheric CO_2 inventories associated with the release of previously sequestered carbon from subsurface waters (Burke and Robinson, 2012; Jaccard et al., 2016; Ronge et al., 2020; Skinner et al., 2010).

The major slowdown in deep ocean circulation occurred mostly after the MIS 5/4 transition. Before, at the onset of the glacial period, other factors contributed to the drawdown of atmospheric carbon. During the first CO_2 drop within MIS 5, cooling sea surface temperatures at high latitudes of both hemispheres led to CO_2 reduction through barrier mechanisms. Sea-ice formation and seasonally induced melt water would lead to stronger surface water stratification and affect air-sea gas exchange and impede lower waters to rise to the productive surface (Watson and Naveira Garabato, 2006; Wolff et al., 2010). This barrier mechanism is consistent with the observed first increase

in nitrate consumption associated with enhanced stratification of the surface ocean (Studer et al., 2015). Only at the second CO_2 drop at the MIS 5/4 transition would deep ocean circulation slow, as is indicated by increased aU and decreased Mn/Ti and in good agreement with other proxy data (Jimenez-Espejo et al., 2020; Kohfeld and Chase, 2017; Oliver et al., 2010; Wilson et al., 2015). This second drop was accompanied by enhanced biological export production north of the PF fueled by enhanced dust input (Lambert et al., 2012). Our results showing a regionally coherent increase in sedimentary aU concentrations, especially after the MIS 5/4 transition, indicate gradually more sluggish overturning circulation that contributed to partitioning carbon into the ocean interior (Gottschalk et al., 2020; Jaccard et al., 2016, 2013; Kohfeld and Chase, 2017).

South of the PF in core PS2609-1 the aU record indicates re-oxygenation during MIS 3, while in the SAZ reducing conditions intensify. This contrasting behavior could be explained by a reorganization of deep-water masses. NADW that forms CDW in which our cores are located in modern times could have retracted northwards and to shallower regions in MIS 3, while the AAWB, generally more oxygenated than NADW, bathe the cores south of the PF (Sigman et al., 2010). Progressing towards the glacial maximum, the upwelled water masses would successively be more insulated from atmospheric forcing by extended sea-ice, leading to more oxygen-depleted and carbon rich AABW being formed (Ferrari et al. 2014), and thus resulting in the increased aU levels in the southern cores during MIS 2.

2.5 Conclusions

Five marine sediment cores from the Indian sector of the Southern Ocean were analyzed in this study. They were retrieved across a transect spanning a latitudinal band of about 15° from the Del Caño Rise, north of the SAF, over the Conrad Rise and as far south as the Enderby Abyssal Plain, close to the Southern ACC Front (SACCF). The redox-sensitive aU and Mn/Ti ratio were studied in detail and compared to ^{230}Th-normalized preserved opal export fluxes to better constrain bottom water oxygenation in the context of carbon sequestration since the last glacial inception. Our results suggest that more sluggish circulation dynamics and thus ventilation changes are the major

contributor accounting for enhanced carbon sequestration in deep-water masses during glacial periods. Our paleoceanographic records covering a meridional transect increase the spatial resolution of deep-water oxygenation records in the Southern Ocean and are overall in agreement with previous reconstructions from other deep-water sites (Chase et al., 2001; Dezileau et al., 2002; Francois et al., 1997; Frank et al., 2000; Jaccard et al., 2016; Thöle et al., 2019).

The influence of enhanced biological export production on oxygenation states due to increased Fe-fertilization by dust input cannot be ruled out completely, especially in the SAZ and at the transition from MIS 5 to 4 (Jaccard et al., 2016, 2013; Martínez-García et al., 2014). In the AZ however, export production likely played a minor role in partitioning carbon from the atmosphere. More importantly, decreased ventilation and the associated slowdown of overall ocean circulation during cold periods led to more carbon being sequestered in the ocean interior. Our results indicate a major drawdown of atmospheric CO_2 by a more sluggish overturning circulation. The most substantial circulation changes are suggested to have occurred at the transition of MIS 5/4 as has been proposed by Kohfeld and Chase (2017).

South of the PF, reducing conditions recede during MIS 3, most likely due to a reorganization of deep-water circulation with larger expansion of AABW, reaching the southern core locations (Ferrari et al., 2014). Later during MIS 2, also these deep waters, that upwell to newly form AABW, were increasingly isolated from atmospheric forcing due to expanded sea ice cover.

Generally, our reconstructions support the hypothesis that ventilation dynamics are the main driver of oxygenation changes in the Southern Ocean and thus exert the major control on the air-sea partitioning of CO_2 over the last glacial cycle.

Author contribution

HEA and SLJ designed the study. HEA, LMT, IS, and WG carried out U/Th measurements and evaluation. HEA and GK carried out biogenic opal measurements. IS and WG conducted the absolute Mn and Ti measurements. MI and GK planned the cruises and gave access to the cores and to XRF-measurements. MI, OE, and HEA obtained tiepoints to develop and refine the age models. HEA wrote the initial version of the manuscript and all co-authors contributed to the manuscript.

Acknowledgments

We thank the captain, crew members and scientists of the R/V Hakuho-maru and R/V Polarstern for the recovery of the sediment cores during KH-10-7 (lead scientist: M. Ikehara) and ANT-XI/4 cruises (lead scientist: G. Kuhn) to the Southern Ocean. We thank Martin Wille, Igor Villa, Jörg Rickli, David Janssen, Edel O'Sullivan, Alessandro Maltese, and Jörg Lippold for their help with the MC-ICP-MS measurements, Julijana Krbanjevic and Hendrik Vogel for helping with the opal measurements, and Takuya Matsuzaki for the Tatscan measurements. Funding for this study was provided by the Swiss National Science Foundation (grants PP00P2_144811 and 2000021_163003). O. Esper, W. Geibert, G. Kuhn and I. Stimac were funded by the Alfred-Wegener-Institut Helmholtz-Zentrum für Polar- und Meeresforschung PACES II research program. M. Ikehara was funded by the Japan Society for the Promotion of Science KAKENHI (Grants-in-Aid for Scientific Research P23244102 and JP17H06318). The isotope data was obtained on a Neptune MC-ICP-mass spectrometer acquired with funds from the NCCR PlanetS supported by the Swiss National Science Foundation grant no. 51NF40-141881.

References

Adkins, J.F., 2013. The role of deep ocean circulation in setting glacial climates. Paleoceanography 28, 539–561. doi: 10.1002/palo.20046

Adkins, J.F., McIntyre, K., Schrag, D.P., 2002. The salinity, temperature, and $\delta^{18}O$ of the glacial deep ocean. Science 298, 69–73. doi: 10.1126/science.1076252

Anderson, R.F., Ali, S., Bradtmiller, L.I., Nielsen, S.H.H., Fleisher, M.Q., Anderson, B.E., Burckle, L.H., 2009. Wind-driven Upwelling in the Southern Ocean and the Deglacial Rise in Atmospheric CO_2. Science 323, 1443–1448. doi: 10.1126/science.1167441

Anderson, R.F., Barker, S., Fleisher, M., Gersonde, R., Goldstein, S.L., Kuhn, G., Mortyn, P.G., Pahnke, K., Sachs, J.P., 2014. Biological response to millennial variability of dust and nutrient supply in the Subantarctic South Atlantic Ocean. Philos. Trans. R. Soc. A 372, 20130054. doi: 10.1098/rsta.2013.0054

Anderson, R.F., Fleer, A.P., 1982. Determination of Natural Actinides and Plutonium in Marine Particulate Material. Anal. Chem. 54, 1142–1147. doi: 10.1021/ac00244a030

Anderson, R.F., Sachs, J.P., Fleisher, M.Q., Allen, K.A., Yu, J., Koutavas, A., Jaccard, S.L., 2019. Deep-sea oxygen depletion and ocean carbon sequestration during the last ice age. Global Biogeochem. Cycles 33, 301–317, doi: 10.1029/2018GB006049.

Basak, C., Fröllje, H., Lamy, F., Gersonde, R., Benz, V., Anderson, R.F., Molina-Kescher, M., Pahnke, K., 2018. Breakup of last glacial deep stratification in the South Pacific. Science 359, 900–904, doi: 10.1126/science.aao2473

Bauska, T.K., Baggenstos, D., Brook, E.J., Mix, A.C., Marcott, S.E., Petrenko, V.V., Schaefer, H., Severinghaus, J.P., Lee, J.E., 2016. Carbon isotopes characterize rapid changes in atmospheric carbon dioxide during the last deglaciation. Proc. Nat. Acad. Sci., doi: 10.1073/pnas.1513868113

Bereiter, B., Eggleston, S., Schmitt, J., Nehrbass-Ahles, C., Stocker, T.F., Fischer, H., Kipfstuhl, S., Chappellaz, J., 2015. Revision of the EPICA Dome C CO_2 record from 800 to 600 kyr before present. Geophys. Res. Lett. 42, 542–549. doi: 10.1002/2014GL061957

Bourne, M.D., Thomas, A.L., Mac Niocaill, C., Henderson, G.M., 2012. Improved determination of marine sedimentation rates using $^{230}Th_{xs}$. Geochemistry, Geophys. Geosystems 13, 1. doi: 10.1029/2012GC00429

Boutorh, J., Moriceau, B., Gallinari, M., Ragueneau, O., Bucciarelli, E., 2016. Effect of trace metal-limited growth on the postmortem dissolution of the marine diatom *Pseudo-nitzschia delicatissima*. Global Biogeochem. Cycles 30, 57–69. doi: 10.1002/2015GB005088

Bouttes, N., Paillard, D., Roche, D.M., 2010. Impact of brine-induced stratification on the glacial carbon cycle. Clim. Past 6, 575–589. doi: 10.5194/cp-6-575-2010

Bradtmiller, L.I., Anderson, R.F., Fleisher, M.Q., Burckle, L.H., 2007. Opal burial in the equatorial Atlantic Ocean over the last 30 ka: Implications for glacial-interglacial changes in the ocean silicon cycle. Paleoceanography 22, PA4216, 1–15. doi: 10.1029/2007PA001443

Brzezinski, M.A., Pride, C.J., Franck, V.M., Sigman, D.M., Matsumoto, K., Gruber, N., Rau, G.H., Coale, K.H., 2002. A switch from $Si(OH)_4$ to NO_3^- depletion in the glacial Southern Ocean. Geophys. Res. Lett. 29, 12, 1564. doi: 10.1029/2001GL014349

Burke, A., Robinson, L.F., 2012. The Southern Ocean's Role in Carbon Exchange During the Last Deglaciation. Science 335, 557–561, doi: 10.1126/science.1208163

Calvert, S.E., Pedersen, T.F., 1993. Geochemistry of Recent oxic and anoxic marine sediments: Implications for the geological record. Mar. Geol. 113, 67–88.

Calvert, S.E., Pedersen, T.F., 1996. Sedimentary geochemistry of manganese: Implications for the environment of formation of manganiferous black shales. Econ. Geol. 91, 36–47. doi: 10.2113/gsecongeo.91.1.36

Chase, Z., Anderson, R.F., Fleisher, M.Q., 2001. Evidence from authigenic uranium for increased productivity of the glacial Subantarctic Ocean. Paleoceanography 16, 5, 468–478. doi: 10.1029/2000PA000542

Chase, Z., Anderson, R.F., Fleisher, M.Q., Kubik, P.W., 2003. Accumulation of biogenic and lithogenic material in the Pacific sector of the Southern Ocean during the past 40,000 years. Deep. Res. Part II Top. Stud. Oceanogr. 50, 799–832. doi: 10.1016/S0967-0645(02)00595-7

Choi, M.S., Francois, R., Sims, K., Bacon, M.P., Brown-Leger, S., Fleer, A.P., Ball, L., Schneider, D., Pichat, S., 2001. Rapid determination of ^{230}Th and ^{231}Pa in seawater by desolvated micro-nebulization Inductively Coupled Plasma magnetic sector mass spectrometry. Mar. Chem. 76, 99–112. doi: 10.1016/S0304-4203(01)00050-0

Colley, S., Thomson, J., Toole, J., 1989. Uranium relocations and derivation of quasi-isochrons for a turbidite/pelagic sequence in the Northeast Atlantic. Geochim. Cosmochim. Acta 53, 1223–1234. doi: 10.1016/0016-7037(89)90058-6

Cortese, G., Gersonde, R., Hillenbrand, C.D., Kuhn, G., 2004. Opal sedimentation shifts in the World Ocean over the last 15 Myr. Earth Planet. Sci. Lett. 224, 509–527. doi: 10.1016/j.epsl.2004.05.035

Costa, K.M., Hayes, C.T., Anderson, R.F., Pavia, F.J., Bausch, A., Deng, F., Dutay, J.C., Geibert, W., Heinze, C., Henderson, G., Hillaire-Marcel, C., Hoffmann, S., Jaccard, S.L., Jacobel, A.W., Kienast, S.S., Kipp, L., Lerner, P., Lippold, J., Lund, D., Marcantonio, F., McGee, D., McManus, J.F., Mekik, F., Middleton, J.L., Missiaen, L., Not, C., Pichat, S., Robinson, L.F., Rowland, G.H., Roy-Barman, M., Tagliabue, A., Torfstein, A., Winckler, G., Zhou, Y., 2020. ^{230}Th normalization: New insights on an essential tool for quantifying sedimentary fluxes in the modern and Quaternary ocean. Paleoceanogr. Paleoclimatology 35, e2019PA003820, 1–36. doi: 10.1029/2019PA003820

Crosta, X., Shukla, S.K., Ther, O., Ikehara, M., Yamane, M., Yokoyama, Y., 2020. Last Abundant Appearance Datum of *Hemidiscus karstenii* driven by climate change. Mar. Micropaleontol. 157. doi: 10.1016/j.marmicro.2020.101861

Dezileau, L., Bareille, G., Reyss, J.-L., 2002. Enrichissement en uranium authigène dans les sédiments glaciaires de l'océan Austral. C. R. Geoscience 334, 1039–1046.

Dezileau, L., Reyss, J.L., Lemoine, F., 2003. Late Quaternary changes in biogenic opal fluxes in the Southern Indian Ocean. Mar. Geol. 202, 143–158. doi: 10.1016/S0025-3227(03)00283-4

Dumont, M., Pichevin, L., Geibert, W., Crosta, X., Michel, E., Moreton, S., Dobby, K., Ganeshram, R., 2020. The nature of deep overturning and reconfigurations of the silicon cycle across the last deglaciation. Nat. Commun. 11, 1534, doi: 10.1038/s41467-020-15101-6

Ferrari, R., Jansen, M.F., Adkins, J.F., Burke, A., Stewart, A.L., Thompson, A.F., 2014. Antarctic sea ice control on ocean circulation in present and glacial climates. Proc. Natl. Acad. Sci. U. S. A. 111, 24, 8753–8758. doi: 10.1073/pnas.1323922111

Francois, R., Altabet, M.A., Yu, E.-F., Sigman, D.M., Bacon, M.P., Frank, M., Bohrmann, G., Bareille, G., Labeyrie, L.D., 1997. Contribution of Southern Ocean surface-water stratification to low atmospheric CO_2 concentrations during the last glacial period. Nature 389, 6654, 929–935, doi: 10.1038/40073

Francois, R., Frank, M., Rutgers van der Loeff, M.M., Bacon, M.P., 2004. ^{230}Th normalization: An essential tool for interpreting sedimentary fluxes during the late Quaternary. Paleoceanography 19, PA1018. doi: 10.1029/2003pa000939

Frank, M., Gersonde, R., Rutgers van der Loeff, M.M., Bohrmann, G., Nürnberg, C.C., Kubik, P.W., Suter, M., Mangini, A., 2000. Similar glacial and interglacial export bioproductivity in the Atlantic sector of the Southern Ocean: Multiproxy evidence and implications for glacial atmospheric CO_2. Paleoceanography 15, 6, 642–658.

Galbraith, E.D., Jaccard, S.L., 2015. Deglacial weakening of the oceanic soft tissue pump: Global constraints from sedimentary nitrogen isotopes and oxygenation proxies. Quat. Sci. Rev. 109, 38–48, doi: 10.1016/j.quascirev.2014.11.012

Galbraith, E.D. Skinner, L.C., 2020. The Biological Pump During the Last Glacial Maximum. Annual Review of Marine Science 12, 559–586, doi: 10.1146/annurev-marine-010419-010906

Galbraith, E.D., Young Kwon, E., Bianchi, D., Hain, M.P., Sarmiento, J.L., 2015. The impact of atmospheric pCO_2 on carbon isotope ratios of the atmosphere and ocean. Global Biogeochem. Cycles 29, 307–324. doi: 10.1002/2014GB004929

Geibert, W., Stimac, I., Rutgers van der Loeff, M.M., Kuhn, G., 2019. Dating Deep-Sea Sediments With ^{230}Th Excess Using a Constant Rate of Supply Model. Paleoceanogr. Paleoclimatology 34, 1895–1912. doi: 10.1029/2019PA003663

Gottschalk, J., Skinner, L.C., Jaccard, S.L., Menviel, L., Nehrbass-Ahles, C., Waelbroeck, C., 2020. Southern Ocean link between changes in atmospheric CO_2 levels and northern-hemisphere climate anomalies during the last two glacial

periods. Quat. Sci. Rev. 230, 106067, doi: 10.1016/j.quascirev.2019.106067

Gottschalk, J., Skinner, L.C., Lippold, J., Vogel, H., Frank, N., Jaccard, S.L., Waelbroeck, C., 2016. Biological and physical controls in the Southern Ocean on past millennial-scale atmospheric CO_2 changes. Nat. Commun. 7. doi: 10.1038/ncomms11539

Hain, M.P., Sigman, D.M., Haug, G.H., 2010. Carbon dioxide effects of Antarctic stratification, North Atlantic Intermediate Water formation, and subantarctic nutrient drawdown during the last ice age: Diagnosis and synthesis in a geochemical box model. Global Biogeochem. Cycles 24, GB4023, 1–19. doi: 10.1029/2010GB003790

Henderson, G.M., 2002. Seawater ($^{234}U/^{238}U$) during the last 800 thousand years. Earth Planet. Sci. Lett. 6183, 1–14. doi: 10.1016/S0012-821X(02)00556-3

Henderson, G.M., Anderson, R.F., 2003. The U-series toolbox for paleoceanography. Rev. Mineral. Geochemistry 52, 493–531. doi: 10.2113/0520493

Hoogakker, B.A.A., Elderfield, H., Schmiedl, G., McCave, I.N., Rickaby, R.E.M., 2015. Glacial–interglacial changes in bottom-water oxygen content on the Portuguese margin. Nat. Geosci. 8, 2–5, doi: 10.1038/ngeo2317

Horn, M.G., Robinson, R.S., Rynearson, T.A., Sigman, D.M., 2011. Nitrogen isotopic relationship between diatom-bound and bulk organic matter of cultured polar diatoms. Paleoceanography 26, PA3208, doi: 10.1029/2010PA002080

Ikehara, M., Katsuki, K., Yamane, M., Yokoyama, Y., Obrochta, S.P., Matsuzaki, T., Sato, H., Kusahara, K., (in prep.). Episodic enhancement of sea ice survivability in the glacial Southern Ocean driven by Antarctic warming.

Jaccard, S.L., Galbraith, E.D., Martínez-García, A., Anderson, R.F., 2016. Covariation of deep Southern Ocean oxygenation and atmospheric CO_2 through the last ice age. Nature 530, 207–210. doi: 10.1038/nature16514

Jaccard, S.L., Galbraith, E.D., Sigman, D.M., Haug, G.H., Francois, R., Pedersen, T.F., Dulski, P., Thierstein, H.R., 2009. Subarctic Pacific evidence for a glacial deepening of the oceanic respired carbon pool. Earth Planet. Sci. Lett. 277, 156–165. doi: 10.1016/j.epsl.2008.10.017

Jaccard, S.L., Hayes, C.T., Hodell, D.A., Anderson, R.F., Sigman, D.M., Haug, G.H., 2013. Two modes of change in SO Productivity. Science 339, 6126, 1419–1423. doi: 10.1126/science.1227545

Jacobel, A.W., McManus, J.F., Anderson, R.F., Winckler, G., 2017. Repeated storage of respired carbon in the equatorial Pacific Ocean over the last three glacial cycles. Nat. Commun. 8. doi: 10.1038/s41467-017-01938-x

Jimenez-Espejo, F.J., Presti, M., Kuhn, G., McKay, R., Crosta, X., Escutia, C., Lucchi, R.G., Tolotti, R., Yoshimura, T., Ortega Huertas, M., Macrì, P., Caburlotto, A., De Santis, L., 2020. Late Pleistocene oceanographic and depositional variations along the Wilkes Land margin (East Antarctica) reconstructed with geochemical proxies in deep-sea sediments. Glob. Planet.

Change 184, 103045, doi: 10.1016/j.gloplacha.2019.103045

Jouzel, J., Masson-Delmotte, V., Cattani, O., Dreyfus, G., Falourd, S., Hoffmann, G., Minster, B., Nouet, J., Barnola, J.M., Chappellaz, J., Fischer, H., Gallet, J.C., Johnsen, S., Leuenberger, M., Loulergue, L., Luethi, D., Oerter, H., Parrenin, F., Raisbeck, G., Raynaud, D., Schilt, A., Schwander, J., Selmo, E., Souchez, R., Spahni, R., Stauffer, B., Steffensen, J.P., Stenni, B., Stocker, T.F., Tison, J.L., Werner, M., Wolff, E.W., 2007. Orbital and millennial antarctic climate variability over the past 800,000 years. Science 317, 5839, 793–796. doi: 10.1126/science.1141038

Klinkhammer, G.P., Palmer, M.R., 1991. Uranium in the oceans: Where it goes and why. Geochim. Cosmochim. Acta 55, 1799–1806. doi: 10.1016/0016-7037(91)90024-Y

Kohfeld, K.E., Chase, Z., 2017. Temporal evolution of mechanisms controlling ocean carbon uptake during the last glacial cycle. Earth Planet. Sci. Lett. 472, 206–215, doi: 10.1016/j.epsl.2017.05.015

Kohfeld, K.E., Le Quéré, C., Harrison, S.P., Anderson, R.F., 2005. Role of marine biology in glacial-interglacial CO_2 cycles. Science 308, 74–78. doi: 10.1126/science.1105375

Korff, L., von Dobeneck, T., Frederichs, T., Kasten, S., Kuhn, G., Gersonde, R., Diekmann, B., 2016. Cyclic magnetite dissolution in Pleistocene sediments of the abyssal northwest Pacific Ocean: Evidence for glacial oxygen depletion and carbon trapping. Paleoceanography 31, 600–624, doi: 10.1002/2015PA002882

Kuhn, G., 2003a. Documentation of sediment core PS2609-1. Alfred Wegener Institute - Polarstern core repository, PANGAEA. doi: 10.1594/PANGAEA.115378

Kuhn, G., 2003b. Documentation of sediment core PS2606-6. Alfred Wegener Institute - Polarstern core repository, PANGAEA. doi: 10.1594/PANGAEA.115376

Kuhn, G., 2003c. Documentation of sediment core PS2603-3. Alfred Wegener Institute - Polarstern core repository, PANGAEA. doi: 10.1594/PANGAEA.115375

Kumar, N., Anderson, R.F., Mortlock, R.A., Froelich, P.N., Kubik, P., Dittrich-Hannen, B., Suter, M., 1995. Increased biological production and export in the glacial Southern Ocean. Nature 378, 675–680. doi: 10.1038/378675a0

Lambert, F., Bigler, M., Steffensen, J.P., Hutterli, M., Fischer, H., 2012. Centennial mineral dust variability in high-resolution ice core data from Dome C, Antarctica. Clim. Past 8, 609–623. doi: 10.5194/cp-8-609-2012

Lamy, F., Gersonde, R., Winckler, G., Esper, O., Jaeschke, A., Kuhn, G., Ullermann, J., Martínez-García, A., Lambert, F., Kilian, R., 2014. Increased dust deposition in the Pacific Southern Ocean during glacial periods. Science 343, 403–407. doi: 10.1126/science.1245424

Langmuir, D., 1978. Uranium solution-mineral equilibria at low temperatures with applications to sedimentary ore deposits. Geochim. Cosmochim. Acta 42, 547–569. doi: 10.1016/0016-7037(78)90001-7

Lippold, J., Grützner, J., Winter, D., Lahaye, Y., Mangini, A., Christi, M., 2009. Does sedimentary $^{231}Pa/^{230}Th$ from the Bermuda Rise monitor past Atlantic Meridional Overturning Circulation? Geophys. Res. Lett. 36, L12601, 1–6. doi: 10.1029/2009GL038068

Lisiecki, L.E., Raymo, M.E., 2005. A Pliocene-Pleistocene stack of 57 globally distributed benthic $\delta^{18}O$ records. Paleoceanography 20, PA1003, 1–17. doi: 10.1029/2004PA001071

Lynch-Stieglitz, J., Ito, T., Michel, E., 2016. Antarctic density stratification and the strength of the circumpolar current during the Last Glacial Maximum. Paleoceanography 31, 539–552, doi: 10.1002/2015PA002915

Mangini, A., Jung, M., Laukenmann, S., 2001. What do we learn from peaks of uranium and of manganese in deep sea sediments? Mar. Geol. 177, 63–78. doi: 10.1016/S0025-3227(01)00124-4

Manoj, M.C., Thamban, M., 2015. Shifting frontal regimes and its influence on bioproductivity variations during the Late Quaternary in the Indian sector of Southern Ocean. Deep. Res. Part II Top. Stud. Oceanogr. 118, 261–274. doi: 10.1016/j.dsr2.2015.03.011

Marshall, J., Speer, K., 2012. Closure of the meridional overturning circulation through Southern Ocean upwelling. Nat. Geosci. 5, 171–180. doi: 10.1038/ngeo1391

Martínez-García, A., Sigman, D.M., Ren, H., Anderson, R.F., Straub, M., Hodell, D.A., Jaccard, S.L., Eglinton, T.I., Haug, G.H., 2014. Iron fertilization of the subantarctic ocean during the last ice age. Science 343, 1347–1350. doi: 10.1126/science.1246848

Matsumoto, K., Sarmiento, J.L., Brzezinski, M.A., 2002. Silicic acid leakage from the Southern Ocean: A possible explanation for glacial atmospheric pCO_2. Global Biogeochem. Cycles 16, 3, 1031, doi: 10.1029/2001GB001442

Meyerink, S.W., Ellwood, M.J., Maher, W.A., Dean Price, G., Strzepek, R.F., 2017. Effects of iron limitation on silicon uptake kinetics and elemental stoichiometry in two Southern Ocean diatoms, *Eucampia antarctica* and *Proboscia inermis*, and the temperate diatom *Thalassiosira pseudonana*. Limnol. Oceanogr. 62, 6, 2445–2462. doi: 10.1002/lno.10578

Morford, J.L., Emerson, S., 1999. The geochemistry of redox sensitive trace metals in sediments. Geochim. Cosmochim. Acta 63, 1735–1750. doi: 10.1016/S0016-7037(99)00126-X

Müller, P.J., Schneider, R., 1993. An automated leaching method for the determination of opal in sediments and particulate matter. Deep. Res. Part I 40, 3, 425–444. doi: 10.1016/0967-0637(93)90140-X

Nameroff, T.J., Balistrieri, L.S., Murray, J.W., 2002. Suboxic trace metal geochemistry in the eastern tropical North Pacific, Geochim. Cosmochim. Acta, 66, 7, 1139–1158. doi: 10.1016/S0016-7037(01)00843-2

Nelson, D.M., Anderson, R.F., Barber, R.T., Brzezinski, M.A., Buesseler, K.O., Chase, Z., Collier, R.W., Dickson, M.L., François, R., Hiscock, M.R., Honjo, S., Marra, J.,

Martin, W.R., Sambrotto, R.N., Sayles, F.L., Sigmon, D.E., 2002. Vertical budgets for organic carbon and biogenic silica in the Pacific sector of the Southern Ocean, 1996–1998. Deep. Res. Part II Top. Stud. Oceanogr. 49, 1645–1674. doi: 10.1016/S0967-0645(02)00005-X

Oiwane, H., Ikehara, M., Suganuma, Y., Miura, H., Nakamura, Y., Sato, T., Nogi, Y., Yamane, M., Yokoyama, Y., 2014. Sediment waves on the Conrad Rise, Southern Indian Ocean: Implications for the migration history of the Antarctic Circumpolar Current. Mar. Geol. 348, 27–36. doi: 10.1016/j.margeo.2013.10.008

Oliver, K.I.C., Hoogakker, B.A.A., Crowhurst, S., Henderson, G.M., Rickaby, R.E.M., Edwards, N.R., Elderfield, H., 2010. A synthesis of marine sediment core $\delta^{13}C$ data over the last 150 000 years. Clim. Past 6, 645–673, doi:10.5194/cp-6-645-2010

Orsi, H., Whitworth, T., Nowlin Jr, W.D., 1995. On the meridional extent and fronts of the Antarctic Circumpolar Current. Deep. Res. Part I 42, 5, 641–673. doi: 10.1016/0967-0637(95)00021-W

Pichat, S., Sims, K.W.W., François, R., McManus, J.F., Leger, S.B., Albarède, F., 2004. Lower export production during glacial periods in the equatorial Pacific derived from $(^{231}Pa/^{230}Th)_{xs,0}$ measurements in deep-sea sediments. Paleoceanography 19, PA4023, 1–21. doi: 10.1029/2003PA000994

Pichevin, L.E., Ganeshram, R.S., Geibert, W., Thunell, R., Hinton, R., 2014. Silica burial enhanced by iron limitation in oceanic upwelling margins. Nat. Geosci. 7, 541–546. doi: 10.1038/ngeo2181

Pollard, R.T., Venables, H.J., Read, J.F., Allen, J.T., 2007. Large-scale circulation around the Crozet Plateau controls an annual phytoplankton bloom in the Crozet Basin. Deep. Res. Part II Top. Stud. Oceanogr. 54, 1915–1929. doi: 10.1016/j.dsr2.2007.06.012

Pondaven, P., Ragueneau, O., Tréguer, P., Hauvespre, A., Dezileau, L., Reyss, J.L., 2000. Resolving the 'opal paradox' in the Southern Ocean. Nature 405, 168–172. doi: 10.1038/35012046

Rae, J.W.B., Burke, A., Robinson, L., Adkins, J.F., Chen, T., Cole, C., Greenop, R., Li, T., Littley, E.F.M., Nita, D.C., Steward, J.A., Taylor, B.J., 2018. CO_2 storage and release in the deep Southern Ocean on millennial to centennial timescales. Nature 562, 569–573, doi: 10.1038/s41586-018-0614-0

Ragueneau, O., Tréguer, P., Leynaert, A., Anderson, R.F., Brzezinski, M.A., DeMaster, D.J., Dugdale, R.C., Dymond, J., Fischer, G., François, R., Heinze, C., Maier-Reimer, E., Martin-Jézéquel, V., Nelson, D.M., Quéguiner, B., 2000. A review of the Si cycle in the modern ocean: Recent progress and missing gaps in the application of biogenic opal as a paleoproductivity proxy. Glob. Planet. Change 26, 317–365. doi: 10.1016/S0921-8181(00)00052-7

Ronge, T.A., Prange, M., Mollenhauer, G., Ellinghausen, M., Kuhn, G., Tiedemann, R., 2020. Radiocarbon Evidence for the Contribution of the Southern Indian Ocean to the Evolution of Atmospheric CO_2 Over the Last 32,000 Years. Paleoceanogr.

Paleoclimatology 35. doi: 10.1029/2019PA003733

Sakamoto, T., Kuroki, K., Sugawara, T., Aoike, K., Iijima, K., Sugisaki, S., 2006. Nondestructive X-ray fluorescence (XRF) core-imaging scanner, TATSCAN-F2. Scientific Drilling 2, 37–39

Sarnthein, M., Schneider, B., Grootes, P.M., 2013. Peak glacial ^{14}C ventilation ages suggest major draw-down of carbon into the abyssal ocean. Clim. Past 9, 2595–9614, doi: 10.5194/cp-9-2595-2013

Sayles, F.L., Martin, W.R., Chase, Z., Anderson, R.F., 2001. Benthic remineralization and burial of biogenic SiO_2, $CaCO_3$, organic carbon, and detrital material in the Southern Ocean along a transect at 170° West. Deep. Res. Part II Top. Stud. Oceanogr. 48, 19–20, 4323–4383. doi: 10.1016/S0967-0645(01)00091-1

Schlitzer, R., 2018. Ocean Data View. Available at http://odv.awi.de

Sigman, D.M., Boyle, E.A., 2000. Glacial/interglacial variations in atmospheric carbon dioxide. Nature 407, 859–869. doi: 10.1038/35038000

Sigman, D.M., Hain, M.P., Haug, G.H., 2010. The polar ocean and glacial cycles in atmospheric CO_2 concentration. Nature 466, 7302, 47–55. doi: 10.1038/nature09149

Skinner, L.C., 2009. Glacial-interglacial atmospheric CO_2 change: a possible "standing volume" effect on deep-ocean carbon sequestration. Clim. Past 5, 537–550. doi: 10.5194/cp-5-537-2009

Skinner, L.C., Fallon, S., Waelbroeck, C., Michel, E., Barker, S., 2010. Ventilation of the Deep Southern Ocean and Deglacial CO_2 Rise. Science 328, 5982, 1147–1151. doi: 10.1126/science.1183627

Skinner, L.C., Primeau, F., Freeman, E., de la Fuente, M., Goodwin, P.A., Gottschalk, J., Huang, E., McCave, I.N., Noble, T.L., Scrivner, A.E., 2017. Radiocarbon constraints on the glacial ocean circulation and its impact on atmospheric CO_2. Nat. Commun. 8, 16010, doi: 10.1038/ncomms16010

Stein, K., Timmermann, A., Young Kwon, E., Friedrich, T., 2020. Timing and magnitude of Southern Ocean sea ice/carbon cycle feedbacks. Proc. Nat. Acad. Sci. 117, 9, doi: 10.1073/pnas.1908670117

Studer, A.S., Sigman, D.M., Martínez-García, A., Benz, V., Winckler, G., Kuhn, G., Esper, O., Lamy, F., Jaccard, S.L., Wacker, L., Oleynik, S., Gersonde, R., Haug, G.H., 2015. Antarctic Zone nutrient conditions during the last two glacial cycles. Paleoceanography 30, 845–862. doi: 10.1002/2014PA002745

Talley, L.D., 2013. Closure of the global overturning circulation through the Indian, Pacific, and Southern Oceans: Schematics and transports. Oceanography 26, 80–97. doi: 10.5670/oceanog.2013.07

Thöle, L.M., Amsler, H.E., Moretti, S., Auderset, A., Gilgannon, J., Lippold, J., Vogel, H., Crosta, X., Mazaud, A., Michel, E., Martínez-García, A., Jaccard, S.L., 2019. Glacial-interglacial dust and export production records from the Southern Indian Ocean. Earth Planet. Sci. Lett. 525. doi: 10.1016/j.epsl.2019.115716

Thomson, J., Wallace, H.E., Colley, S., Toole, J., 1990. Authigenic uranium in Atlantic sediments of the last glacial stage – a diagenetic phenomenon. Earth Planet. Sci. Lett. 98, 222–232, doi: 10.1016/0012-821x(90)90061-2

Toggweiler, J.R., 1999. Variation of atmospheric CO_2 by ventilation of the ocean's deepest water. Paleoceanography 14, 5, 571–588. doi: 10.1029/1999PA900033

Tribovillard, N., Algeo, T.J., Lyons, T., Riboulleau, A., 2006. Trace metals as paleoredox and paleoproductivity proxies: An update. Chem. Geol. 232, 1–2, 12–32, doi: 10.1016/j.chemgeo.2006.02.012

Vogel, H., Meyer-Jacob, C., Thöle, L., Lippold, J.A., Jaccard, S.L., 2016. Quantification of biogenic silica by means of Fourier transform infrared spectroscopy (FTIRS) in marine sediments. Limnol. Oceanogr. Methods 14, 828–838. doi: 10.1002/lom3.10129

Watson, A.J., Naveira Garabato, A.C., 2006. The role of Southern Ocean mixing and upwelling in glacial-interglacial atmospheric CO_2 change. Tellus, Ser. B Chem. Phys. Meteorol. 58, 1, 73–87. doi: 10.1111/j.1600-0889.2005.00167.x

Watson, A.J., Vallis, G.K., Nikurashin, M., 2015. Southern Ocean buoyancy forcing of ocean ventilation and glacial atmospheric CO_2. Nat. Geosci. 8, 11, 861–864. doi: 10.1038/ngeo2538

Wilson, D.J., Piotrowski, A.M., Galy, A., Banakar, V.K., 2015. Interhemispheric controls on deep ocean circulation and carbon chemistry during the last two glacial cycles. Paleoceanography 30, 621–641. doi: 10.1002/2014PA002707

Wolff, E.W., Barbante, C., Becagli, S., Bigler, M., Boutron, C.F., Castellano, E., de Angelis, M., Federer, U., Fischer, H., Fundel, F., Hansson, M., Hutterli, M., Jonsell, U., Karlin, T., Kaufmann, P., Lambert, F., Littot, G.C., Mulvaney, R., Röthlisberger, R., Ruth, U., Severi, M., Siggaard-Andersen, M.L., Sime, L.C., Steffensen, J.P., Stocker, T.F., Traversi, R., Twarloh, B., Udisti, R., Wagenbach, D., Wegner, A., 2010. Changes in environment over the last 800,000 years from chemical analysis of the EPICA Dome C ice core. Quat. Sci. Rev. 29, 285–295. doi: 10.1016/j.quascirev.2009.06.013

Xiao, W., Esper, O., Gersonde, R., 2016. Last Glacial - Holocene climate variability in the Atlantic sector of the Southern Ocean. Quat. Sci. Rev. 135, 115–137. doi: 10.1016/j.quascirev.2016.01.023

Yu, J., Menviel, L., Jin, Z.D., Thornalley, D.J.R., Barker, S., Marino, G., Rohling, E.J., Cai, Y., Zhang, F., Wang, X., Dai, Y., Chen, P., Broecker, W.S., 2016. Sequestration of carbon in the deep Atlantic during the last glaciation. Nat. Geosci. 9, 319–324, doi:10.1038/ngeo2657

Zielinski, U., Gersonde, R., 2002. Plio-Pleistocene diatom biostratigraphy from ODP Leg 177, Atlantic sector of the Southern Ocean. Mar. Micropaleontol. 45, 225–268. doi: 10.1016/S0377-8398(02)00031-2

CHAPTER 3

Spatio-temporal variations in lithogenic fluxes in the Southern Indian Ocean across the last glacial cycle

H. Eri Amsler[a,b], Lena M. Thöle[a,b,c], Walter Geibert[d], Gerhard Kuhn[d], Ingrid Stimac[d], Minoru Ikehara[e], Samuel L. Jaccard[a,b]

[a]Institute of Geological Sciences, University of Bern, Switzerland
[b]Oeschger Centre for Climate Change Research, University of Bern, Switzerland
[c]Department of Earth Sciences, Utrecht University, the Netherlands
[d]Alfred-Wegener-Institut Helmholtz-Zentrum für Polar- und Meeresforschung, Bremerhaven, Germany
[e]Center for Advanced Marine Core Research, Kochi University, Japan

in preparation for *EPSL*

ABSTRACT

Dust input into the ocean-atmosphere system plays a significant role as a source of micronutrients in biogeochemical cycles and global climate. Ice cores and marine sediments have shown higher dust and lithogenic fluxes during glacial periods than during interglacials. Here we present downcore records of lithogenic fluxes in a set of five marine sediment cores from the Indian Ocean based on measurements of thorium isotopes for the Subantarctic Zone (SAZ) and the Antarctic Zone (AZ) during the past glacial cycle. Lithogenic fluxes are generally low in interglacials (0.05 g/cm^2/ka) and rise in both SAZ and AZ to values of up to 0.5 g/cm^2/ka during glacial conditions. Comparing our results with lithogenic fluxes from other cores in the Southern Indian and the Southern Atlantic Ocean shows consistent regional patterns. Besides dust from southern America, we suggest additional input of lithogenic material from southern Africa and locally derived sources. Increased lithogenic input and associated iron-fertilization during glacial periods in the SAZ, combined with increased stratification in the AZ may have contributed to sequester CO_2 away from the atmosphere.

3.1 Introduction

Sedimentary records of mineral dust from around the world suggest a two- to four-fold increase in emission and deposition during late Pleistocene ice ages compared to interglacial periods (e.g. Kienast et al., 2016; Kohfeld and Harrison, 2001; Maher et al., 2010; Mahowald et al., 2006; Martínez-García et al., 2009; McGee et al., 2010). Similarly, polar ice cores show consistently higher dust fluxes during ice ages (e.g. Lambert et al., 2012, 2008; Ruth et al., 2007), which has been attributed to a variety of processes (e.g. Lunt and Valdes, 2002; Maher et al., 2010), including greater atmospheric dust load and stronger prevailing winds (McGee et al., 2010; Werner et al., 2002), increased dust production under generally colder and more arid/less vegetated conditions (Mahowald et al., 1999, 2006; Rea, 1994), longer atmospheric residence time of dust (Kohfeld and Harrison, 2001), changes in glaciogenic sediment supply (Reader et al., 1999; Sugden et al., 2009), changes in source regions (Fischer et al., 2007), and exposure of continental shelves as a result of lowered sea-level

(De Angelis et al., 1997). Furthermore, dust concentration in the atmosphere plays a major role in the climate system, directly impacting radiative forcing by scattering and absorption or indirectly with mineral dust particles acting as nuclei for cloud formation (Mahowald and Kiehl, 2003; Takemura et al., 2009; Tegen and Lacis, 1996; Werner et al., 2002). Lastly, mineral dust provides an important source of essential micronutrients such as iron (Fe) to pelagic ecosystems (e.g. Boyd et al., 2000; Boyd and Ellwood, 2010; Duce et al., 2008; Martin, 1990; Watson et al., 2000) with consequences for the marine carbon cycle.

Marine sediment records in the Southern Ocean are consistent with a regional increase in dust deposition (Anderson et al., 2014; Durand et al., 2017; Kumar et al., 1995; Lamy et al., 2014; Martínez-García et al., 2014; Thöle et al., 2019). While dust transport and deposition increased ubiquitously in the southern hemisphere, Patagonia and central western Argentina appear to represent major sources of dust to the Southern Ocean as inferred by both proxy records (e.g. Delmonte et al., 2008; Gili et al., 2017) and model simulations (Li et al., 2008; Lunt and Valdes, 2002; Mahowald et al., 1999, 2006). Increased Fe-bearing dust supply to the Southern Ocean during the last ice ages has been proposed to have alleviated the limitation chronic Fe-scarcity imposes on phytoplankton growth, thus potentially impacting the air-sea partitioning of CO_2 with implications for climate (Hain et al., 2010; Jaccard et al., 2013; Kumar et al., 1995; Martin, 1990; Martínez-García et al., 2014; Thöle et al., 2019). For the Indian sector of the Southern Ocean, additional sources of lithogenic material have been proposed, such as dust originating from southern Africa (Li et al., 2008; Sicre et al., 2006), remote islands and/or volcanic material eroded from oceanic plateaus by ocean currents (Thöle et al., 2019), and transport not only by winds, but also by ocean currents, such as the Antarctic Circumpolar Current (ACC) (Anderson et al., 2014; Dezileau et al., 2000; Franzese et al., 2006).

Here, we present downcore sedimentary lithogenic flux reconstructions of five marine sediment cores spanning a meridional transect in the southwestern Indian sector of the Southern Ocean. We further compare these observations with previously published sedimentary records from the SE Atlantic basin (Anderson et al., 2014) as well as east of Kerguelen Plateau (Thöle et al., 2019),

further downwind from the Patagonian dust plume, and offer a regional reconstruction of deposition of lithogenic material for the last glacial cycle in the yet sparsely sampled Indian sector of the Southern Ocean.

3.2 Study site, materials and methods

3.2.1 Core locations and material

Analyses were carried out on a suite of marine sediment cores from the Indian Ocean, collected on the flanks of salient bathymetric highs, including Del Caño Rise, Conrad Rise, and as far south as the Enderby Abyssal Plain (Figure 3.1). The core locations cover a meridional transect encompassing the Subantarctic and Antarctic zones of the Southern Ocean (Orsi et al., 1995) and are located downwind of South America, the major source of dust to the Atlantic and Indian sectors of the Southern Ocean (Li et al., 2008; Mahowald et al., 2006). The cores are thus ideally located to record past changes in dust input by the prevailing southern hemisphere westerly winds.

Cores DCR-1PC (46°01.34'S, 44°15.24'E, 2632 mbsl) and COR-1bPC (54°16.04'S, 39°45.98'E, 2828 mbsl) were retrieved during expedition KH-10-7 on R/V Hakuho-maru in 2010–2011. Cores PS2609-1 (51°29.9'S, 41°35.8'E, 3113 mbsl), PS2606-6 (53°13.9'S, 40°48.1'E, 2545 mbsl) and PS2603-3 (58°59.2'S, 37°37.7'E, 5289 mbsl) were retrieved during ANT-XI/4 expedition on R/V Polarstern in 1994. The northernmost core DCR-1PC lies in the Subantarctic Zone (SAZ) of the Southern Ocean close to the Subantarctic Front (SAF) and consists of nannofossil and diatom ooze with variable amounts of clay. The remaining cores lie in the Antarctic Zone (AZ) of the Southern Ocean, south of today's position of the Polar Front (PF) and are mainly composed of diatom ooze.

For the regional overview, these records were compared to additional cores. Two cores, MD11-3357 (44°40.8'S, 80°25.8'E, 3349 mbsl) and MD11-3353 (50°34.2'S, 68°23.4'E, 1568 mbsl), were recovered further to the east, in the vicinity of the Kerguelen Archipelago by R/V Marion Dufresne in 2011. MD11-3357 is located in the SAZ close to the SAF, whereas MD11-3353 is located in the AZ, just south of the modern PF. Another two cores from the Southern Atlantic, TN057-21 (41.13°S, 7.81°E, 4981 mbsl) and TN057-06

(42.91°S, 8.9°E, 3751 mbsl), were used for the regional comparison (Anderson et al., 2014). TN057-06 was retrieved at the same location as ODP core 1090 (Martínez-García et al., 2009). Combining the datasets allows for increasing the spatial and temporal resolution of marine records in the Southern Indian Ocean, helping to better appraise regional paleoclimatic dynamics and identify potential drivers of change.

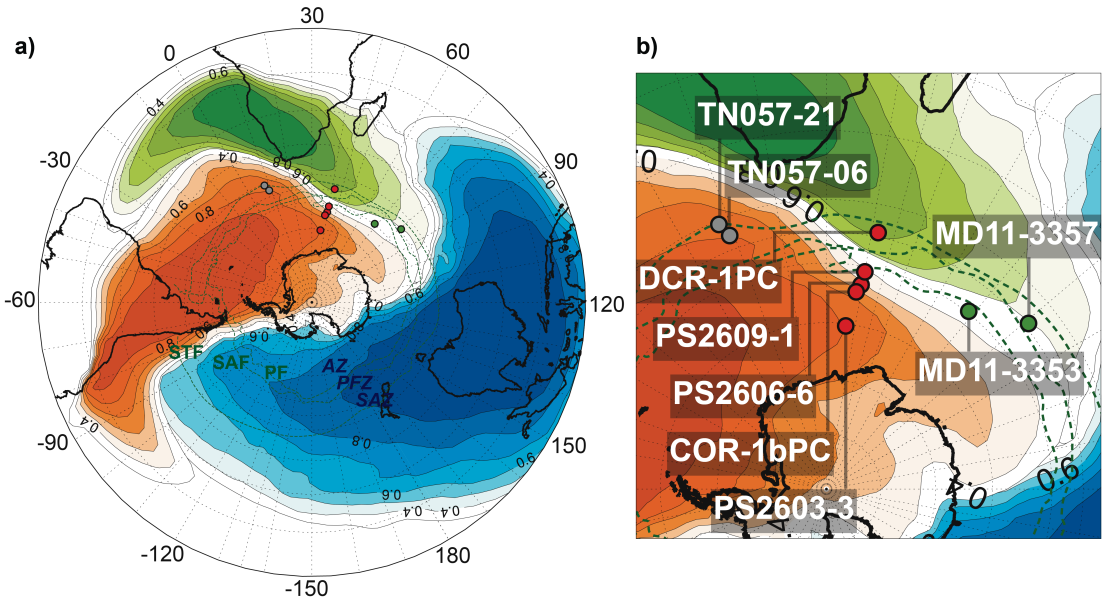

Figure 3.1: Core locations (red: this study; green: cores of Thöle et al. (2019); grey: cores from Anderson et al. (2014)). a) View of southern hemisphere with simulated extent of dust plumes in present climate (adapted from Li et al., 2008). The fronts (green dashed lines) are labeled from north to south: Subtropical Front (STF), Subantarctic Front (SAF) and Polar Front (PF). The zones are labeled in blue from north to south: Subantarctic Zone (SAZ), Polar Frontal Zone (PFZ) and Antarctic Zone (AZ). b) Zoom of the study site with the core locations labeled.

3.2.2 Age models

Age models were determined based on a different approach for each core (see Chapter 2 for more details). Briefly, for DCR-1PC, seven ^{14}C-dates were measured and additional tiepoints were defined comparing the diatom-based summer sea surface temperature (SST) record to the EDC δD local temperature record, assuming synchronicity (Crosta et al., 2020). The stratigraphy for core COR-1bPC is based on 23 calibrated ^{14}C measurements on planktic foraminifera *neogloboquadrina pachyderma (sinistral)* (Ikehara et al., *in prep.*; Oiwane et al., 2014). For PS2609-1, PS2606-6, and PS2603-3, tie points have been established based on graphical alignment of magnetic susceptibility and XRF-data (Fe, Si,

Ti, Ca) to the LR04 $\delta^{18}O$ stack (Lisiecki and Raymo, 2005), and XRF-data (Ti) to the EDC dust record (Lambert et al., 2012), assuming synchronous temporal variability.

For PS2606-6 and PS2603-3, ^{14}C-data (Ronge et al., 2020; Xiao et al., 2016) and diatom species extinction events provided additional tiepoints, respectively.

3.2.3 Lithogenic fluxes

Common thorium (^{232}Th) has widely been used as a robust proxy to reconstruct (past) changes in lithogenic fluxes to the ocean (e.g. Anderson et al., 2014; Jacobel et al., 2016; Kienast et al., 2016; Martínez-García et al., 2009; McGee et al., 2016; Sayles et al., 2001; Serno et al., 2014; Thöle et al., 2019; Wengler et al., 2019; Winckler et al., 2008). ^{232}Th is a trace element, typically enriched in the continental crust and comparatively low in volcanic material (Kienast et al., 2016; McGee et al., 2016; Winckler et al., 2008). ^{232}Th is predominantly supplied to the pelagic sedimentary record via winds, given that the open ocean is far removed from riverine and continental slope inputs. However, besides eolian transport, lithogenic particles can be also transported over significant distances by ocean currents while in suspension (Anderson et al., 2014; Dezileau et al., 2000). Dust sources around the world show relatively tightly-constrained ^{232}Th concentrations averaging 10.7 ± 2 ppm (Kienast et al., 2016; McGee et al., 2007; Taylor and McLennan, 1995). A slightly higher average concentration of 14 ppm was proposed by McGee et al. (2016) for sediments predominantly constituted of grains <5 µm. In the sediment cores considered in this study, sediments mainly consist of diatom and calcareous nannofossil ooze, and the detrital material was predominantly in the silt fraction (2–63 µm). Furthermore, calculation with the traditional value of 10.7 ppm allows for a quantitative comparison with other cores from the region. The validity of ^{232}Th as a dust proxy is supported by the strong correlation between ^{232}Th and terrigenous *n*-alkane fluxes in several sedimentary records of the Southern Ocean (Lamy et al., 2014; Martínez-García et al., 2009; Thöle et al., 2019).

The vertical flux of lithogenic material is quantified using the ^{230}Th-normalization approach (e.g. Bourne et al., 2012; Costa et al., 2020; Francois et al., 2004; Henderson and Anderson, 2003), which is based on the premise that the flux of ^{230}Th reaching the seafloor along with sinking particles equals its

known production rate (β_{230}) within the overlying water column (z) from the radioactive decay of dissolved uranium (U). Therefore, the vertical flux of any sedimentary constituent can be calculated when normalized to ^{230}Th: $^{pr}F_v = \frac{\beta_{230} \times z}{A^{scav}_{Th230,(0)}}$. Excess sedimentary ^{230}Th ($A^{scav}_{Th230,(0)}$) is calculated and corrected for i) ^{230}Th produced in situ from the decay of authigenic ^{238}U, ii) ^{230}Th produced in situ from the decay of detrital ^{238}U, and iii) in situ decay of ^{230}Th since deposition. The lithogenic flux can thus be determined as follows:

$$lith.\,flux = \frac{A^{total}_{Th232}}{10.7\ ppm} \times \frac{\beta_{230} \times z}{A^{scav}_{Th230,(0)}} \qquad \text{Eq. (3.1)}$$

The Th and U isotopic compositions were quantified by isotope dilution following Anderson and Fleer (1982) and adjusted to match the analytical set-up (Choi et al., 2001; Lippold et al., 2009; Pichat et al., 2004). For cores DCR-1PC and COR-1bPC, freeze-dried sediment samples (150–200 mg) were double spiked (^{229}Th, ^{236}U) and completely digested with concentrated HNO_3, HCl and HF in a pressure-assisted microwave (T_{max} = 180°C). The Th and U fractions were separated and purified by anion exchange chromatography using AG1-X8 resin (Pichat et al., 2004) and measured separately on a Thermo Fisher Scientific Neptune Plus multi-collector inductively coupled plasma mass spectrometer (MC-ICP-MS) at the University of Bern, Switzerland. Approximately half of the samples from cores PS2609-1, PS2606-6, and PS2603-3 had been prepared earlier (by I. Stimac and S. Kretschmer at AWI) following a similar procedure, with U and Th fractions being separated chromatographically using UTEVA resin (Eichrom). The samples of these cores were measured on a single-collector ICP-MS (Thermo Fisher Scientific Element 2) at the Alfred Wegener Institute (AWI) in Bremerhaven. The isotope measurements were corrected with a calibrated standard that was run along with the samples as reference material (UREM-11 Sarm 31) and yielded a relative standard deviation of less than 3.8% and 3.5% for ^{238}U and ^{234}U, and less than 5.7% and 4.9% for ^{230}Th and ^{232}Th, respectively. The measurement differences between the two mass spectrometers were within these errors.

3.2.4 Preserved opal export

In the Southern Ocean, especially south of the Polar Front, biogenic export production is dominated by diatoms (Cortese et al., 2004; Ragueneau et al., 2000). Sedimentary biogenic opal concentrations (bSi) were measured using Fourier transform infrared spectroscopy (FTIRS – Vogel et al., 2016) at the University of Bern on cores DCR-1PC and COR-1bPC. For the PS cores, the sedimentary opal content was determined by alkaline extraction of silica according to Müller and Schneider (1993) at AWI, Bremerhaven. Both methods provide comparable results and were converted to vertical fluxes via the ^{230}Th-normalization method:

$$preserved\ opal\ flux = bSi_{(conc.)} \times \frac{\beta_{230} \times z}{A^{scav}_{Th230,(0)}} \qquad \text{Eq. (3.2)}$$

3.3 Results

3.3.1 Reconstruction of lithogenic fluxes in the Subantarctic Zone

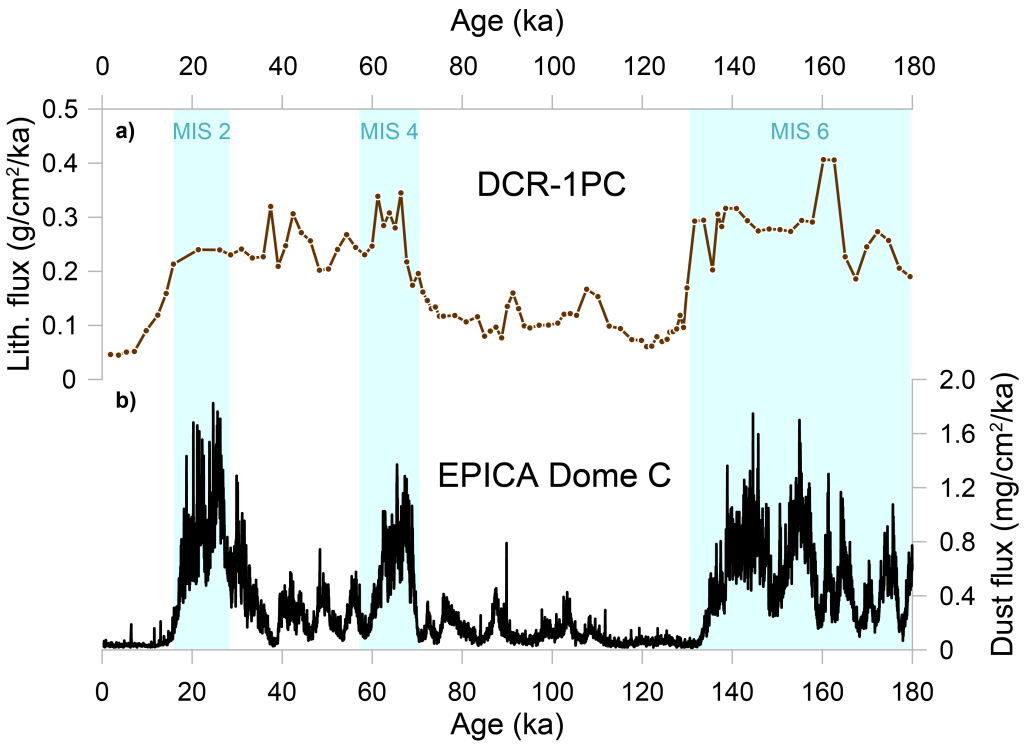

Figure 3.2: Lithogenic fluxes in the Subantarctic Zone. a) Lithogenic fluxes (brown) in northernmost core DCR-1PC. b) Dust flux record from EPICA Dome C ice core (Lambert et al., 2012). Light blue bars show cold periods MIS 2, 4, and 6 (Lisiecki and Raymo, 2005).

Lithogenic fluxes in northernmost SAZ core DCR-1PC follow a typical glacial-interglacial pattern characterized by higher values during cold periods and substantially lower values during warmer intervals. The lowest values (<0.1 g/cm²/ka) are found during intervals of Marine Isotope Stage (MIS) 5 and the Holocene. The overall highest values of up to 0.4 g/cm²/ka are reached during MIS 6, before they decrease rapidly at TERM II at the onset of MIS 5. During MIS 5 there are transient increases of up to 0.2 g/cm²/ka at around 115–105 ka and 95–85 ka, possibly coinciding with MIS 5b and MIS 5d. At the MIS 5/4 transition, dust fluxes increase substantially. Peak values (0.35 g/cm²/ka) are reached during MIS 4 and remain elevated throughout MIS 3. The lithogenic flux values plateau around these levels during the first half of MIS 2, before they start decreasing steadily from 18 ka before reaching their lowest levels at around 7 ka.

3.3.2 Reconstruction of lithogenic fluxes in the Antarctic Zone

The three northern cores of the Antarctic Zone all show coherent downcore patterns in lithogenic flux with typically higher values during cold periods and lower values typical for warm climate intervals. The lowest values (<0.1 g/cm²/ka) are found during parts of MIS 5 and the Holocene. In the northern AZ we observe slight increases up to 0.2 g/cm²/ka during MIS 5 at around 115–105 ka and at around 95–85 ka. At the MIS 5/4 transition, lithogenic flux values increase steadily until reaching peak values during MIS 3 (0.4–0.5 g/cm²/ka). Flux values decrease rapidly after 40 ka before increasing gradually again, although without reaching the high values of MIS 3. During peak glacial conditions the values hover between 0.3 and 0.35 g/cm²/ka, before declining abruptly across TERM I. The record of COR-1bPC starts during MIS 3 when the values are in the steep decrease at around 40 ka. The pattern that follows is very similar to the other two cores described with a gradual increase to the LGM peak before a sudden drop to background Holocene values.

The southernmost core PS2603-3 retrieved from Enderby Abyssal Plain is an exception within the AZ cores. During MIS 5, between 90–75 ka, values reach 5 g/cm²/ka in a prominent peak. Otherwise, background values are generally more elevated than in the northern AZ; lithogenic fluxes remain consistently and uniformly between 0.2 and 0.4 g/cm²/ka throughout MIS 4, 3 and 2 and rise after TERM I to values slightly above 0.6 g/cm²/ka, before they fall again

to levels around 0.3 g/cm²/ka in the Holocene; a similar transient rise at the start of MIS 5 after TERM II is observed.

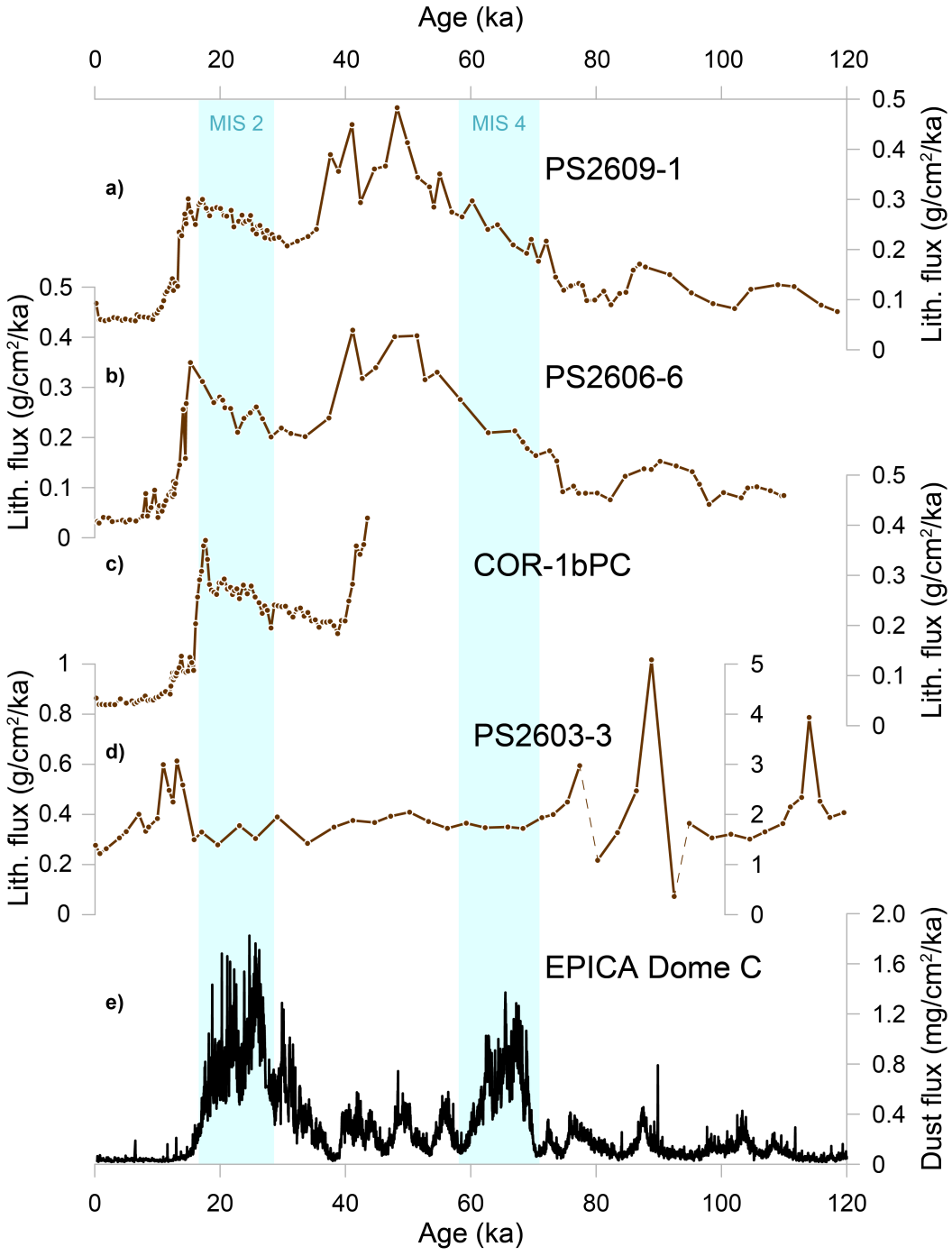

Figure 3.3: Lithogenic fluxes in the Antarctic Zone from north to south. a) Core PS2609-1, b) core PS2606-6, c) core COR-1bPC, d) core PS2603-3 with adjusted y-axis for the peak at 90–75 ka, e) dust flux record from EPICA Dome C ice core (Lambert et al., 2012). Light blue bars show cold periods MIS 2 and 4 (Lisiecki and Raymo, 2005).

3.4 Interpretation and discussion

3.4.1 Regional variations in lithogenic fluxes

The sedimentary lithogenic flux records show broad similarities with Antarctic ice core dust reconstructions (Lambert et al., 2012, 2008), albeit with much smaller amplitude. Dust accumulation over Antarctica was up to 25 times higher during past ice ages than during interglacials, consistent with higher atmospheric dust load, but also with changes in dust transport and deposition specific to the Antarctic continent (Lambert et al., 2008). The major difference between the ice core and sediment records relates to sustained input of lithogenic material to the SW Indian Ocean throughout the last glacial period, whereas the Antarctic dust flux record shows a marked decrease during MIS 3 (Figures 3.2b and 3.3e).

All cores in the SAZ and AZ show significant similarities in their lithogenic flux records, both in the downcore evolution as well as in the flux values, except for the southernmost core PS2603-3.

In SAZ core DCR-1PC, MIS 4 flux values are higher than those of MIS 3 and MIS 2, and the MIS 4 values in the three northern AZ cores. In both SAZ and northern AZ, MIS 3 values are higher than during MIS 2, unlike EPICA Dome C, where dust fluxes are highest during the LGM (Figures 3.2 and 3.3). We suggest that the notable difference between the ice-core and marine sediment records possibly reflects enhanced lithogenic input from local/regional sources during the last ice age, in addition to the supply of lithogenic material from South America, which predominates in the ice-core record (Delmonte et al., 2008; Gili et al., 2017; Grousset et al., 1992). Additional glacial sources of lithogenic material to the SW Indian Ocean possibly include southern Africa (Sicre et al., 2006), Antarctica (via CDW/AABW and to a lesser extent ice rafting) (Bareille et al., 1994; Ikehara et al., *in prep.*), exposed shelf-areas (Bareille et al., 1994), increased transport by stronger ACC (Franzese et al., 2006; Manoj and Thamban, 2015; Mazaud et al., 2010), and/or more localized, volcanogenic sources from ocean highs (Bareille et al., 1994; Dezileau et al., 2000; Oiwane et al., 2014). However, local volcanogenic sources would contribute to a lesser degree to the downcore ^{232}Th flux values due to the generally lower (yet variable) ^{232}Th concentrations in volcanic rocks compared

to continental material. Measurements of southeastern Indian Ridge basalts yielded ^{232}Th concentrations that were two orders of magnitude lower than the global average value for continental crust (Russo et al., 2009), similar to other mid-ocean ridge basalt material (Kienast et al., 2016). However, there is evidence of incorporation of continental crust material into the Kerguelen Plateau (Bénard et al., 2010; Frey et al., 2002; Ingle et al., 2002). Furthermore, the ^{232}Th concentrations measured on the lithogenic fraction separated from SW Indian Ocean sediments vary between 1.76 and 6.18 ppm (Dezileau et al., 2000), which are close to the values typical for volcanogenic material sampled around Crozet Island averaging 6.3 ppm (Gunn et al., 1970; Marsh et al., 2007). Therefore, local sources may bear sufficiently high ^{232}Th concentrations to partially account for the glacial increase in ^{232}Th fluxes. Downcore reconstructions of ^{230}Th-derived total vertical fluxes diverging from ^{232}Th concentrations further support this interpretation (*data-CD of thesis*).

The southernmost core PS2603-3, located afar from the main westerly wind belt, behaves differently. The prominent peak observed during MIS 5 (Figure 3.3) could be related to a 30-ka long sedimentary hiatus (see Chapter 2). This sediment disturbance could be related to a turbidite (Kuhn, 2003c), possibly associated with remobilizing old sediments low in ^{230}Th. Compared to the other AZ cores, the overall higher values consistently above 0.2 g/cm^2/ka, could be explained as due to its southern location and being under influence of Antartic input. The rise after TERM II and TERM I we interpret to be an increased IRD (ice-rafted debris) signal during deglaciation and breakup of continental ice.

3.4.2 Comparison with South Atlantic and East Indian cores

In order to further investigate regional similarities and potential sources different from Patagonia, we compare our reconstructions to other sediment cores in the region.

The South Atlantic records (Anderson et al., 2014) show a very similar glacial-interglacial pattern to the SAZ as well as the AZ records of the Indian Ocean cores of this study (Figure 3.4a). These two marine sediment cores (TN057-21 and TN057-06 – Anderson et al., 2014) were retrieved from the South Atlantic basin, west of southern Africa. The South Atlantic lithogenic flux

reconstructions show a similar pattern, but consistently higher values (offset of ~0.2–0.3 g/cm²/ka) than those reported for the SW Indian Ocean, pointing to South America as the dominant dust source for the South Atlantic region and decreasing dust supply further away from the source.

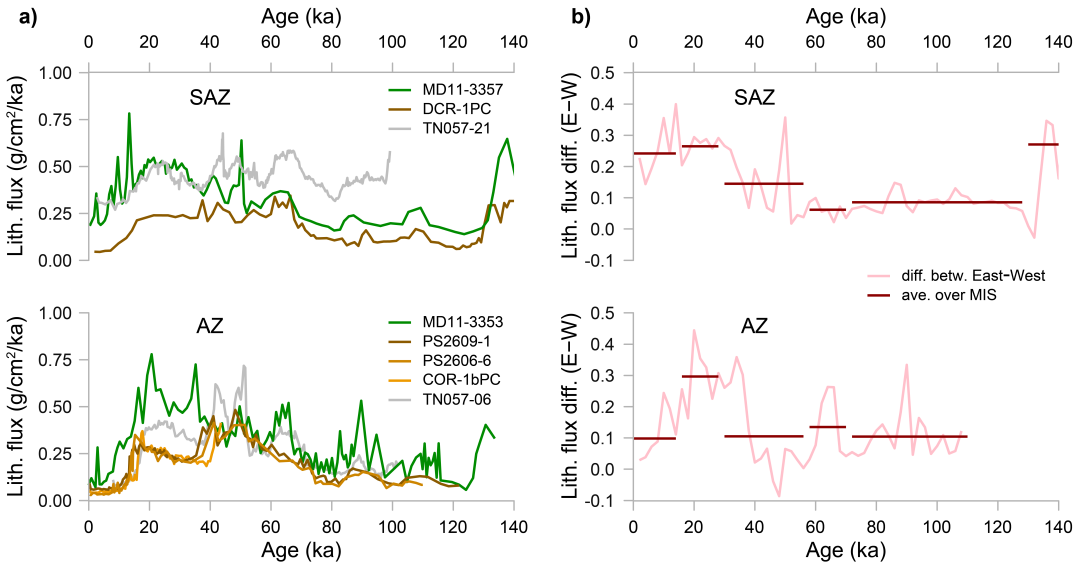

Figure 3.4: Regional comparison of lithogenic fluxes. Top panels: SAZ, bottom panels: AZ. a) Lithogenic fluxes of western cores in brown; lith. fluxes of eastern cores in green (Thöle et al., 2019); grey fluxes are from the eastern South Atlantic (Anderson et al., 2014). b) Gradient between eastern cores (green) and western cores (brown). For the AZ, the PS2609-1 and PS2606-6 were stacked (2-ka interpolation); light pink: gradients of values interpolated to 2-ka intervals; red: average of the gradients for each MIS.

A recent study focusing on two marine sediment cores located eastwards, in the vicinity of Kerguelen Plateau, presents lithogenic flux reconstructions on the basis of ^{232}Th as well as *n*-alkanes (Thöle et al., 2019). In the context of providing a broader regional perspective, the lithogenic fluxes of these different cores were compared. In Figure 3.4 we report a detailed comparison between the eastern and western lithogenic flux reconstructions for the SAZ (top) and the AZ (bottom). In order to facilitate data intercomparison, a 2-ka interpolation stack of cores PS2609-1 and PS2606-6 has been generated (Figure 3.4b). The generally positive values suggest that in both SAZ and AZ, the eastern cores are characterized by higher lithogenic fluxes than in the west.

The lithogenic flux reconstructions in the eastern cores generally show a similar pattern to the ones in the west. Major differences can be observed during the last (MIS 2) and penultimate (MIS 6) glacial maxima, during which flux values

in the east substantially exceed those in the western cores. Additionally, in the AZ there is a distinct peak during MIS 4 that is not apparent in the SW Indian Ocean (Figure 3.4). The lowest values in the eastern cores are consistently found during the warm periods of the Holocene and parts of MIS 5. Furthermore, the average zonal gradients (Figure 3.4b) clearly show that during the cold periods the eastern cores exhibit higher lithogenic fluxes than in the west.

We suggest that the distinct glacial peak observed in both the eastern SAZ and AZ cores and the smaller, yet noticeable peak in the AZ during MIS 4 may be associated with additional lithogenic sources, related to the Kerguelen Plateau, which is located between the two sets of cores. Enhanced erosion of the volcanic structures by vigorous bottom currents (Bareille et al., 1994; Dezileau et al., 2000) and/or enhanced glacial erosion of emerged landmasses during peak glacial times and sediment destabilization on shelves (Dezileau et al., 2000) may have increased the lithogenic contribution to the core sites, in addition to aeolian material transported from South America and possibly southern Africa.

In the western sites, the proximity to the African continent leads us to assume that dust originating from southern Africa may have reached the core sites. Modeling data (Li et al., 2008) suggest the influence of African dust to decrease with increasing distance from the continent towards the south and the east. This being said, the absolute flux values in the western cores do not exceed those in the east; to the contrary, MD11-3357 shows a constant positive offset when compared to DCR-1PC (Figure 3.4a). Furthermore, the contribution of southern African dust would be more pronounced in the northern cores than further to the south, which is not the case either. Indeed, enhanced influx of African lithogenic material may well be contributing to the overall increase observed during cold periods, but this contribution would have been surpassed by yet stronger influx from the Kerguelen Plateau, as illustrated by the distinct MIS 2 and 4 peaks. Also, an influence from enhanced Agulhas return current during glacials, that only affected the eastern cores, cannot effectively be ruled out (e.g. Lutjeharms and Ansorge, 2001; Nair et al., 2019). Higher dust accumulation across large swaths of the Southern Indian Ocean is consistent with stronger winds and a generally drier atmosphere, which would have conspired to enhance particle lifetime in the atmosphere (Lunt and Valdes,

2002). But also and perhaps more importantly, stronger currents during MIS 4 and MIS 2, possibly as a result of a previously postulated northward shift of the frontal system (Gersonde et al., 2005; Thöle et al., 2019), would lead to more lithogenic material being eroded and transported from the Kerguelen Plateau (Bareille et al., 1994) to the core site locations.

Overall, comparison of the lithogenic fluxes in the SW Indian Ocean cores with the South Atlantic cores and the cores east of the Kerguelen Plateau show that the flux records are remarkably consistent. There are slight differences between SAZ and AZ, as well as some zonal variations, but all in all the results confirm a regional pattern, that can reliably be inferred from ^{232}Th-analyses.

3.4.3 Impact of dust fertilization and possible implications for carbon export

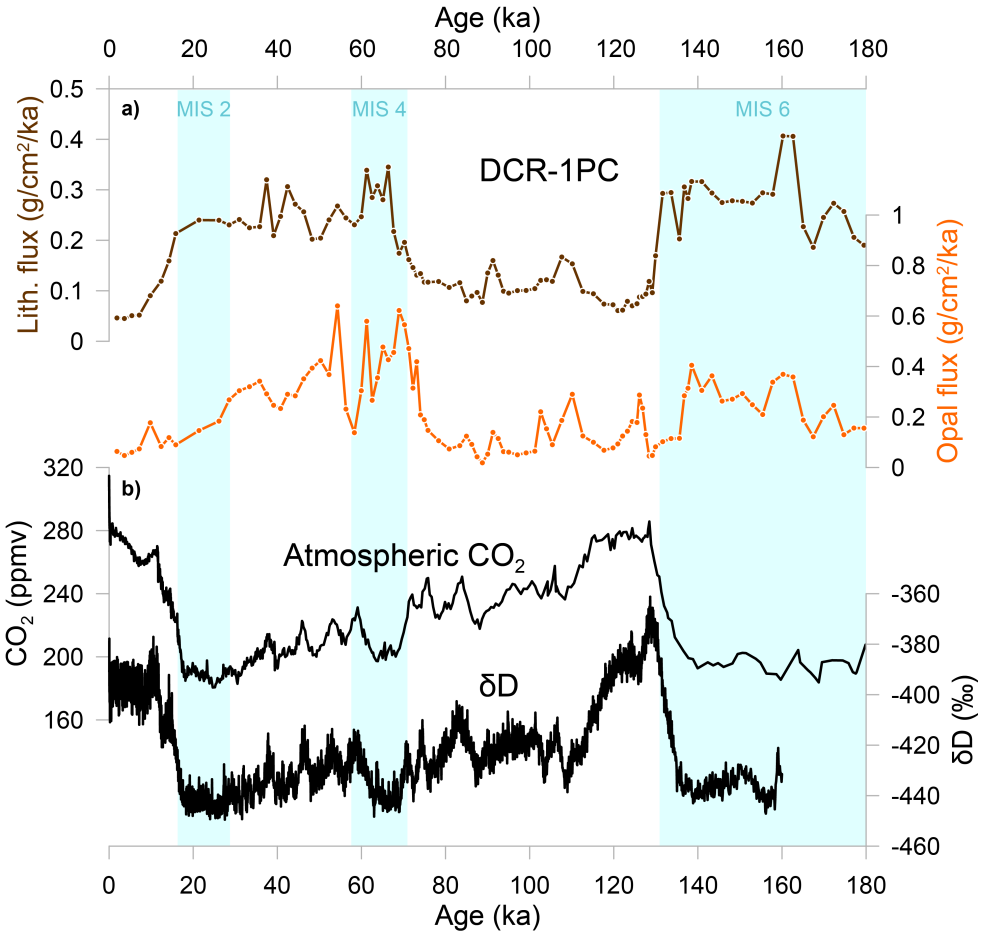

Figure 3.5: a) Lithogenic fluxes and preserved opal fluxes in the Subantarctic Zone. b) Atmospheric CO_2 from EPICA Dome C ice core, composite record (Bereiter et al., 2015 *and references therein*) and δD record from EPICA Dome C ice core reflecting Antarctic air temperatures (Jouzel et al., 2007). Light blue bars show cold periods MIS 2, 4, and 6 (Lisiecki and Raymo, 2005).

Comparison of the lithogenic flux records with the preserved opal flux reconstructions shows contrasted evolutions in the SAZ and the AZ (Figures 3.5 and 3.6). In the SAZ, both proxies follow a consistent temporal variability, with generally lower flux values during warmer intervals and comparatively higher values during cold periods. This suggests that phytoplankton growth in the SAZ of the Indian sector of the Southern Ocean responded to enhanced availability of bioavailable Fe, similar to the other sectors of the Southern Ocean (Anderson et al., 2014; Durand et al., 2017; Lamy et al., 2014; Martin, 1990; Martínez-García et al., 2014; Studer et al., 2015). However, from MIS 3 onwards the correlation weakens as biogenic opal fluxes decrease while lithogenic fluxes remain high. A potential explanation relates to the hypothesis that phytoplankton growth became limited by an overall decrease in nitrate and/or silicate availability due to a generally reduced supply from upwelling (Brzezinski et al., 2002; Dumont et al., 2020) and/or due to a northward shift of the PF (Gersonde et al., 2005; Thöle et al., 2019; Toggweiler et al., 2006). The early decrease in opal fluxes can be also observed during the penultimate glacial maximum, where lithogenic and opal fluxes are transiently decoupled prior to the glacial termination.

In the AZ, the preserved opal and lithogenic flux records show opposite patterns (Figure 3.6). Biogenic opal flux values increase abruptly at the onset of the last glacial termination, whereas the lithogenic flux rapidly decreases. We interpret the rise in biogenic opal fluxes during the deglaciation to result from increased nutrient supply from upwelled waters (see Chapter 2) induced by a reinvigoration of subsurface ocean circulation at the end of the last glacial period (e.g. Anderson et al., 2009; Jaccard et al., 2016; Skinner et al., 2010; Studer et al., 2015). Increased Fe-bearing dust input to the fertile surface ocean during glacial periods was insufficient to enhance biological export production, as ecosystems remained limited by the scarcity of nitrate as a result of decreased vertical exchange and/or sea-ice extent (Ferrari et al., 2014; François et al., 1997; Jaccard et al., 2013; Studer et al., 2015). There is however, an ongoing discussion about the scope of preserved opal flux as productivity proxy and how Fe-limitation influences the Si-uptake ratio in diatom cells (Boutorh et al., 2016; Meyerink et al., 2017; Pichevin et al., 2014). We suggest that the combination of Fe-fertilization in the SAZ together with generally more stratified conditions in the AZ contributed to sequester carbon away from the

atmosphere during past ice ages (Jaccard et al., 2016, 2013; Sigman et al., 2010).

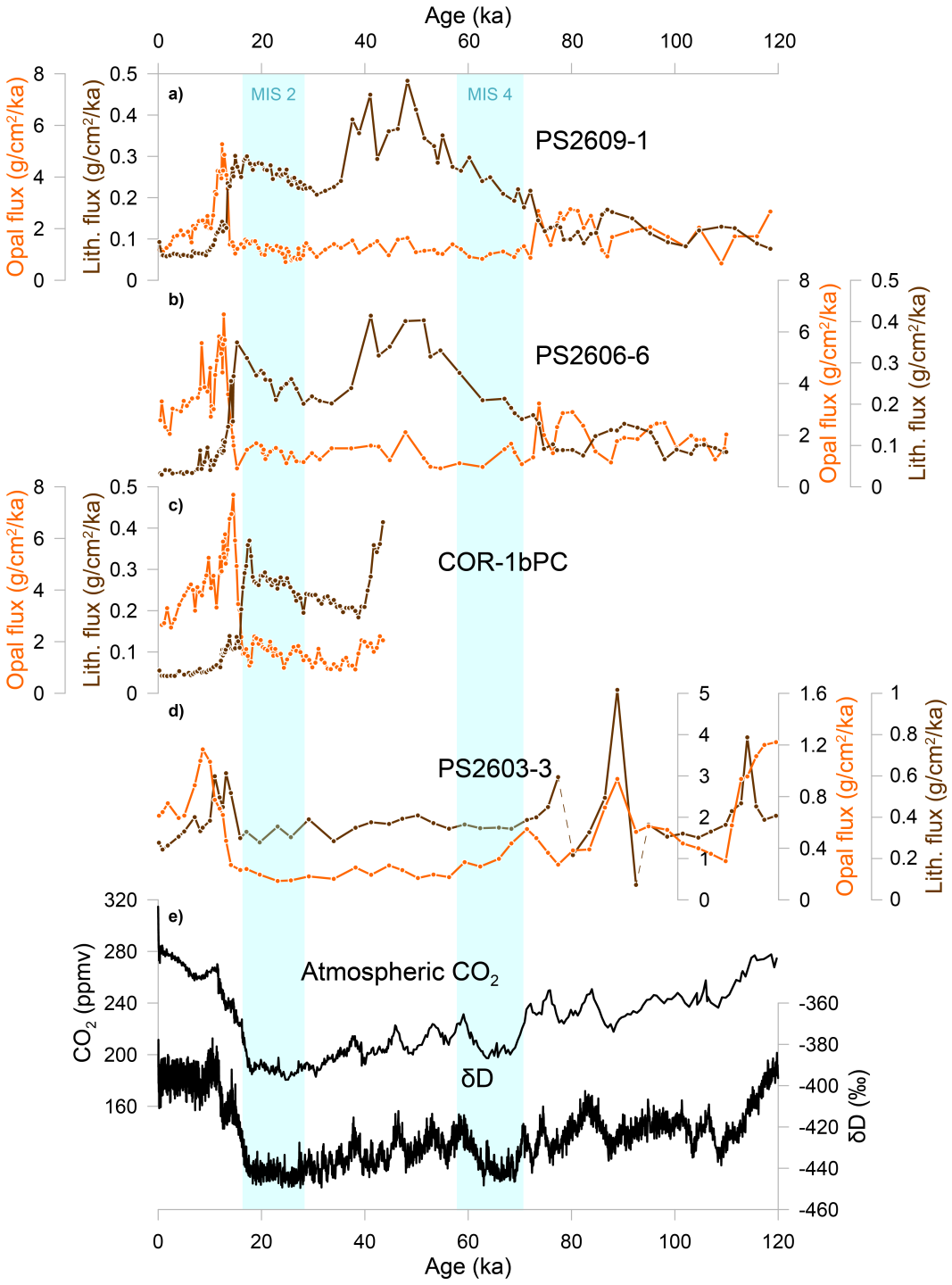

Figure 3.6: a)–d) Lithogenic fluxes and preserved opal fluxes in the Antarctic Zone. e) Atmospheric CO_2 from EPICA Dome C ice core, composite record (Bereiter et al., 2015 *and references therein*) and δD record from EPICA Dome C ice core reflecting Antarctic air temperatures (Jouzel et al., 2007). Light blue bars show cold periods MIS 2 and 4 (Lisiecki and Raymo, 2005).

3.5 Conclusions

In this study the temporal evolution of lithogenic input on a meridional transect of five cores from the Southwestern Indian Ocean was investigated. The core locations span a latitudinal band of around 15°S from north of Del Caño Rise in the SAZ, across Conrad Rise and far into the AZ in the Enderby Abyssal Plain. The lithogenic fluxes were quantified using ^{232}Th, which is relatively enriched in the continental crust and has been shown to record terrigenous input. The results were compared to previously published records from the South Atlantic (Anderson et al., 2014) and the east of Kerguelen Plateau (Thöle et al., 2019) to provide a regional overview of lithogenic fluxes across the last glacial cycle and to investigate additional sources and dynamics.

Our results, which show excellent quantitative agreement between records, suggest that the core site locations were under the influence of more than one source of lithogenic material during the last ice age. Besides dust originating from Patagonia, the SW Indian Ocean most probably also received lithogenic material sourced in southern Africa and/or more locally in agreement with previously published work (Anderson et al., 2014; Thöle et al., 2019). The absolute lithogenic flux values east of the Kerguelen Plateau are slightly higher (max. 0.7–0.8 g/cm^2/ka) than those in the Southwestern Indian Ocean (max. 0.4–0.5 g/cm^2/ka), indicating a direct influence of these ocean islands and bathymetric highs, especially during the cold periods MIS 4 and 2. The seemingly prominent peak during MIS 3 in the AZ of the western cores is in terms of absolute values, comparable to the values in the east (Figure 3.4a). The southernmost core of the Enderby Abyssal Plain shows fluxes with overall higher background values (0.2–0.4 g/cm^2/ka) than the other AZ and SAZ cores (background <0.1 g/cm^2/ka), indicating its proximity to Antarctica to be the cause. Thus, Patagonian, southern African and possibly Antarctic sources are the most probable sources of lithogenic material to the core sites. The glacial peaks in the eastern cores are likely derived from local sources such as the Kerguelen Plateau. Provenance analyses in future work would help distinguish between different sources of lithogenic material.

In the SAZ, fertilization by bioavailable Fe-input through dust is in line with previous studies (Anderson et al., 2014; Lamy et al., 2014; Martin, 1990; Martínez-García et al., 2009, 2014; Thöle et al., 2019). Combined with enhanced

stratification in the AZ during the glacial periods, the Indian sector of the Southern Ocean possibly contributed to sequester carbon away from the atmosphere (Jaccard et al., 2016, 2013; Sigman et al., 2010).

Author contribution

HEA and SLJ designed the study. HEA, LMT, IS, and WG carried out U/Th measurements and evaluation. HEA and GK carried out biogenic opal measurements. MI and GK planned the research expeditions and provided access to the sediment core material. HEA wrote the initial version of the manuscript and all co-authors contributed to the manuscript.

Acknowledgments

We thank the captain, crew members and scientists of the R/V Hakuho-maru and R/V Polarstern for the recovery of the sediment cores during KH-10-7 (lead scientist: M. Ikehara) and ANT-XI/4 cruises (lead scientist: G. Kuhn) to the Southern Ocean, respectively. Furthermore, we thank Martin Wille, Igor Villa, Jörg Rickli, David Janssen, Edel O'Sullivan, Alessandro Maltese, and Sven Kretschmer for their help with the MC-ICP-MS measurements as well as Julijana Krbanjevic and Hendrik Vogel for helping with the biogenic opal measurements. Funding for this study was provided by the Swiss National Science Foundation (grants PP00P2_144811 and 2000021_163003). I. Stimac, W. Geibert, and G. Kuhn were funded by the Alfred-Wegener-Institut Helmholtz-Zentrum für Polar- und Meeresforschung PACES II research program. M. Ikehara was funded by the Japan Society for the Promotion of Science KAKENHI (Grants-in-Aid for Scientific Research P23244102 and JP17H06318). The isotope data was obtained on a Neptune MC-ICP-mass spectrometer acquired with funds from the NCCR PlanetS supported by the Swiss National Science Foundation grant no. 51NF40-141881.

References

Anderson, R.F., Ali, S., Bradtmiller, L.I., Nielsen, S.H.H., Fleisher, M.Q., Anderson, B.E., Burckle, L.H., 2009. Wind-driven Upwelling in the Southern Ocean and the Deglacial Rise in Atmospheric CO_2. Science 323, 1443–1448. doi: 10.1126/science.1167441

Anderson, R.F., Barker, S., Fleisher, M., Gersonde, R., Goldstein, S.L., Kuhn, G., Mortyn, P.G., Pahnke, K., Sachs, J.P., 2014. Biological response to millennial variability of dust and nutrient supply in the Subantarctic South Atlantic Ocean. Philos. Trans. R. Soc. A 372, 20130054. doi: 10.1098/rsta.2013.0054

Anderson, R.F., Fleer, A.P., 1982. Determination of Natural Actinides and Plutonium in Marine Particulate Material. Anal. Chem. 54, 1142–1147. doi: 10.1021/ac00244a030

Bareille, G., Grousset, F.E., Labracherie, M., Labeyrie, L.D., 1994. Origin of detrital fluxes in during the last climatic cycles. Paleoceanography 9, 799–819. doi: 10.1029/94PA01946

Bénard, F., Callot, J.P., Vially, R., Schmitz, J., Roest, W., Patriat, M., Loubrieu, B., 2010. The Kerguelen plateau: Records from a long-living/composite microcontinent. Mar. Pet. Geol. 27, 633–649. doi: 10.1016/j.marpetgeo.2009.08.011

Bereiter, B., Eggleston, S., Schmitt, J., Nehrbass-Ahles, C., Stocker, T.F., Fischer, H., Kipfstuhl, S., Chappellaz, J., 2015. Revision of the EPICA Dome C CO_2 record from 800 to 600 kyr before present. Geophys. Res. Lett. 42, 542–549. doi: 10.1002/2014GL061957

Bourne, M.D., Thomas, A.L., Niocaill, C. Mac, Henderson, G.M., 2012. Improved determination of marine sedimentation rates using $^{230}Th_{xs}$. Geochemistry, Geophys. Geosystems 13, 1. doi: 10.1029/2012GC004295

Boutorh, J., Moriceau, B., Gallinari, M., Ragueneau, O., Bucciarelli, E., 2016. Effect of trace metal-limited growth on the postmortem dissolution of the marine diatom *Pseudo-nitzschia delicatissima*. Global Biogeochem. Cycles 30, 57–69. doi: 10.1002/2015GB005088

Boyd, P.W., Ellwood, M.J., 2010. The biogeochemical cycle of iron in the ocean. Nat. Geosci. 3, 675–682. doi: 10.1038/ngeo964

Boyd, P.W., Watson, A.J., Law, C.S., Abraham, E.R., Trull, T., Murdoch, R., Bakker, D.C.E., Bowie, A.R., Buesseler, K.O., Chang, H., Charette, M., Croot, P., Downing, K., Frew, R., Gall, M., Hadfield, M., Hall, J., Harvey, M., Jameson, G., LaRoche, J., Liddicoat, M., Ling, R., Maldonado, M.T., McKay, R.M., Nodder, S., Pickmere, S., Pridmore, R., Rintoul, S., Safi, K., Sutton, P., Strzepek, R., Tanneberger, K., Turner, S., Waite, A., Zeldis, J., 2000. A mesoscale phytoplankton bloom in the polar Southern Ocean stimulated by iron fertilization. Nature 407, 695–702. doi: 10.1038/35037500

Choi, M.S., Francois, R., Sims, K., Bacon, M.P., Brown-Leger, S., Fleer, A.P., Ball, L., Schneider, D., Pichat, S., 2001. Rapid determination of ^{230}Th and ^{231}Pa in seawater

by desolvated micro-nebulization Inductively Coupled Plasma magnetic sector mass spectrometry. Mar. Chem. 76, 99–112. doi: 10.1016/S0304-4203(01)00050-0

Cortese, G., Gersonde, R., Hillenbrand, C.D., Kuhn, G., 2004. Opal sedimentation shifts in the World Ocean over the last 15 Myr. Earth Planet. Sci. Lett. 224, 509–527. doi: 10.1016/j.epsl.2004.05.035

Costa, K.M., Hayes, C.T., Anderson, R.F., Pavia, F.J., Bausch, A., Deng, F., Dutay, J.C., Geibert, W., Heinze, C., Henderson, G., Hillaire-Marcel, C., Hoffmann, S., Jaccard, S.L., Jacobel, A.W., Kienast, S.S., Kipp, L., Lerner, P., Lippold, J., Lund, D., Marcantonio, F., McGee, D., McManus, J.F., Mekik, F., Middleton, J.L., Missiaen, L., Not, C., Pichat, S., Robinson, L.F., Rowland, G.H., Roy-Barman, M., Tagliabue, A., Torfstein, A., Winckler, G., Zhou, Y., 2020. ^{230}Th normalization: New insights on an essential tool for quantifying sedimentary fluxes in the modern and Quaternary ocean. Paleoceanogr. Paleoclimatology 35, e2019PA003820, 1–36. doi: 10.1029/2019PA003820

Crosta, X., Shukla, S.K., Ther, O., Ikehara, M., Yamane, M., Yokoyama, Y., 2020. Last Abundant Appearance Datum of *Hemidiscus karstenii* driven by climate change. Mar. Micropaleontol. 157. doi: 10.1016/j.marmicro.2020.101861

De Angelis, M., Steffensen, J.P., Legrand, M., Clausen, H., Hammer, C., 1997. Primary aerosol (sea salt and soil dust) deposited in Greenland ice during the last climatic cycle: Comparison with east Antarctic records. J. Geophys. Res. Ocean. 102, 26681–26698. doi: 10.1029/97JC01298

Delmonte, B., Andersson, P.S., Hansson, M., Schöberg, H., Petit, J.R., Basile-Doelsch, I., Maggi, V., 2008. Aeolian dust in East Antarctica (EPICA-Dome C and Vostok): Provenance during glacial ages over the last 800 kyr. Geophys. Res. Lett. 35, 2–7. doi: 10.1029/2008GL033382

Dezileau, L., Bareille, G., Reyss, J.L., Lemoine, F., 2000. Evidence for strong sediment redistribution by bottom currents along the southeast Indian ridge. Deep. Res. Part I Oceanogr. Res. Pap. 47, 1899–1936. doi: 10.1016/S0967-0637(00)00008-X

Duce, R.A., LaRoche, J., Altieri, K., Arrigo, K.R., Baker, A.R., Capone, D.G., Cornell, S., Dentener, F., Galloway, J., Ganeshram, R.S., Geider, R.J., Jickells, T., Kuypers, M.M., Langlois, R., Liss, P.S., Liu, S.M., Middelburg, J.J., Moore, C.M., Nickovic, S., Oschlies, A., Pedersen, T., Prospero, J., Schlitzer, R., Seitzinger, S., Sorensen, L.L., Uematsu, M., Ulloa, O., Voss, M., Ward, B., Zamora, L., 2008. Impacts of atmospheric anthropogenic nitrogen on the open ocean. Science 320, 893–897. doi: 10.1126/science.1150369

Durand, A., Chase, Z., Noble, T.L., Bostock, H., Jaccard, S.L., Kitchener, P., Townsend, A.T., Jansen, N., Kinsley, L., Jacobsen, G., Johnson, S., Neil, H., 2017. Export production in the New-Zealand region since the Last Glacial Maximum. Earth Planet. Sci. Lett. 469, 110–122. doi: 10.1016/j.epsl.2017.03.035

Ferrari, R., Jansen, M.F., Adkins, J.F., Burke, A., Stewart, A.L., Thompson, A.F., 2014. Antarctic sea ice control on ocean circulation in present and glacial climates. Proc. Natl. Acad. Sci. U. S. A. 111, 24, 8753–8758. doi: 10.1073/pnas.1323922111

Fischer, H., Siggaard-Andersen, M.L., Ruth, U., Röthlisberger, R., Wolff, E., 2007. Glacial/interglacial changes in mineral dust and sea-salt records in polar ice cores: Sources, transport, and deposition. Rev. Geophys. 45, 1–26. doi: 10.1029/2005RG000192

François, R., Altabett, M.A., Yu, E.F., Sigman, D.M., Bacon, M.P., Frank, M., Bohrmann, G., Bareille, G., Labeyrie, L.D., 1997. Contribution of Southern Ocean surface-water stratification to low atmospheric CO_2 concentrations during the last glacial period. Nature 389, 929–935. doi: 10.1038/40073

Francois, R., Frank, M., Rutgers van der Loeff, M.M., Bacon, M.P., 2004. ^{230}Th normalization: An essential tool for interpreting sedimentary fluxes during the late Quaternary. Paleoceanography 19, PA1018. doi: 10.1029/2003pa000939

Franzese, A.M., Hemming, S.R., Goldstein, S.L., Anderson, R.F., 2006. Reduced Agulhas Leakage during the Last Glacial Maximum inferred from an integrated provenance and flux study. Earth Planet. Sci. Lett. 250, 72–88. doi: 10.1016/j.epsl.2006.07.002

Frey, F.A., Weis, D., Borisova, A.Y., Xu, G., 2002. Involvement of continental crust in the formation of the Cretaceous Kerguelen Plateau: New perspectives from ODP Leg 120 sites. J. Petrol. 43, 1207–1239. doi: 10.1093/petrology/43.7.1207

Gersonde, R., Crosta, X., Abelmann, A., Armand, L., 2005. Sea-surface temperature and sea ice distribution of the Southern Ocean at the EPILOG Last Glacial Maximum - A circum-Antarctic view based on siliceous microfossil records. Quat. Sci. Rev. 24, 869–896. doi: 10.1016/j.quascirev.2004.07.015

Gili, S., Gaiero, D.M., Goldstein, S.L., Chemale, F., Jweda, J., Kaplan, M.R., Becchio, R.A., Koester, E., 2017. Glacial/interglacial changes of Southern Hemisphere wind circulation from the geochemistry of South American dust. Earth Planet. Sci. Lett. 469, 98–109. doi: 10.1016/j.epsl.2017.04.007

Grousset, F.E., Biscaye, P.E., Revel, M., Petit, J.R., Pye, K., Joussaume, S., Jouzel, J., 1992. Antarctic (Dome C) ice-core dust at 18 k.y. B.P.: Isotopic constraints on origins. Earth Planet. Sci. Lett. 111, 175–182. doi: 10.1016/0012-821X(92)90177-W

Gunn, B.M., Coy-Yll, R., Watkins, N.D., Abranson, C.E., Nougier, J., 1970. Geochemistry of an oceanite-ankaramite-basalt suite from East Island, Crozet Archipelago. Contrib. to Mineral. Petrol. 28, 319–339. doi: 10.1007/BF00388954

Hain, M.P., Sigman, D.M., Haug, G.H., 2010. Carbon dioxide effects of Antarctic stratification, North Atlantic Intermediate Water formation, and subantarctic nutrient drawdown during the last ice age: Diagnosis and synthesis in a geochemical box model. Global Biogeochem. Cycles 24, GB4023, 1–19. doi: 10.1029/2010GB003790

Henderson, G.M., Anderson, R.F., 2003. The U-series toolbox for paleoceanography. Rev. Mineral. Geochemistry 52, 493–531. doi: 10.2113/0520493

Ikehara, M., Katsuki, K., Yamane, M., Yokoyama, Y., Obrochta, S.P., Matsuzaki, T., Sato, H., Kusahara, K., (in prep.). Episodic enhancement of sea ice survivability in

the glacial Southern Ocean driven by Antarctic warming.

Ingle S., D., Weis, Frey, F.A., 2002. Indian Continental Crust Recovered from Elan Bank, Kerguelen Plateau (ODP Leg 183, Site 1137). J. Petrol. 43, 1241–1257. doi: 10.1093/petrology/43.7.1241

Jaccard, S.L., Galbraith, E.D., Martínez-García, A., Anderson, R.F., 2016. Covariation of deep Southern Ocean oxygenation and atmospheric CO_2 through the last ice age. Nature 530, 207–210. doi: 10.1038/nature16514

Jaccard, S.L., Hayes, C.T., Hodell, D.A., Anderson, R.F., Sigman, D.M., Haug, G.H., 2013. Two modes of change in SO Productivity. Science 339, 6126, 1419–1423. doi: 10.1126/science.1227545

Jacobel, A.W., McManus, J.F., Anderson, R.F., Winckler, G., 2016. Large deglacial shifts of the Pacific Intertropical Convergence Zone. Nat. Commun. 7. doi: 10.1038/ncomms10449

Jouzel, J., Masson-Delmotte, V., Cattani, O., Dreyfus, G., Falourd, S., Hoffmann, G., Minster, B., Nouet, J., Barnola, J.M., Chappellaz, J., Fischer, H., Gallet, J.C., Johnsen, S., Leuenberger, M., Loulergue, L., Luethi, D., Oerter, H., Parrenin, F., Raisbeck, G., Raynaud, D., Schilt, A., Schwander, J., Selmo, E., Souchez, R., Spahni, R., Stauffer, B., Steffensen, J.P., Stenni, B., Stocker, T.F., Tison, J.L., Werner, M., Wolff, E.W., 2007. Orbital and millennial antarctic climate variability over the past 800,000 years. Science 317, 5839, 793–796. doi: 10.1126/science.1141038

Kienast, S.S., Winckler, G., Lippold, J., Albani, S., Mahowald, N.M., 2016. Tracing dust input to the global ocean using thorium isotopes in marine sediments: ThoroMap. Global Biogeochem. Cycles 30, 1526–1541. doi: 10.1002/2016GB005408

Kohfeld, K.E., Harrison, S.P., 2001. DIRTMAP: The geological record of dust. Earth-Science Rev. 54, 81–114. doi: 10.1016/S0012-8252(01)00042-3

Kuhn, G., 2003. Documentation of sediment core PS2603-3. Alfred Wegener Institute - Polarstern core repository, *PANGAEA*. doi: 10.1594/PANGAEA.115375

Kumar, N., Anderson, R.F., Mortlock, R.A., Froelich, P.N., Kubik, P., Dittrich-Hannen, B., Suter, M., 1995. Increased biological production and export in the glacial Southern Ocean. Nature 378, 675–680. doi: 10.1038/378675a0

Lambert, F., Bigler, M., Steffensen, J.P., Hutterli, M., Fischer, H., 2012. Centennial mineral dust variability in high-resolution ice core data from Dome C, Antarctica. Clim. Past 8, 609–623. doi: 10.5194/cp-8-609-2012

Lambert, F., Delmonte, B., Petit, J.R., Bigler, M., Kaufmann, P.R., Hutterli, M.A., Stocker, T.F., Ruth, U., Steffensen, J.P., Maggi, V., 2008. Dust - Climate couplings over the past 800,000 years from the EPICA Dome C ice core. Nature 452, 616–619. doi: 10.1038/nature06763

Lamy, F., Gersonde, R., Winckler, G., Esper, O., Jaeschke, A., Kuhn, G., Ullermann, J., Martínez-García, A., Lambert, F., Kilian, R., 2014. Increased dust deposition in the Pacific Southern Ocean during glacial periods. Science 343, 403–407. doi:

10.1126/science.1245424

Li, F., Ginoux, P., Ramaswamy, V., 2008. Distribution, transport, and deposition of mineral dust in the Southern Ocean and Antarctica: Contribution of major sources. J. Geophys. Res. Atmos. 113, 1–15. doi: 10.1029/2007JD009190

Lippold, J., Grützner, J., Winter, D., Lahaye, Y., Mangini, A., Christi, M., 2009. Does sedimentary $^{231}Pa/^{230}Th$ from the Bermuda Rise monitor past Atlantic Meridional Overturning Circulation? Geophys. Res. Lett. 36, L12601, 1–6. doi: 10.1029/2009GL038068

Lisiecki, L.E., Raymo, M.E., 2005. A Pliocene-Pleistocene stack of 57 globally distributed benthic $\delta^{18}O$ records. Paleoceanography 20, PA1003, 1–17. doi: 10.1029/2004PA001071

Lunt, D.J., Valdes, P.J., 2002. The modern dust cycle: Comparison of model results with observations and study of sensitivities. J. Geophys. Res. Atmos. 107, AAC 1-1-AAC 1-16. doi: 10.1029/2002JD002316

Lutjeharms, J.R.E., Ansorge, I.J., 2001. The Agulhas Return Current. J. Mar. Syst. 30, 115–138. doi: 10.1016/S0924-7963(01)00041-0

Maher, B.A., Prospero, J.M., Mackie, D., Gaiero, D., Hesse, P.P., Balkanski, Y., 2010. Global connections between aeolian dust, climate and ocean biogeochemistry at the present day and at the last glacial maximum. Earth-Science Rev. 99, 61–97. doi: 10.1016/j.earscirev.2009.12.001

Mahowald, N., Kohfeld, K., Hansson, M., Balkanski, Y., Harrison, S.P., Prentice, I.C., Schulz, M., Rodhe, H., 1999. Dust sources and deposition during the last glacial maximum and current climate: A comparison of model results with paleodata from ice cores and marine sediments. J. Geophys. Res. Atmos. 104, 15895–15916. doi: 10.1029/1999JD900084

Mahowald, N.M., Kiehl, L.M., 2003. Mineral aerosol and cloud interactions. Geophys. Res. Lett. 30, 9, 1475. doi: 10.1029/2002GL016762

Mahowald, N.M., Muhs, D.R., Levis, S., Rasch, P.J., Yoshioka, M., Zender, C.S., Luo, C., 2006. Change in atmospheric mineral aerosols in response to climate: Last glacial period, preindustrial, modern, and doubled carbon dioxide climates. J. Geophys. Res. Atmos. 111. doi: 10.1029/2005JD006653

Manoj, M.C., Thamban, M., 2015. Shifting frontal regimes and its influence on bioproductivity variations during the Late Quaternary in the Indian sector of Southern Ocean. Deep. Res. Part II Top. Stud. Oceanogr. 118, 261–274. doi: 10.1016/j.dsr2.2015.03.011

Marsh, R., Mills, R.A., Green, D.R.H., Salter, I., Taylor, S., 2007. Controls on sediment geochemistry in the Crozet region. Deep. Res. Part II Top. Stud. Oceanogr. 54, 2260–2274. doi: 10.1016/j.dsr2.2007.06.004

Martin, J.H., 1990. Glacial-interglacial CO_2 change: The Iron Hypothesis. Paleoceanography 5, 1–13. doi: 10.1029/PA005i001p00001

Martínez-García, A., Rosell-Melé, A., Geibert, W., Gersonde, R., Masqué, P., Gaspari,

V., Barbante, C., 2009. Links between iron supply, marine productivity, sea surface temperature, and CO_2 over the last 1.1 Ma. Paleoceanography 24, 1–14. doi: 10.1029/2008PA001657

Martínez-García, A., Sigman, D.M., Ren, H., Anderson, R.F., Straub, M., Hodell, D.A., Jaccard, S.L., Eglinton, T.I., Haug, G.H., 2014. Iron fertilization of the Subantarctic Ocean during the Last Ice Age. Science 343, 1347–1350. doi: 10.1126/science.1246848

Mazaud, A., Michel, E., Dewilde, F., Turon, J.L., 2010. Variations of the Antarctic Circumpolar Current intensity during the past 500 ka. Geochemistry, Geophys. Geosystems 11, 1–10. doi: 10.1029/2010GC003033

McGee, D., Broecker, W.S., Winckler, G., 2010. Gustiness: The driver of glacial dustiness? Quat. Sci. Rev. 29, 2340–2350. doi: 10.1016/j.quascirev.2010.06.009

McGee, D., Marcantonio, F., Lynch-Stieglitz, J., 2007. Deglacial changes in dust flux in the eastern equatorial Pacific. Earth Planet. Sci. Lett. 257, 215–230. doi: 10.1016/j.epsl.2007.02.033

McGee, D., Winckler, G., Borunda, A., Serno, S., Anderson, R.F., Recasens, C., Bory, A., Gaiero, D., Jaccard, S.L., Kaplan, M., McManus, J.F., Revel, M., Sun, Y., 2016. Tracking eolian dust with helium and thorium: Impacts of grain size and provenance, Geochim. Cosmochim. Acta. Elsevier Ltd. doi: 10.1016/j.gca.2015.11.023

Meyerink, S.W., Ellwood, M.J., Maher, W.A., Dean Price, G., Strzepek, R.F., 2017. Effects of iron limitation on silicon uptake kinetics and elemental stoichiometry in two Southern Ocean diatoms, *Eucampia antarctica* and *Proboscia inermis*, and the temperate diatom *Thalassiosira pseudonana*. Limnol. Oceanogr. 62, 6, 2445–2462. doi: 10.1002/lno.10578

Müller, P.J., Schneider, R., 1993. An automated leaching method for the determination of opal in sediments and particulate matter. Deep. Res. Part I 40, 3, 425–444. doi: 10.1016/0967-0637(93)90140-X

Nair, A., Mohan, R., Crosta, X., Manoj, M.C., Thamban, M., Marieu, V., 2019. Southern Ocean sea ice and frontal changes during the Late Quaternary and their linkages to Asian summer monsoon. Quat. Sci. Rev. 213, 93–104, doi: 10.1016/j.quascirev.2019.04.007

Oiwane, H., Ikehara, M., Suganuma, Y., Miura, H., Nakamura, Y., Sato, T., Nogi, Y., Yamane, M., Yokoyama, Y., 2014. Sediment waves on the Conrad Rise, Southern Indian Ocean: Implications for the migration history of the Antarctic Circumpolar Current. Mar. Geol. 348, 27–36. doi: 10.1016/j.margeo.2013.10.008

Orsi, H., Whitworth, T., Nowlin Jr, W.D., 1995. On the meridional extent and fronts of the Antarctic Circumpolar Current. Deep. Res. Part I 42, 5, 641–673. doi: 10.1016/0967-0637(95)00021-W

Pichat, S., Sims, K.W.W., François, R., McManus, J.F., Leger, S.B., Albarède, F., 2004. Lower export production during glacial periods in the equatorial Pacific

derived from $(^{231}Pa/^{230}Th)_{xs,0}$ measurements in deep-sea sediments. Paleoceanography 19, PA4023, 1–21. doi: 10.1029/2003PA000994

Pichevin, L.E., Ganeshram, R.S., Geibert, W., Thunell, R., Hinton, R., 2014. Silica burial enhanced by iron limitation in oceanic upwelling margins. Nat. Geosci. 7, 541–546. doi: 10.1038/ngeo2181

Ragueneau, O., Tréguer, P., Leynaert, A., Anderson, R.F., Brzezinski, M.A., DeMaster, D.J., Dugdale, R.C., Dymond, J., Fischer, G., François, R., Heinze, C., Maier-Reimer, E., Martin-Jézéquel, V., Nelson, D.M., Quéguiner, B., 2000. A review of the Si cycle in the modern ocean: Recent progress and missing gaps in the application of biogenic opal as a paleoproductivity proxy. Glob. Planet. Change 26, 317–365. doi: 10.1016/S0921-8181(00)00052-7

Rea, D.K., 1994. The paleoclimatic record provided by eolian deposition in the deep sea: The geologic history of wind. Rev. Geophys. 32, 159–195. doi: 10.1029/93RG03257

Reader, M.C., Fung, I., McFarlane, N., 1999. The mineral dust aerosol cycle during the Last Glacial Maximum. J. Geophys. Res. Atmos. 104, 9381–9398. doi: 10.1029/1999JD900033

Ronge, T.A., Prange, M., Mollenhauer, G., Ellinghausen, M., Kuhn, G., Tiedemann, R., 2020. Radiocarbon Evidence for the Contribution of the Southern Indian Ocean to the Evolution of Atmospheric CO_2 Over the Last 32,000 Years. Paleoceanogr. Paleoclimatology 35. doi: 10.1029/2019PA003733

Russo, C.J., Rubin, K.H., Graham, D.W., 2009. Mantle melting and magma supply to the Southeast Indian Ridge: The roles of lithology and melting conditions from U-series disequilibria. Earth Planet. Sci. Lett. 278, 55–66, https://doi:10.1016/j.epsl.2008.11.016

Ruth, U., Bigler, M., Röthlisberger, R., Siggaard-Andersen, M.L., Kipfstuhl, S., Goto-Azuma, K., Hansson, M.E., Johnsen, S.J., Lu, H., Steffensen, J.P., 2007. Ice core evidence for a very tight link between North Atlantic and east Asian glacial climate. Geophys. Res. Lett. 34, 1–5. doi: 10.1029/2006GL027876

Sayles, F.L., Martin, W.R., Chase, Z., Anderson, R.F., 2001. Benthic remineralization and burial of biogenic SiO_2, $CaCO_3$, organic carbon, and detrital material in the Southern Ocean along a transect at 170° West. Deep. Res. Part II Top. Stud. Oceanogr. 48, 19–20, 4323–4383. doi: 10.1016/S0967-0645(01)00091-1

Serno, S., Winckler, G., Anderson, R.F., Hayes, C.T., McGee, D., Machalett, B., Ren, H., Straub, S.M., Gersonde, R., Haug, G.H., 2014. Eolian dust input to the Subarctic North Pacific. Earth Planet. Sci. Lett. 387, 252–263. doi: 10.1016/j.epsl.2013.11.008

Sicre, M.A., Labeyrie, L., Ezat, U., Mazaud, A., Turon, J.L., 2006. A 27 kyr terrestrial biomarker record in the southern Indian Ocean. Geochemistry, Geophys. Geosystems 7. doi: 10.1029/2005GC001234

Sigman, D.M., Hain, M.P., Haug, G.H., 2010. The polar ocean and glacial cycles in

atmospheric CO_2 concentration. Nature 466, 7302, 47–55. doi: 10.1038/nature09149

Skinner, L.C., Fallon, S., Waelbroeck, C., Michel, E., Barker, S., 2010. Ventilation of the Deep Southern Ocean and Deglacial CO_2 Rise. Science 328, 5982, 1147–1151. doi: 10.1126/science.1183627

Studer, A.S., Sigman, D.M., Martínez-García, A., Benz, V., Winckler, G., Kuhn, G., Esper, O., Lamy, F., Jaccard, S.L., Wacker, L., Oleynik, S., Gersonde, R., Haug, G.H., 2015. Antarctic Zone nutrient conditions during the last two glacial cycles. Paleoceanography 30, 845–862. doi: 10.1002/2014PA002745

Sugden, D.E., McCulloch, R.D., Bory, A.J.M., Hein, A.S., 2009. Influence of Patagonian glaciers on Antarctic dust deposition during the last glacial period. Nat. Geosci. 2, 281–285. doi: 10.1038/ngeo474

Takemura, T., Egashira, M., Matsuzawa, K., Ichijo, H., O'Ishi, R., Abe-Ouchi, A., 2009. A simulation of the global distribution and radiative forcing of soil dust aerosols at the Last Glacial Maximum. Atmos. Chem. Phys. 9, 3061–3073. doi: 10.5194/acp-9-3061-2009

Taylor, S.R., McLennan, S.M., 1995. The geochemical the continental evolution crust. Rev. Mineral. Geochemistry 33, 241–265

Tegen, I., Lacis, A.A., 1996. Modeling of particle size distribution and its influence on the radiative properties of mineral dust aerosol. J. Geophys. Res. Atmos. 101, 19237–19244. doi: 10.1029/95jd03610

Thöle, L.M., Amsler, H.E., Moretti, S., Auderset, A., Gilgannon, J., Lippold, J., Vogel, H., Crosta, X., Mazaud, A., Michel, E., Martínez-García, A., Jaccard, S.L., 2019. Glacial-interglacial dust and export production records from the Southern Indian Ocean. Earth Planet. Sci. Lett. 525. doi: 10.1016/j.epsl.2019.115716

Toggweiler, J.R., Russell, J.L., Carson, S.R., 2006. Midlatitude westerlies, atmospheric CO_2, and climate change during the ice ages. Paleoceanography 21, 1–15. doi: 10.1029/2005PA001154

Vogel, H., Meyer-Jacob, C., Thöle, L., Lippold, J.A., Jaccard, S.L., 2016. Quantification of biogenic silica by means of Fourier transform infrared spectroscopy (FTIRS) in marine sediments. Limnol. Oceanogr. Methods 14, 828–838. doi: 10.1002/lom3.10129

Watson, A.J., Bakker, D.C.E., Ridgwell, A.J., Boyd, P.W., Law, C.S., 2000. Effect of iron supply on Southern Ocean CO_2 uptake and implications for glacial atmospheric CO_2. Nature 407, 730–733. doi: 10.1038/35037561

Wengler, M., Lamy, F., Struve, T., Borunda, A., Böning, P., Geibert, W., Kuhn, G., Pahnke, K., Roberts, J., Tiedemann, R., Winckler, G., 2019. A geochemical approach to reconstruct modern dust fluxes and sources to the South Pacific. Geochim. Cosmochim. Acta 264, 205–223. doi: 10.1016/j.gca.2019.08.024

Werner, M., Tegen, I., Harrison, S.P., Kohfeld, K.E., Prentice, I.C., Balkanski, Y., Rodhe, H., Roelandt, C., 2002. Seasonal and interannual variability of the mineral dust cycle under present and glacial climate conditions. J. Geophys. Res. Atmos.

107, D24, 4744. doi: 10.1029/2002JD002365

Winckler, G., Anderson, R.F., Fleisher, M., McGee, D., Mahowald, N., 2008. Covariant Glacial-Interglacial Dust Fluxes. Science 320, 93–96. doi: 10.1126/science.1150595

Xiao, W., Esper, O., Gersonde, R., 2016. Last Glacial - Holocene climate variability in the Atlantic sector of the Southern Ocean. Quat. Sci. Rev. 135, 115–137. doi: 10.1016/j.quascirev.2016.01.023

CHAPTER 4

Strong variations in ACC flow dynamics across the last glacial cycle in the Southern Indian Ocean

H. Eri Amsler[a,b], Nicole Schmid[a,b], Lena M. Thöle[a,b,c], Gerhard Kuhn[d], Minoru Ikehara[e], I. Nick McCave[f], Samuel L. Jaccard[a,b]

[a]Institute of Geological Sciences, University of Bern, Switzerland
[b]Oeschger Centre for Climate Change Research, University of Bern, Switzerland
[c]Department of Earth Sciences, Utrecht University, the Netherlands
[d]Alfred-Wegener-Institut Helmholtz-Zentrum für Polar- und Meeresforschung, Bremerhaven, Germany
[e]Center for Advanced Marine Core Research, Kochi University, Japan
[f]Godwin Laboratory for Palaeoclimate Research, Department of Earth Sciences, University of Cambridge, UK

in preparation

ABSTRACT

The Antarctic Circumpolar Current (ACC) connects all ocean basins and enables upwelling of deep-water masses, connecting the deep and shallow layers of the Southern Ocean and promoting large-scale air-sea CO_2 exchange. On glacial-interglacial timescales, meridional frontal migration and/or changes in the strength of the ACC flow have been proposed to modulate upwelling intensity, and thus global climate.

We present sortable silt records in four marine sediment cores retrieved along a meridional transect across the ACC in the western part of the Southern Indian Ocean. The highly resolved downcore records cover the last glacial cycle and allow reconstructing the spatio-temporal variability of ACC flow dynamics in a region where the ACC flow path is largely influenced by complex bathymetry. At each core location, spanning the Subantarctic (SAZ) and Antarctic (AZ) zones of the Southern Ocean, mean bottom water flow has varied between 10 and 15 cm/s across the last glacial cycle. Our results are consistent with a northward shift as well as an overall strengthening of the ACC during glacial periods. Abrupt changes in near-bottom flow intensity argue for the ACC overcoming bathymetrical constraints. Contrasting bottom flow dynamics show the ACC's complex behavior and the importance of seabed topography in directing the flow path. A glacial equatorward shift of the ACC, combined with intensified flow may have contributed to modulate oceanic CO_2 sequestration with counterbalancing effects. Despite being more intensive, upwelling of shallower, CO_2-depleted water masses might have played a role in reducing the release of previously sequestered CO_2 and thereby contributing to maintenance of reduced atmospheric CO_2 levels.

4.1 Introduction

The Antarctic Circumpolar Current (ACC) is a dominant feature of the global ocean circulation and thus plays an important role in the climate system (e.g. Rintoul et al., 2001; Rintoul, 2018; Talley, 2013). Uninhibited by land barriers, the ACC flows eastwards around Antarctica, connecting all major ocean basins and (re)distributing heat, fresh water, (micro)nutrients and carbon around the globe (Marshall and Speer, 2012; Rintoul et al., 2001). The ACC is a deep-

reaching current, partly constrained by the complex bathymetry around Antarctica (Gille et al., 2004; Gordon et al., 1978; Marshall and Speer, 2012; Orsi et al., 1995; Rintoul, 2018; Rintoul et al., 2001). The meridional extent of the circumpolar current ranges from the Subtropical Front (STF) in the north to the Southern boundary of the ACC (SBy) towards Antarctica (Orsi et al., 1995). Within these boundaries, the ACC is accompanied by regions of strong flow regimes, characterized as oceanographic fronts, including the Subantarctic Front (SAF), Polar Front (PF), and Southern ACC Front (SACCF), separating water masses with distinct physicochemical properties (Orsi et al., 1995). As such, the ACC is not a meridionally uniform flow, but rather a vigorously eddying current, characterized by a braided structure (Chapman et al., 2020; Marshall and Speer, 2012). A major part of the ACC's transport occurs within these fronts, driven by wind stress at the surface (Allison et al., 2010; Marshall and Speer, 2012; Rintoul et al., 2001; Toggweiler and Russell, 2008) as well as by buoyancy forcing associated with heat gain and freshwater supply (Marshall and Speer, 2012; Watson and Naveira Garabato, 2006). As a result of the strong wind stress exerted across the Southern Ocean by the southern hemisphere westerly winds (SHW), approximately at 45°–50°S (Toggweiler and Russell, 2008), surface waters are transported northwards by Ekman flow, leading to upwelling of old, nutrient-rich subsurface waters along tilted isopycnals (Marshall and Speer, 2012; Rintoul et al., 2001; Talley, 2013). These southward rising isopycnals act as conduits for deep water to be transported to the surface ocean, thereby modulating air-sea partitioning of CO_2. Therefore, changes in ACC dynamics have been proposed to play an important role in driving glacial-interglacial climate variability (e.g. Lamy et al., 2014; McCave et al., 2014; Sigman et al., 2010).

However, there is no consensus as to how the SHW have evolved during past ice ages (Chavaillaz et al., 2013; Kohfeld et al., 2013), and the associated response of the ACC is still debated (Franzese et al., 2006; Lamy et al., 2015; Manoj and Thamban, 2015; Mazaud et al., 2010; McCave et al., 2014; Molyneux et al., 2007; Pahnke et al., 2003; Toyos et al., 2020). Similarly, the future evolution of the SHW in response to anthropogenic climate forcing remains debated (e.g. Fyfe and Saenko, 2006; Saenko et al., 2005; Toggweiler and Russell, 2008; Tschumi et al., 2008). It is thus important to gain further insight on the spatio-temporal evolution of ACC dynamics to better understand their sensitivity to

different climate boundary conditions and identify major drivers of change (Gottschalk et al., 2019).

To date, limited data on paleocurrent intensity are available and most observations are based on sortable silt records using marine sediment cores retrieved from the Drake Passage and adjacent Scotia Sea (Lamy et al., 2015; McCave et al., 2014; Roberts et al., 2017; Toyos et al., 2020), the SE Atlantic basin (Krueger et al., 2012; Martínez-Méndez et al., 2008; Molyneux et al., 2007) and to a much lesser extent, the Indian sector of the Southern Ocean (Mazaud et al., 2010).

Around the Drake Passage, paleoceanographic reconstructions signal a slowdown of bottom current intensities during glacial periods, consistent with a northward deflection of the ACC along the western margin of South America (Lamy et al., 2015; McCave et al., 2014; Roberts et al., 2017; Toyos et al., 2020). On the other hand, Mazaud et al. (2010) have suggested a faster flow in the Indian Ocean east of Kerguelen Plateau during glacial times for the last 500 ka, based on magnetic grain size variation and abundance. However, these recorded variations in magnetic properties could reflect fluctuations in current strength, but also changes in the source and nature of magnetic minerals, bacterial activity and IRD input (Channell et al., 2016). Closer to the African continent in the SE Atlantic, further studies have reported stronger glacial near-bottom flow speeds based on sortable silt records for the southern Agulhas Plateau and the western slope of Agulhas Bank off South Africa (Krueger et al., 2012; Martínez-Méndez et al., 2008; Molyneux et al., 2007).

Since both local and regional considerations have to be taken into account to provide a synoptic reconstruction on past changes in ACC dynamics, it is difficult to get robust insights based on single core locations. Here, we use a transect of four marine sediment cores spanning the major oceanic fronts in the Southern Indian Ocean. To reconstruct the spatio-temporal variability of the ACC dynamics over the past glacial cycle, we use sortable silt mean size ($\overline{\text{SS}}$) as a direct proxy for changes in relative bottom current speed.

4.2 Study site, materials and methods

4.2.1 Core locations and material

Our study comprises sortable silt records of four marine sediment cores, retrieved along a meridional transect in the SW Indian Ocean (Figure 4.1). Core DCR-1PC (46°01.34'S, 44°15.24'E, 2632 mbsl) was recovered during expedition KH-10-7 on R/V Hakuho-maru in 2010–2011 on the southern flank of Del Caño Rise. The core lies in the Subantarctic Zone (SAZ) just north of today's position of the Subantarctic Front (SAF) and is composed of nannofossil and diatom ooze with variable amounts of clay.

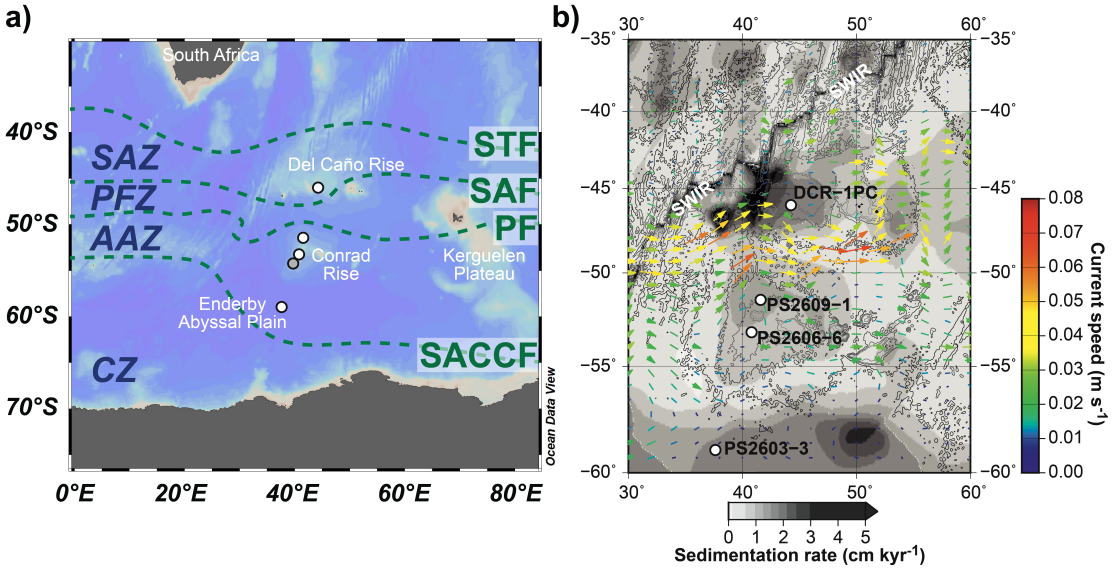

Figure 4.1: Study region with core locations (white circles) and surrounding ocean highs. a) Bathymetry and approximate positions of today's main oceanic fronts from north to south (Orsi et al., 1995): Subtropical Front (STF), Subantarctic Front (SAF), Polar Front (PF), and the Southern ACC Front (SACCF); the zones between these fronts are defined as the Subantarctic (SAZ), Polar Frontal (PFZ), Antarctic (AZ), and Continental zones (CZ) (plotted with the ODV-software, Schlitzer, 2018). b) Contoured bathymetric map (courtesy of J. Gottschalk) illustrating the average speed (colors) and direction (vectors) of ocean currents at mid-depth (1.0–3.5 km) based on the Global Ocean Data Assimilation System (GODAS) data base (NOAA/OAR/ESRL PSD, Boulder, Colorado, USA; www.esrl.noaa.gov/psd/), i.e., the pathway of the Antarctic Circumpolar Current (ACC) core at mid-depth (Park et al., 2008). The study area is located south of the Southwest Indian Ridge (SWIR), grey shading indicate simulated sedimentation rate patterns (Dutkiewicz et al., 2016).

Cores PS2609-1 (51°29.9'S, 41°35.8'E, 3113 mbsl), PS2606-6 (53°13.9'S, 40°48.1'E, 2545 mbsl) and PS2603-3 (58°59.2'S, 37°37.7'E, 5289 mbsl) were

collected during ANT-XI/4 expedition on R/V Polarstern in 1994. PS2609-1 and PS2606-6 were retrieved from Conrad Rise and PS2603-3 from the Enderby Abyssal Plain. These three cores all lie in the Antarctic Zone (AZ) between the Polar Front (PF) to the north and the Southern ACC Front (SACCF) to the south. They consist predominantly of diatom ooze with little detrital material (Kuhn, 2003a, 2003b, 2003c).

In the Indian sector of the Southern Ocean the oceanic fronts show a complex structure as a result of the seabed topography (Durgadoo et al., 2008; Katsuki et al., 2012; Pollard et al., 2007; Pollard and Read, 2001; Sokolov and Rintoul, 2009) (Figure 4.1a). Today, the ACC branches on the western side of Conrad Rise, forming two intense jets around the rise. At Del Caño Rise the current is guided around the south of the rise (Pollard et al., 2007) (Figure 4.1b).

4.2.2 Age models

The age models are based on different approaches for each core (see Chapter 2). Briefly, for DCR-1PC seven ^{14}C-dates were determined and additional tiepoints were defined from comparing the diatom-based summer sea surface temperature (SST) record to the EDC δD local temperature record, assuming in-phase temporal evolution (Crosta et al., 2020). The age models for PS2609-1, PS2606-6, and PS2603-3 are based on tiepoints determined from graphical alignment of magnetic susceptibility and XRF-data (Fe, Si, Ti, Ca) to the LR04 δ^{18}O stack (Lisiecki and Raymo, 2005) and XRF-data (Ti) to the EDC dust record (Lambert et al., 2012), assuming synchronous temporal variability. In the two southernmost cores PS2606-6 and PS2603-3, ^{14}C-data (Ronge et al., 2020; Xiao et al., 2016) and diatom species extinction events provided additional tiepoints.

4.2.3 Sortable silt

Changes in the mean size of terrigenous silt in the grain size fraction between 10 and 63 µm within current-sorted marine sediments, are considered to robustly record past variations in near-bottom flow speeds (e.g. Bianchi et al., 1999; McCave et al., 2017, 1995; Tegzes et al., 2015). Coarser sediment compositions indicate intervals of higher flow intensity, whereas smaller grain sizes are consistent with slower bottom currents. The signal arises from selective deposition under different flow regimes; faster currents maintain fine grains in

suspension and only coarser grains can settle, whereas generally slower currents allow successively finer sediment grains to be sedimented. As ocean currents rarely transport grains larger than 63 µm, this defines the upper limit of the proxy. On the lower end, finer silt and clay particles (<10 µm) tend to behave cohesively, acting as aggregates and are thus not suitable to record past changes in current intensities (McCave et al., 1995).

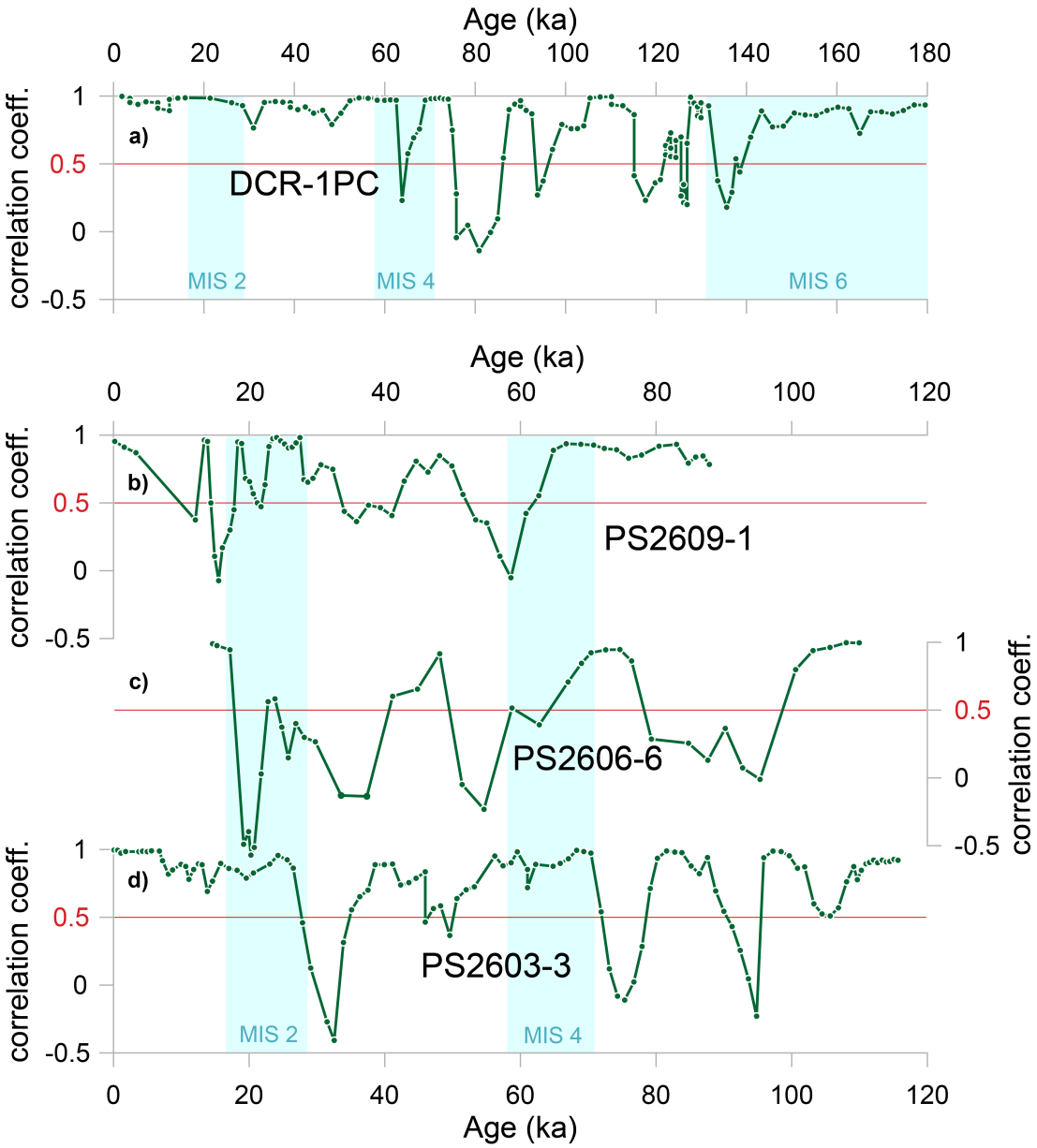

Figure 4.2: Running downcore correlation (7-point) between sortable silt mean size and sortable silt percentage. The red line represents the correlation coefficient r = 0.5. Only sediment samples above this line are considered current-sorted and used in Figure 4.3. Light blue bars show cold periods MIS 2, 4, and 6 (Lisiecki and Raymo, 2005).

If the deposition rate of finer material (<10 µm) decreases with faster bottom currents, the ratio of 10–63 µm material to the total fine fraction (all grains <63 µm), is expected to increase with current speed. Thus, in current-sorted sediments, sortable silt mean size ($\overline{SS}$) correlates linearly with the percentage of sortable silt (SS%) in the fine fraction (McCave et al., 1995; McCave and Andrews, 2019). Therefore, the degree of correlation can be used as an indication of the sediment being sorted by bottom currents (McCave and Andrews, 2019) (Figure 4.2).

To prepare the samples for sortable silt analysis, 1 g of freeze-dried sediment was wet sieved through a 63 µm net. After a one-week settling time, the samples were transferred to centrifuge tubes in a disaggregating solution (0.2% Calgon, $(NaPO_3)_6$). The organic matter, carbonate, and biogenic silica fractions were successively dissolved in a series of chemical treatments using 10% H_2O_2, 1M acetic acid, and 20% NaOH, respectively, separated by multiple steps of rinsing and vortexing. Remaining diatom frustules were physically removed by density separation using sodium polytungstate (SPT) at a density of 2.25 g/cm^3. The samples were kept in Calgon to help the samples disperse until measurement on a Malvern Mastersizer 2000 laser diffractometer (Sperazza et al., 2004) at the Institute of Geography (GIUB), University of Bern.

The grain sizes are computed by the level and angle of scattering of light energy of a specific wavelength by the grains (Sperazza et al., 2004). The Mastersizer 2000 utilizes Mie theory to convert this scatter to grain size and reports grain-size distributions as volume percentage for each size bin. The grain sizes are reported in 0.5 to 1 µm step size bins from 10–63 µm. The geometric mean of each size bin was used for computing the sortable silt mean size (McCave and Andrews, 2019). Three internal standards were processed along every batch of 37 sediment samples. The procedural error of two of these three standards yielded a standard deviation of less than 2%. Yet for the third internal standard, the error was somewhat higher (8.23%). The analytical error was estimated using a poorly sorted glacial sediment collected in Sillikers (Bista et al., 2016) and yielded a standard deviation of 1.37%.

4.3 Results

The downcore comparison between $\overline{SS}$ and SS% does neither follow a typical glacial-interglacial pattern, nor does it correlate with sortable silt mean size itself (Figure 4.2). Thus, for samples with a correlation coefficient above 0.5, we assume that downcore variations in $\overline{SS}$ are primarily driven by current sorting and not by changes in the sediment source, for instance (McCave and Andrews, 2019).

In SAZ core DCR-1PC, $\overline{SS}$ values vary between 20-29 µm, with generally higher values during warm periods and comparatively lower values during colder periods (Figure 4.3a). MIS 6 is characterized by intermediate $\overline{SS}$ values (hovering around 25–27 µm) preceding an abrupt increase at the onset of the penultimate glacial termination (MIS 6/5). The record reaches the highest $\overline{SS}$ values (26–29 µm) during MIS 5 with transient decreases between 115 and 110 ka, possibly corresponding to MIS 5d. The $\overline{SS}$ levels show a sudden decrease to relatively low grain size values (20–22 µm) at the MIS 5/4 transition and remain low throughout MIS 3 and MIS 2. After a sharp rise during the last glacial termination, $\overline{SS}$ values decrease steadily during the Holocene.

In the AZ, the sediment mainly consists of diatom ooze. Thus, some of the samples yielded too little detrital material to allow for reproducible grain size analyses. Therefore, some samples could not be measured and the $\overline{SS}$ records are accordingly somewhat fragmentary, especially for core PS2606-6. Nevertheless, the three AZ cores show a generally consistent pattern with characteristically high $\overline{SS}$ values during cold periods and comparatively lower values during warm intervals. Sediment cores PS2609-1 and PS2606-6 generally show grain size values ranging between 18 and 26 µm and southernmost core PS2603-3 between 14 and 24 µm. All three cores show a distinct increase in $\overline{SS}$ during MIS 4, whereas during MIS 2 an increase is only clearly visible in PS2609-1. The lowest values in PS2603-3 during 90–80 ka of around 14–16 µm may coincide with a sediment disturbance (see Chapters 2 and 3).

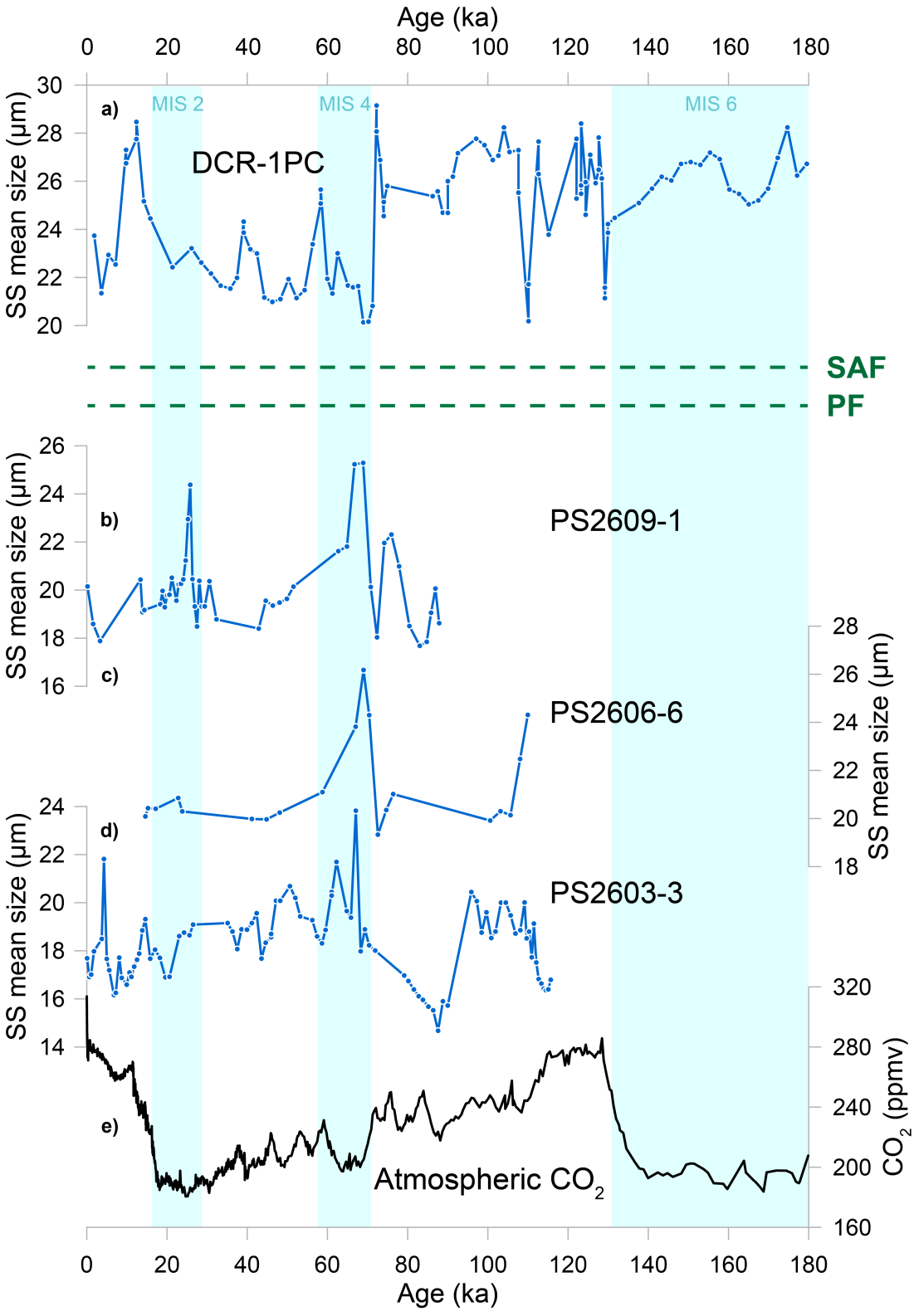

Figure 4.3: a)–d) Sortable silt mean size ($\overline{SS}$) of all four cores. Only samples with a downcore correlation coefficient of r >0.5 are shown. Higher $\overline{SS}$ values translate to stronger current speeds. e) Atmospheric CO_2 from EPICA Dome C ice core, composite record (Bereiter et al., 2015 *and references therein*). Light blue bars show cold periods MIS 2, 4, and 6 (Lisiecki and Raymo, 2005). Green dashed lines schematically show today's position of the Subantarctic Front (SAF) and Polar Front (PF).

4.4 Interpretation and discussion

The $\overline{SS}$ range spans 8–10 µm within each core, which translates into near-bottom current speed changes of around 10–15 cm/s (McCave et al., 2017). SAZ core DCR-1PC typically shows the highest inferred bottom current flow speeds, whereas the southernmost AZ core PS2603-3 shows the lowest ones, with PS2609-1 and PS2606-6 having similar values and ranging in between. This may hint towards higher bottom flow speeds in the SAZ, yet it is difficult to directly translate $\overline{SS}$ values into absolute flow intensities unless there is a local calibration (McCave et al., 2017). Therefore, we focus on relative bottom current speed changes at individual core locations, while inter-core comparisons need to be treated more carefully. Additional factors may explain the meridional differences (McCave et al., 2017); first, the sediment supply might not contain the same amount of coarse grains in all cores and second, the supply of coarse silt might have been reduced by deposition further upstream along the current flow path (McCave et al., 2017). Additionally, as PS2603-3 lies in greater water depth in the Enderby Abyssal Plain, this core may be primarily influenced by Antarctic Bottom Water (AABW).

The different patterns in the SAZ and the AZ core locations suggest regionally distinct bottom current regimes in the Southern Indian Ocean. SAZ core DCR-1PC records faster (slower) bottom flow intensities during warm (cold) intervals, respectively, in line with previous studies from the Drake Passage (Lamy et al., 2015; Roberts et al., 2017; Toyos et al., 2020). In contrast, the AZ core locations suggest faster near-bottom flow regimes during cold periods, in agreement with studies from the southeastern Indian Ocean (Mazaud et al., 2010) and from the vicinity of South Africa (Krueger et al., 2012; Martínez-Méndez et al., 2008; Molyneux et al., 2007). The latter studies describe cores located NW of DCR-1PC. Yet, the variations in bottom water flow behave differently from DCR-1PC, with generally opposing trends during the MIS 5/4 transition and throughout MIS 4 and 3. The difference in the records – despite their geographic proximity – might be ascribed to the Southwest Indian Ridge (SWIR) separating the Agulhas Bank/Plateau from Del Cañ o Rise (Figure 4.1). The ridge is located just NW of Del Cañ o Rise and inhibits water from the west of the ridge flowing straight to the DCR-1PC core location, potentially accounting for the contrasting flow patterns.

Due to the complex bathymetry in the Southwest Indian Ocean, the flow direction of the ACC is highly channeled (Durgadoo et al., 2008; Pollard et al., 2007; Pollard and Read, 2001; Sokolov and Rintoul, 2009). Bathymetry that is shallower than 2000 m has the largest impact on deep reaching currents and thus Del Caño Rise and Conrad Rise largely obstruct the ACC flow (Durgadoo et al., 2008; Pollard and Read, 2001). Today, the highest velocities are found between Del Caño Rise and Conrad Rise (Figure 4.1). This region of high velocity has been interpreted as merged SAF and PF (Pollard and Read, 2001) and has been described later as corresponding to the SAF (Pollard et al., 2007). Since bathymetry is crucial for channeling the currents, the flow paths in the study region are locked and may only migrate within a limited meridional range. But in some instances, meridional shifts of the ACC could pass a threshold that leads the main current path to "jump", creating an abrupt change in the downcore $\overline{\text{SS}}$ records. Such a drastic change can be observed at the MIS 5/4 transition in DCR-1PC, where the values drop suddenly. The rise of the values slightly before the transition, might indicate increasing flow speeds until a certain threshold was reached. The rapid increases at the glacial terminations could imply a similar mechanism, yet in opposing direction. We suggest that at the MIS 5/4 transition, the SAF passed Del Caño Rise to the north, so that the core location lay in a slower flow regime during MIS 4 and 3. Molyneux et al. (2007) observe a simultaneous drastic rise in flow speeds, consistent with the main flow path leading through the channel between SWIR and Del Caño Rise or even further to the north of SWIR. These observations would be in line with previous studies suggesting a northward shift of the frontal system during cold periods (e.g. Gersonde et al., 2005; Thöle et al., 2019) and studies suggesting reduced Agulhas leakage during cold periods (e.g. Caley et al., 2012; Nair et al., 2019). Furthermore, a northward shift of the frontal system would be consistent with increased preserved opal fluxes in the SAZ at the MIS 5/4 boundary (see Chapters 2 and 3), as this would push the SAZ in more AZ-like biogeochemical conditions close to the upwelling region, allowing for enhanced siliceous export production (e.g. Anderson et al., 2009), additional to contributions of fertilization through a rise in lithogenic flux (see Chapter 3).

Contrary to the SAZ, the AZ sortable silt records suggest slower flow regimes during warm periods and stronger near-bottom current speeds during the colder

period of MIS 4 (Figure 4.3). In PS2609-1 the data suggest that the current flow speed in MIS 2 and 4 were both increased and did not substantially differ. Whereas PS2603-3 shows a similar peak of flow speed in MIS 4, but seems to be insensitive to the peak glacial conditions in MIS 2 compared to MIS 3 as well as the Holocene. This decoupling indicates that the northern part of the AZ was influenced by a general strengthening of the ACC during glacials, while the southern part was not. For PS2609-1 (and possibly PS2606-6) to be under the influence of SACCF, a northward shift of approximately 10° of latitude would have been necessary. Due to the large distance between the PF and the SACCF today, we consider this scenario rather unlikely. The southern PS2603-3 was most probably influenced by the SACCF during MIS 4. For the Last Glacial Maximum (LGM), extended sea-ice could account for the muted response in the downcore $\overline{\text{SS}}$ record (Crosta et al., 1998; Katsuki et al., 2012). In the Indian Ocean, sea-ice extent has been shown to have extended to at least the southern flanks of Conrad Rise (Katsuki et al., 2012). Dezileau et al. (2000) report evidence for weaker bottom-water current velocities associated with the AABW during glacial periods, that bathes PS2603-3.

Durgadoo et al. (2008) observe a bifurcation of the currents into two strong jets north and south of Conrad Rise. Today, both PS2609-1 and PS2606-6 are close to the maximum strength of these flows (Durgadoo et al., 2008). Possibilities to increase $\overline{\text{SS}}$ values as seen during MIS 4 and MIS 2 in PS2609-1, include an overall increase in current velocity and/or a widening of the currents, that are currently restricted to 1°–1.5° latitude (Durgadoo et al., 2008).

A northward shift of the frontal system has previously been suggested to have led to a deflection of the ACC along the west coast of South America truncating the SAF (Gersonde et al., 2005; Lamy et al., 2015; Roberts et al., 2017; Toyos et al., 2020), thereby reducing ACC flow through the Drake Passage (Lamy et al., 2015). That this deflection of the ACC could have an impact further downstream, possibly decreasing flow speed in the SAZ of the Indian Ocean is rather unlikely. Local and regional influence of bottom topography is greater than the deflection west of South America. Furthermore, its effect should be the same for the cores off South Africa as for DCR-1PC and should be seen in their sortable silt record, which is not the case (Krueger et al., 2012; Molyneux et al., 2007).

A similar deflection at the west coast of Africa leading to a reduced throughflow is unlikely. The passage between southern Africa and Antarctica being much wider than between Patagonia and Antarctic Peninsula allows for uninhibited throughflow, without the fronts of the ACC being "compressed". A northward shift of the frontal system however, would reduce Agulhas leakage, the flow of warm water masses from the Indian Ocean along the African coast and into the Atlantic (Caley et al., 2012), keeping these water masses within the Indian sector and increasing the Agulhas Return Current (ARC) (Nair et al., 2019; Simon et al., 2013). Influence of the ARC on our sortable silt records is yet unlikely, because the ARC is a surface current (Lutjeharms and Ansorge, 2001) and would not impact near-bottom current flow reconstructions.

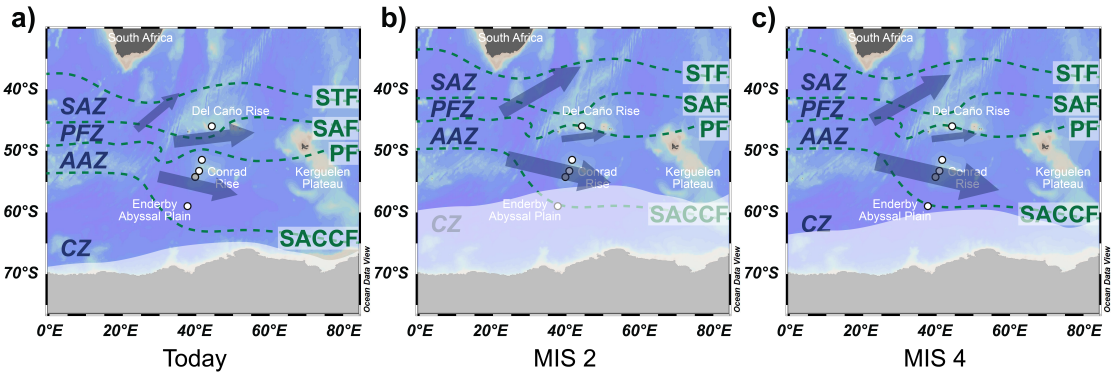

Figure 4.4: Schematic evolution of ACC in the SW Indian Ocean. a) Today's position of fronts with ACC strength schematically illustrated as arrows, and approximate sea-ice extent (white shading). b) MIS 2 shows glacial maximum with northward shifted fronts and maximum expanded sea-ice extent; ACC dynamics at Del Caño Rise show a slowdown, whereas in AZ the ACC is faster, but only affects northern AZ; southernmost core PS2603-3 is covered by sea-ice and thus protected from intensive ACC. c) MIS 4 with a northward shift of fronts and expanded sea-ice extent; ACC dynamics at Del Caño Rise are slow, whereas in AZ the ACC is faster; here southernmost core PS2603-3 is ice-free. Fronts from north to south (Orsi et al., 1995): Subtropical Front (STF), Subantarctic Front (SAF), Polar Front (PF), and the Southern ACC Front (SACCF); the zones between them are the Subantarctic Zone (SAZ), Polar Frontal Zone (PFZ), Antarctic Zone (AZ), and Continental Zone (CZ) (plotted with the ODV-software, Schlitzer, 2018).

Local and regional aspects have to be taken into consideration when reconstructing ACC dynamics based on downcore sortable silt records. We suggest a northward shift of the frontal system during glacial periods, leading the SAF and PF to overcome the bathymetric constraints after reaching a certain threshold (Figure 4.4). Furthermore, the AZ cores suggest an overall

strengthening of the ACC during glacial periods, possibly associated with stronger winds, as various model results imply (Gottschalk et al., 2019 *and references therein*). At the same time, more extensive sea-ice cover would have protected the cores in the southern regimes from vigorous flows (Figure 4.4). A northward migration of the ACC would contribute to decrease upwelling intensities, bringing shallower, more CO_2-depleted waters to the surface (Sigman and Boyle, 2000; Toggweiler and Russell, 2008; Watson et al., 2015). A concomitant strengthening of the ACC would lead to stronger upwelling and release of CO_2 to the atmosphere, which may have been counteracted by increased sea-ice extent.

Modern observations show both a strengthening and poleward shift of the SHW over the last decades (Böning et al., 2008; Toggweiler and Russell, 2008), often ascribed to stratospheric ozone depletion over Antarctica, and to a lesser degree as a reaction to the thermal contrast increased by elevated atmospheric CO_2 concentrations (Thompson et al., 2011; Toggweiler and Russell, 2008; Waugh et al., 2013). Recent findings show that the poleward intensified SHW are also associated with a positive Southern Annular Mode (SAM) (Paterne et al., 2019). Ocean models supported by observations suggest that the intensification and concomitant poleward migration of the westerlies enhance upwelling, without much change in the isopycnal tilt of the ACC and its transport (Böning et al., 2008; Gottschalk et al., 2019; Rintoul, 2018). Furthermore, wind-forced increase in upwelling can impact ice-sheets by basal melting (Pritchard et al., 2012; Rintoul, 2018). A more southwards shifted ACC, as implied for warm periods by our study, might lead to upwelling of deeper, more CO_2-rich waters, helping to accelerate the global CO_2 trend. However, other processes, e.g. enhanced buoyancy forcing (Böning et al., 2008; Rintoul, 2018) may partly balance this process. Furthermore, observations over the last few decades show highly variable upwelling changes in the Southern Ocean, suggesting its balance of CO_2 uptake/outgassing being prone to change in the future (DeVries et al., 2017). Thus, it is crucial to understand the interplay of the various mechanisms and the connection of the upper overturning circulation with the deep, and to observe future responses of the ACC to continuing changes in climatic drivers.

4.5 Conclusions

We report detailed, highly resolved sortable silt mean size ($\overline{SS}$) measurements from four cores to determine near-bottom flow changes in the Southern Indian Ocean over the last glacial cycle. The paleoceanographic reconstructions spanning a meridional transect suggest contrasting ACC dynamics, substantiating the ACC's inhomogeneous behavior with possible implications on upwelling intensities and thus climate.

In SAZ core DCR-1PC, $\overline{SS}$ values suggest a generally weaker flow during cold periods and a comparatively stronger flow during warm climate intervals. The abrupt changes at Terminations I and II, and the MIS 5/4 transition, indicate possible jumps in the current path of the otherwise largely bathymetrically locked flow. We interpret the northernmost core DCR-1PC to have experienced jumps of the SAF (possibly amalgamated with PF) towards the north during MIS 4 through MIS 2, leaving the core location in relatively calm flow regime of the Polar Frontal Zone and back to the southern flanks of the Del Caño Rise during warm periods. This northward shift was possibly accompanied by a strengthening of current speed as seen in the AZ cores.

The cores in the AZ show a weaker flow regime during warm periods and stronger flow during cold periods. Southernmost core PS2603-3 shows generally stable flow intensities during the LGM, probably due to expanded sea-ice, inhibiting large current variability.

Local and regional parameters and bathymetry play a major role in directing the ACC flow path and thus in the reconstructed sortable silt record. However, a northward shift and a concomitant strengthening during cold periods would be consistent with the observed data.

Seemingly contradicting previous studies suggesting either a slower ACC close to the Drake Passage during glacial times (Lamy et al., 2015; McCave et al., 2014; Roberts et al., 2017; Toyos et al., 2020) or a faster ACC during glacials in the Southeast Atlantic (Krueger et al., 2012; Martínez-Méndez et al., 2008; Molyneux et al., 2007) and Indian Ocean (Mazaud et al., 2010), can be partly reconciled. We conclude that ACC dynamics are sensitive to regional and spatial differences and thus require a high spatio-temporal resolution to gain a deeper understanding.

We suggest that the ACC strengthening during glacial intervals did not lead to a net increase in CO_2 flux to the atmosphere, for two main reasons: first, the northward shift would upwell shallower waters carrying less CO_2 than deep waters upwelled with a more southern ACC position (Sigman and Boyle, 2000; Toggweiler and Russell, 2008; Watson et al., 2015) and second, an ACC strengthening associated with increased upwelling would be counteracted by an increase in sea-ice extent (Dezileau et al., 2000).

Author contribution

HEA, NS and SLJ designed the study. HEA and NS refined the SS sample preparation for diatom-rich samples and NS carried out the grain-size measurements and data evaluation. MI and GK planned the cruises and gave access to the cores. LMT and NM contributed with insights on sample preparation and data interpretation. HEA wrote the original version of the manuscript and all co-authors contributed to the manuscript.

Acknowledgments

We thank the captain, crew members and scientists of R/V Hakuho-maru and R/V Polarstern for the recovery of the sediment cores during KH-10-7 (lead scientist: M. Ikehara) and ANT-XI/4 cruises (lead scientist: G. Kuhn) to the Southern Ocean. We thank Daniela Fischer at GIUB, University of Bern, for helping with the sortable silt measurements, Julia Gottschalk for helping with the sample preparation and for providing Figure 4.1b, Peter Abbott for his help for the diatom removal procedure, and Priska Bähler for support in the laboratory. Funding for this study was provided by the Swiss National Science Foundation (grants PP00P2_144811 and 2000021_163003). G. Kuhn was funded by the Alfred-Wegener-Institut Helmholtz-Zentrum für Polar- und Meeresforschung PACES II research program. M. Ikehara was funded by the Japan Society for the Promotion of Science KAKENHI (Grants-in-Aid for Scientific Research P23244102 and JP17H06318).

References

Allison, L.C., Johnson, H.L., Marshall, D.P., Munday, D.R., 2010. Where do winds drive the antarctic circumpolar current? Geophys. Res. Lett. 37, 1–5. doi: 10.1029/2010GL043355

Anderson, R.F., Ali, S., Bradtmiller, L.I., Nielsen, S.H.H., Fleisher, M.Q., Anderson, B.E., Burckle, L.H., 2009. Wind-driven Upwelling in the Southern Ocean and the Deglacial Rise in Atmospheric CO_2. Science 323, 1443–1448

Bereiter, B., Eggleston, S., Schmitt, J., Nehrbass-Ahles, C., Stocker, T.F., Fischer, H., Kipfstuhl, S., Chappellaz, J., 2015. Revision of the EPICA Dome C CO_2 record from 800 to 600 kyr before present. Geophys. Res. Lett. 42, 542–549. doi: 10.1002/2014GL061957

Bianchi, G.G., Hall, I.R., McCave, I.N., Joseph, L., 1999. Measurement of the sortable silt current speed proxy using the Sedigraph 5100 and Coulter Multisizer Ile: Precision and accuracy. Sedimentology 46, 1001–1014. doi: 10.1046/j.1365-3091.1999.00256.x

Bista, D., Kienast, S.S., Hill, P.S., Kienast, M., 2016. Sediment sorting and focusing in the eastern equatorial Pacific. Mar. Geol. 382, 151–161. doi: 10.1016/j.margeo.2016.09.016

Böning, C.W., Dispert, A., Visbeck, M., Rintoul, S.R., Schwarzkopf, F.U., 2008. The response of the antarctic circumpolar current to recent climate change. Nat. Geosci. 1, 864–869. doi: 10.1038/ngeo362

Caley, T., Giraudeau, J., Malaizé, B., Rossignol, L., Pierre, C., 2012. Agulhas leakage as a key process in the modes of Quaternary climate changes. Proc. Natl. Acad. Sci. U. S. A. 109, 6835–6839. doi: 10.1073/pnas.1115545109

Channell, J.E.T., Harrison, R.J., Lascu, I., McCave, I.N., Hibbert, F.D., Austin, W.E.N., 2016. Magnetic record of deglaciation using FORC-PCA, sortable-silt grain size, and magnetic excursion at 26 ka, from the Rockall Trough (NE Atlantic). Geochemistry Geophys. Geosystems 17, 1823–1841. doi: 10.1002/2016GC006300

Chavaillaz, Y., Codron, F., Kageyama, M., 2013. Southern westerlies in LGM and future (RCP4.5) climates. Clim. Past 9, 517–524. doi: 10.5194/cp-9-517-2013

Crosta, X., Pichon, J.-J., Burckle, L.H., 1998. Application of modern analog technique to marine Antarctic diatoms: Reconstruction of maximum sea-ice extent at the Last Glacial Maximum. Paleoceanography 13, 284–297. doi: 10.1029/98PA00339

Crosta, X., Shukla, S.K., Ther, O., Ikehara, M., Yamane, M., Yokoyama, Y., 2020. Last Abundant Appearance Datum of *Hemidiscus karstenii* driven by climate change. Mar. Micropaleontol. 157. doi: 10.1016/j.marmicro.2020.101861

DeVries, T., Holzer, M., Primeau, F., 2017. Recent increase in oceanic carbon uptake driven by weaker upper-ocean overturning. Nature 542, 215–218. doi: 10.1038/nature21068

Dezileau, L., Bareille, G., Reyss, J.L., Lemoine, F., 2000. Evidence for strong sediment redistribution by bottom currents along the southeast Indian ridge. Deep. Res. Part I Oceanogr. Res. Pap. 47, 1899–1936. doi: 10.1016/S0967-0637(00)00008-X

Durgadoo, J.V., Lutjeharms, J.R.E., Biastoch, A., Ansorge, I.J., 2008. The Conrad Rise as an obstruction to the Antarctic Circumpolar Current. Geophys. Res. Lett. 35, 1–6. doi: 10.1029/2008GL035382

Dutkiewicz, A., Dietmar Müller, R., Hogg, A.M.C., Spence, P., 2016. Vigorous deep-sea currents cause global anomaly in sediment accumulation in the Southern Ocean. Geology 44, 663–666. doi: 10.1130/G38143.1

Franzese, A.M., Hemming, S.R., Goldstein, S.L., Anderson, R.F., 2006. Reduced Agulhas Leakage during the Last Glacial Maximum inferred from an integrated provenance and flux study. Earth Planet. Sci. Lett. 250, 72–88. doi: 10.1016/j.epsl.2006.07.002

Fyfe, J.C., Saenko, O.A., 2006. Simulated changes in the extratropical Southern Hemisphere winds and currents. Geophys. Res. Lett. 33, 1–4. doi: 10.1029/2005GL025332

Gersonde, R., Crosta, X., Abelmann, A., Armand, L., 2005. Sea-surface temperature and sea ice distribution of the Southern Ocean at the EPILOG Last Glacial Maximum - A circum-Antarctic view based on siliceous microfossil records. Quat. Sci. Rev. 24, 869–896. doi: 10.1016/j.quascirev.2004.07.015

Gille, S.T., Joseph Metzger, E., Tokmakian, R., 2004. Seafloor topography and ocean circulation. Oceanography 17, 47–54. doi: 10.5670/oceanog.2004.66

Gordon, A.L., Molinelli, E., Baker, T., 1978. Large-scale relative dynamic topography of the Southern Ocean. J. Geophys. Res. 83, 3023. doi: 10.1029/jc083ic06p03023

Gottschalk, J., Battaglia, G., Fischer, H., Frölicher, T.L., Jaccard, S.L., Jeltsch-Thömmes, A., Joos, F., Köhler, P., Meissner, K.J., Menviel, L., Nehrbass-Ahles, C., Schmitt, J., Schmittner, A., Skinner, L.C., Stocker, T.F., 2019. Mechanisms of millennial-scale atmospheric CO_2 change in numerical model simulations. Quat. Sci. Rev. 220, 30–74. doi: 10.1016/j.quascirev.2019.05.013

Katsuki, K., Ikehara, M., Yokoyama, Y., Yamane, M., Khim, B.K., 2012. Holocene migration of oceanic front systems over the Conrad Rise in the Indian Sector of the Southern Ocean. J. Quat. Sci. 27, 203–210. doi: 10.1002/jqs.1535

Kohfeld, K.E., Graham, R.M., de Boer, A.M., Sime, L.C., Wolff, E.W., Le Quéré, C., Bopp, L., 2013. Southern Hemisphere westerly wind changes during the Last Glacial Maximum: Paleo-data synthesis. Quat. Sci. Rev. 68, 76–95. doi: 10.1016/j.quascirev.2013.01.017

Krueger, S., Leuschner, D.C., Ehrmann, W., Schmiedl, G., Mackensen, A., 2012. North Atlantic Deep Water and Antarctic Bottom Water variability during the last 200 ka recorded in an abyssal sediment core off South Africa. Glob. Planet. Change 80–81, 180–189. doi: 10.1016/j.gloplacha.2011.10.001

Kuhn, G., 2003a. Documentation of sediment core PS2609-1. Alfred Wegener Institute

- Polarstern core repository, PANGAEA. doi: 10.1594/PANGAEA.115378

Kuhn, G., 2003b. Documentation of sediment core PS2606-6. Alfred Wegener Institute - Polarstern core repository, PANGAEA. doi: 10.1594/PANGAEA.115376

Kuhn, G., 2003c. Documentation of sediment core PS2603-3. Alfred Wegener Institute - Polarstern core repository, PANGAEA. doi: 10.1594/PANGAEA.115375

Lambert, F., Bigler, M., Steffensen, J.P., Hutterli, M., Fischer, H., 2012. Centennial mineral dust variability in high-resolution ice core data from Dome C, Antarctica. Clim. Past 8, 609–623. doi: 10.5194/cp-8-609-2012

Lamy, F., Arz, H.W., Kilian, R., Lange, C.B., Lembke-Jene, L., Wengler, M., Kaiser, J., Baeza-Urrea, O., Hall, I.R., Harada, N., Tiedemann, R., 2015. Glacial reduction and millennial-scale variations in Drake Passage throughflow. Proc. Natl. Acad. Sci. U. S. A. 112, 13496–13501. doi: 10.1073/pnas.1509203112

Lamy, F., Gersonde, R., Winckler, G., Esper, O., Jaeschke, A., Kuhn, G., Ullermann, J., Martínez-García, A., Lambert, F., Kilian, R., 2014. Increased dust deposition in the Pacific Southern Ocean during glacial periods. Science 343, 403–407. doi: 10.1126/science.1245424

Lisiecki, L.E., Raymo, M.E., 2005. A Pliocene-Pleistocene stack of 57 globally distributed benthic $\delta^{18}O$ records. Paleoceanography 20, PA1003, 1–17. doi: 10.1029/2004PA001071

Lutjeharms, J.R.E., Ansorge, I.J., 2001. The Agulhas Return Current. J. Mar. Syst. 30, 115–138. doi: 10.1016/S0924-7963(01)00041-0

Manoj, M.C., Thamban, M., 2015. Shifting frontal regimes and its influence on bioproductivity variations during the Late Quaternary in the Indian sector of Southern Ocean. Deep. Res. Part II Top. Stud. Oceanogr. 118, 261–274. doi: 10.1016/j.dsr2.2015.03.011

Marshall, J., Speer, K., 2012. Closure of the meridional overturning circulation through Southern Ocean upwelling. Nat. Geosci. 5, 171–180. doi: 10.1038/ngeo1391

Martínez-Méndez, G., Zahn, R., Hall, I.R., Pena, L.D., Cacho, I., 2008. 345,000-year-long multi-proxy records off South Africa document variable contributions of Northern versus Southern Component Water to the Deep South Atlantic. Earth Planet. Sci. Lett. doi: 10.1016/j.epsl.2007.11.050

Mazaud, A., Michel, E., Dewilde, F., Turon, J.L., 2010. Variations of the Antarctic Circumpolar Current intensity during the past 500 ka. Geochemistry, Geophys. Geosystems 11, 1–10. doi: 10.1029/2010GC003033

McCave, I.N., Andrews, J.T., 2019. Distinguishing current effects in sediments delivered to the ocean by ice. I. Principles, methods and examples. Quat. Sci. Rev. 212, 92–107. doi: 10.1016/j.quascirev.2019.03.031

McCave, I.N., Crowhurst, S.J., Kuhn, G., Hillenbrand, C.D., Meredith, M.P., 2014. Minimal change in antarctic circumpolar current flow speed between the last glacial and holocene. Nat. Geosci. 7, 113–116. doi: 10.1038/ngeo2037

McCave, I.N., Manighetti, B., Robinson, S.G., 1995. Sortable silt and fine sediment size/composition slicing: Parameters for palaeocurrent speed and palaeoceanography. Paleoceanography 10, 593–610. doi: 10.1029/94PA03039

McCave, I.N., Thornalley, D.J.R., Hall, I.R., 2017. Relation of sortable silt grain-size to deep-sea current speeds: Calibration of the 'Mud Current Meter.' Deep. Res. Part I Oceanogr. Res. Pap. 127, 1–12. doi: 10.1016/j.dsr.2017.07.003

Molyneux, E.G., Hall, I.R., Zahn, R., Diz, P., 2007. Deep water variability on the southern Agulhas Plateau: Interhemispheric links over the past 170 ka. Paleoceanography 22, 1–14. doi: 10.1029/2006PA001407

Nair, A., Mohan, R., Crosta, X., Manoj, M.C., Thamban, M., Marieu, V., 2019. Southern Ocean sea ice and frontal changes during the Late Quaternary and their linkages to Asian summer monsoon. Quat. Sci. Rev. 213, 93–104. doi: 10.1016/j.quascirev.2019.04.007

Orsi, A.H., Whitworth, T., Nowlin, W.D., 1995. On the meridional extent and fronts of the Antarctic Circumpolar Current. Deep Sea Res. 42, 641–673. doi: 10.1016/0967-0637(95)00021-W

Pahnke, K., Zahn, R., Elderfield, H., Schulz, M., 2003. 340,000-Year Centennial-Scale Marine Record of Southern Hemisphere Climatic Oscillation. Science 301, 948–952. doi: 10.1126/science.1084451

Park, Y.H., Roquet, F., Durand, I., Fuda, J.L., 2008. Large-scale circulation over and around the Northern Kerguelen Plateau. Deep. Res. Part II Top. Stud. Oceanogr. 55, 566–581. doi: 10.1016/j.dsr2.2007.12.030

Paterne, M., Michel, E., Héros, V., 2019. Variability of marine ^{14}C reservoir ages in the Southern Ocean highlighting circulation changes between 1910 and 1950. Earth Planet. Sci. Lett. 511, 99–104. doi: 10.1016/j.epsl.2019.01.029

Pollard, R.T., Read, J.F., 2001. Circulation pathways and transports of the Southern Ocean in the vicinity of the Southwest Indian Ridge. J. Geophys. Res. Ocean. 106, 2881–2898. doi: 10.1029/2000jc900090

Pollard, R.T., Venables, H.J., Read, J.F., Allen, J.T., 2007. Large-scale circulation around the Crozet Plateau controls an annual phytoplankton bloom in the Crozet Basin. Deep. Res. Part II Top. Stud. Oceanogr. 54, 1915–1929. doi: 10.1016/j.dsr2.2007.06.012

Pritchard, H.D., Ligtenberg, S.R.M., Fricker, H.A., Vaughan, D.G., Van Den Broeke, M.R., Padman, L., 2012. Antarctic ice-sheet loss driven by basal melting of ice shelves. Nature 484, 502–505. doi: 10.1038/nature10968

Rintoul, S.R., 2018. The global influence of localized dynamics in the Southern Ocean. Nature 558, 209–218. doi: 10.1038/s41586-018-0182-3

Rintoul, S.R., W. Hughes, C., Olbers, D., 2001. Chapter 4.6 The antarctic circumpolar current system. International Geophysics. in Ocean Circulation and Climate, edited by G. Siedler, J. Church, and J. Gould, 271–302, Elsevier, New York. doi: 10.1016/S0074-6142(01)80124-8

Roberts, J., McCave, I.N., McClymont, E.L., Kender, S., Hillenbrand, C.D., Matano, R., Hodell, D.A., Peck, V.L., 2017. Deglacial changes in flow and frontal structure through the Drake Passage. Earth Planet. Sci. Lett. 474, 397–408. doi: 10.1016/j.epsl.2017.07.004

Ronge, T.A., Prange, M., Mollenhauer, G., Ellinghausen, M., Kuhn, G., Tiedemann, R., 2020. Radiocarbon Evidence for the Contribution of the Southern Indian Ocean to the Evolution of Atmospheric CO_2 Over the Last 32,000 Years. Paleoceanogr. Paleoclimatology 35. doi: 10.1029/2019PA003733

Saenko, O.A., Fyfe, J.C., England, M.H., 2005. On the response of the oceanic wind-driven circulation to atmospheric CO_2 increase. Clim. Dyn. 25, 415–426. doi: 10.1007/s00382-005-0032-5

Schlitzer, R., 2018. Ocean Data View. Available at http://odv.awi.de

Sigman, D.M., Boyle, E.A., 2000. Glacial/interglacial variations in atmospheric carbon dioxide. Nature 407, 859–869. doi: 10.1038/35038000

Sigman, D.M., Hain, M.P., Haug, G.H., 2010. The polar ocean and glacial cycles in atmospheric CO_2 concentration. Nature 466, 7302, 47–55. doi: 10.1038/nature09149

Simon, M.H., Arthur, K.L., Hall, I.R., Peeters, F.J.C., Loveday, B.R., Barker, S., Ziegler, M., Zahn, R., 2013. Millennial-scale Agulhas Current variability and its implications for salt-leakage through the Indian-Atlantic Ocean Gateway. Earth Planet. Sci. Lett. 383, 101–112. doi: 10.1016/j.epsl.2013.09.035

Sokolov, S., Rintoul, S.R., 2009. Circumpolar structure and distribution of the Antarctic Circumpolar Current fronts: 1. Mean circumpolar paths. J. Geophys. Res. Ocean. 114, 1–19. doi: 10.1029/2008JC005108

Sperazza, M., Moore, J.N., Hendrix, M.S., 2004. High-Resolution Particle Size Analysis of Naturally Occurring Very Fine-Grained Sediment Through Laser Diffractometry. J. Sediment. Res. 74, 736–743. doi: 10.1306/031104740736

Talley, L.D., 2013. Closure of the global overturning circulation through the Indian, Pacific, and Southern Oceans: Schematics and transports. Oceanography 26, 80–97. doi: 10.5670/oceanog.2013.07

Tegzes, A.D., Jansen, E., Telford, R.J., 2015. Which is the better proxy for paleocurrent strength: Sortable-silt mean size ($\overline{SS}$) or sortable-silt mean grain diameter ($\bar{d}_{SS}$)? A case study from the Nordic Seas. Geochemistry, Geophys. Geosystems 16, 3456–3471. doi: 10.1002/2014GC005655

Thöle, L.M., Amsler, H.E., Moretti, S., Auderset, A., Gilgannon, J., Lippold, J., Vogel, H., Crosta, X., Mazaud, A., Michel, E., Martínez-García, A., Jaccard, S.L., 2019. Glacial-interglacial dust and export production records from the Southern Indian Ocean. Earth Planet. Sci. Lett. 525. doi: 10.1016/j.epsl.2019.115716

Thompson, D.W.J., Solomon, S., Kushner, P.J., England, M.H., Grise, K.M., Karoly, D.J., 2011. Signatures of the Antarctic ozone hole in Southern Hemisphere surface climate change. Nat. Geosci. 4, 741–749. doi: 10.1038/ngeo1296

Toggweiler, J.R., Russell, J., 2008. Ocean circulation in a warming climate. Nature 451, 286–288. doi: 10.1038/nature06590

Toyos, M.H., Lamy, F., Lange, C.B., Lembke-Jene, L., Saavedra-Pellitero, M., Esper, O., Arz, H.W., 2020. Antarctic Circumpolar Current dynamics at the Pacific entrance to the Drake Passage over the past 1.3 million years. Paleoceanogr. Paleoclimatology 35. doi: 10.1029/2019PA003773

Tschumi, T., Joos, F., Parekh, P., 2008. How important are Southern Hemisphere wind changes for low glacial carbon dioxide? A model study. Paleoceanography 23, 1–20. doi: 10.1029/2008PA001592

Watson, A.J., Naveira Garabato, A.C., 2006. The role of Southern Ocean mixing and upwelling in glacial-interglacial atmospheric CO_2 change. Tellus, Ser. B Chem. Phys. Meteorol. 58, 1, 73–87. doi: 10.1111/j.1600-0889.2005.00167.x

Watson, A.J., Vallis, G.K., Nikurashin, M., 2015. Southern Ocean buoyancy forcing of ocean ventilation and glacial atmospheric CO_2. Nat. Geosci. 8, 11, 861–864. doi: 10.1038/ngeo2538

Waugh, D.W., Primeau, F., DeVries, T., Holzer, M., 2013. Recent changes in the ventilation of the southern oceans. Science 339, 568–570. doi: 10.1126/science.1225411

Xiao, W., Esper, O., Gersonde, R., 2016. Last Glacial - Holocene climate variability in the Atlantic sector of the Southern Ocean. Quat. Sci. Rev. 135, 115–137. doi: 10.1016/j.quascirev.2016.01.023

CHAPTER 5

Synthesis and outlook

Synthesis and outlook

In this PhD thesis we present a series of paleoceanographic records based on marine sediment cores retrieved from the SW Indian Ocean spanning a meridional transect across major hydrographic fronts and covering the last glacial cycle. Our main objective was to investigate the biogeochemical and physical processes that may have contributed to the evolution of atmospheric CO_2, based on a multi-proxy approach, including both sedimentological and geochemical tools. These processes include changes in ocean circulation and biogenic export production and their combined leverage on deep ocean oxygenation, ultimately controlling CO_2 storage and release (Chapter 2). As biogenic export production in the Subantarctic Zone (SAZ) of the Southern Ocean is modulated by the availability of the micronutrient iron (Fe), predominantly supplied to the ocean surface via dust, a regional comparison of lithogenic fluxes was conducted (Chapter 3). The dynamics of bottom water flow of the Antarctic Circumpolar Current (ACC), that influence circulation and ventilation changes allowing previously sequestered CO_2 to outgas and (micro)nutrients to upwell, were investigated (Chapter 4). Despite an increasing number of studies focusing on these aspects, ambiguities still remain and the exact interplay of different processes is yet not fully understood. With this study, we aim to address these questions by increasing the spatial and temporal resolution of existing Southern Ocean sediment records to provide a more complete understanding of the dynamics in the Southern Indian Ocean.

The main conclusions of this thesis are:

1) Bottom water oxygenation changes are mainly controlled by ocean ventilation and circulation dynamics. Our reconstructions covering both the SAZ and AZ of the Southern Ocean, show a consistent pattern of reduced glacial oxygenation and increased interglacial oxygenation of bottom waters. Detailed comparison with preserved opal fluxes, and by inference organic carbon export and respiration, reveals a contribution from enhanced glacial export productivity on the local oxygen demand in the SAZ only, but not in the AZ. Our reconstructions support the notion

of more sluggish circulation dynamics to provide a dominant control on enhanced remineralized carbon sequestration during glacial intervals.

2) Regional comparison of lithogenic fluxes shows very good quantitative agreement and coherent downcore patterns from the Southeast Atlantic to the Southeast Indian Ocean. The input of lithogenic material increased in both the SAZ and AZ during glacial periods. We suggest that glacial lithogenic sources primarily stem from southern America, with contributions from southern Africa and local bathymetric highs. The covariation observed between lithogenic flux reconstructions and preserved opal points towards Fe fertilizing biological production in the glacial SAZ, yet with a weakening response due to limitation by other (macro)nutrients during peak glacial conditions.

3) Bathymetry plays an important role in directing the ACC flow. The sortable silt records highlight the inhomogeneous behavior of the ACC along the meridional core transect. The data suggest a glacial northward migration of the ACC, and the current overcoming bathymetric constraints when certain thresholds are reached. A northward migration of the ACC contributed to enhanced upwelling of younger, shallower water masses, possibly decreasing CO_2 outgassing to the atmosphere. The concomitant strengthening of the ACC in the AZ may have increased upwelling intensity, but this mechanism may have been curbed by expanded sea-ice cover.

4) The combined changes in ocean circulation, nutrient biogeochemistry and export production patterns in the SW Indian Ocean contributed to sequestering carbon away from the atmosphere during glacial periods. In the SAZ, the glacial increase in lithogenic flux partly fueled export production, which enhanced organic carbon respiration at depth and contributed to removing oxygen from the ocean interior. In the AZ, glacial bottom-water oxygen content generally decreased despite reduced export production, suggesting that the ocean was strongly stratified, prohibiting exchange with the atmosphere, even with a stronger ACC flow. The rapid rise of export production during the deglaciation, concomitant with increased ventilation further supports this interpretation.

In summary, the results of this thesis illustrate the role of the Southern Ocean as a dynamic player in the climate system, and highlight the importance of future studies to increase the spatio-temporal resolution of well-dated paleoceanographic reconstructions. To gain a yet more complete insight into the details of the sediment records investigated in the framework of this thesis and to improve our overall understanding related to Southern Ocean dynamics, future studies may investigate the following aspects:

1) Geochemical and mineralogical analyses focusing on the detrital fraction of the sediment could provide useful constraints on the provenance of the lithogenic material over time.
2) Variations in microfossil assemblages (e.g. diatoms, foraminifera) could help reconstructing frontal migration and support our sedimentological reconstructions.
3) Additional export production proxies, such as total organic carbon, $CaCO_3$, biogenic barium, and biomarkers could complement the reconstructions of biological export production to support the conclusions based on the preserved opal flux records.
4) The potential influence of Fe-limitation on biogenic opal could be further addressed, in particular the impact of Fe-availability on nutrient uptake rates, or on diatom shell silicification, which might impact frustule preservation in sediments.

CHAPTER 6

Appendix

Appendix

6.1 Sediment cores

All sedimentological and geochemical analyses have been conducted on marine sediment cores retrieved from the Southwestern Indian Ocean. Cores DCR-1PC and COR-1bPC were recovered during expedition KH-10-7 on R/V Hakuho-maru in 2010–2011. Cores PS2609-1, PS2606-6 and PS2603-3 were retrieved during the ANT XI/4 expedition on R/V Polarstern in 1994. With exception of PS2603-3, which is a gravity core, all other cores were retrieved with a piston corer (see Chapter 1, Table 1.1 and Figure 1.4).

DCR-1PC is composed of nannofossil and diatom ooze with variable amounts of clay. The sedimentation rate is 2–4 cm/ka and the core contains sediments covering a time interval ranging back to MIS 11. This core lies in the Subantarctic Zone (SAZ) just north of today's position of the Subantarctic Front (SAF) and was retrieved from the southern slope of the Del Caño Rise. To the northern and southern side of the peak of another bathymetric high, the Conrad Rise, the two cores PS2609-1 and PS2606-6 were retrieved, both consisting predominantly of diatom ooze with sedimentation rates ranging between 10–20 cm/ka and 5–40 cm/ka, respectively (Kuhn, 2003a, 2003b). Both cores are located south of the Polar Front (PF) in the Antarctic Zone (AZ) and reach back to 120 and 110 ka, respectively. Core COR-1bPC was collected a bit further to the southwest, on the southern flank of Conrad Rise. The sediment is composed of homogeneous diatom ooze with a sedimentation rate amounting to 10–40 cm/ka. The sediments reach MIS 3; as such the last glacial, deglaciation and Holocene sequences are highly resolved temporally. The southernmost core PS2603-3 was retrieved from Enderby Abyssal Plain, close to the Southern ACC Front (SACCF). The sediment consists of diatom ooze with a sedimentation rate of 1–5 cm/ka and reaches back to about MIS 9 (Kuhn, 2003c). In this study, samples dating back as far as 120 ka are presented to cover the last glacial cycle.

The cores are located along a meridional transect from the Subantarctic Zone north of the Subantarctic Front over the Polar Front far into the Antarctic Zone almost to the Southern ACC Front, covering around 15° of latitude. The sediment archives span different oceanographic zones and thus have the

potential to record past changes in chemical and sedimentological characteristics affecting the Southern Ocean.

Additionally, literature data from cores retrieved in the vicinity of the Kerguelen Archipelago MD11-3357 (44°40.8'S, 80°25.8'E, 3349 mbsl) and MD11-3353 (50°34.2'S, 68°23.4'E, 1568 mbsl) are presented in this thesis (Chapter 3) (Thöle et al., 2019). MD11-3357 is located in the SAZ close to the SAF with sedimentation rates of 10–25 cm/ka and MD11-3353 is located in the AZ with sedimentation rates of 3–15 cm/ka. Both cores were retrieved by R/V Marion Dufresne during cruises in 2011 and 2012.

Data from another two cores TN057-21 (41°08'S, 7°49'E, 4981 mbsl) and TN057-06 (42°54.8'S, 8°54'E, 3751 mbsl) are used for comparison (Chapter 3). Both cores are located north of the Subantarctic Front in the Southern Atlantic off southern Africa (Anderson et al., 2014). TN057-21 was retrieved from the southern Cape Basin from a sediment drift with sedimentation rates amounting to around 12.5 cm/ka (Sachs and Anderson, 2003) and TN057-06 was retrieved from the Agulhas Ridge with lower sedimentation rates of around 3.4 cm/ka (Hodell et al., 2000).

6.2 Age models

For DCR-1PC, seven ^{14}C-dates were determined and the diatom-based SST record was tuned to the deuterium record of EPICA Dome C, assuming both records are synchronous (Crosta et al., 2020). The stratigraphy for core COR-1bPC is based on 23 calibrated ^{14}C-measurements on planktic foraminifera *neogloboquadrina pachyderma (sinistral)* (Oiwane et al., 2014; Ikehara et al., *in prep.*).

For PS2609-1 and PS2606-6 tie points have been established based on graphical alignment of the magnetic susceptibility record to the global δ^{18}O LR04-stack (Lisiecki and Raymo, 2005). The alignments were fine-tuned using the XRF-scanning data of iron (Fe), silicon (Si), titanium (Ti), and calcium (Ca). For PS2606-6, seven ^{14}C-dates have been determined (Xiao et al., 2016). Additional tie points were added for core PS2609-1 based on graphical alignment of XRF-scanning titanium (Ti) measurements with the EPICA Dome C dust record (Lambert et al., 2012), assuming synchronous temporal variability. The Ti- and Ca/Ti-records from core PS2606-6 were compared to those of PS2609-1 to

define a common stratigraphic framework (Table 2.1). Our age model was compared to the recently published ^{14}C-based age model of PS2606-6 (Ronge et al., 2020) and both independently determined age models are consistent with one another.

The age model for core PS2603-3 was determined based on graphical alignment of magnetic susceptibility, XRF-data, and biogenic silica with the LR04-stack (Lisiecki and Raymo, 2005). The extinctions of three diatom species served as additional, independent biostratigraphic markers: *rouxia leventerae* at 130 ka, *hemidiscus karstenii* at 191 ka and *rouxia constricta* at 300 ka (Zielinski and Gersonde, 2002). There is evidence for a 30-ka long hiatus associated with a sediment disturbance, possibly a turbidite close to the MIS 5/4 boundary (Kuhn, 2003c). Independent absolute age constraints with the CRS-method (Geibert et al., 2019) yielded similar ages for PS2603-3, except for the interval around the hiatus, where a deviation of around 30 ka is observed.

6.3 Methods

6.3.1 Biogenic opal measurements

Sedimentary biogenic opal (bSi) concentrations were measured at the University of Bern by Fourier transform infrared spectroscopy (FTIRS). Basis for this independent FTIRS bSi calibration is an empirical relationship between known concentrations of bSi and their FTIR spectral signatures (Meyer-Jacob et al., 2014; Vogel et al., 2016). The principle of this technique is that molecules with polar bonds are excited by infrared (IR) radiation. Depending on the structural and atomic composition of the molecule, the IR radiation is absorbed at molecule-specific spectral wavelengths (Vogel et al., 2008).

For the measurement, 11 ± 0.1 mg of freeze-dried bulk sediment were mixed with 500 ± 0.5 mg of dry spectroscopic-grade potassium bromide (KBr) (Uvasol®, Merck Corp., oven-dried over night at 150°C) and then mortared. The homogenized sample powder was filled and flattened into measurement cups and dried again (2 hours at 200°C) to avoid biases related to adsorbed water. The measurements were performed using a Bruker Vertex 70 spectrometer equipped with a liquid nitrogen cooled MCT (Mercury-Cadmium-Telluride)

detector, a KBr beam splitter, and a HTS-XT multisampler accessory unit (Vogel et al., 2016).

The initial calibration proved to be robust, yet a drift in the standard (mix of marine sediments) was observed with time between freeze-drying and the measurement. Also, samples composed almost exclusively of diatom ooze showed bSi contents of >100%.

This continuous increase of the measured opal values within several months is likely resulting from water absorption from ambient humidity between the tetrahedral sheets of clay minerals abundant in marine sediments. The salt content in marine sediments could also facilitate OH^-- or H_2O-molecules to adsorb to the sediment, changing the spectral signature (H. Vogel, *pers. comm.*). To prevent the sediments from absorbing water, an additional drying step (60°C over night) was introduced before weighing the freeze-dried samples, and the time limit from weighing to measurement was set to a maximum of five days.

Deviations from the initial calibration associated with sediment composition cannot be ruled out, since the initial calibration was carried out on synthetic mixtures composed of purified diatom frustules from lake diatomites (Meyer-Jacob et al., 2014). To verify the robustness of this relatively new method, another set of tests was carried out. A pure biogenic opal standard was prepared with diatoms separated from marine sediments from the Atlantic sector of the Southern Ocean following the description by Studer et al. (2015). This sample consisting of 100% biogenic silica was mixed with other pure mineral phases to reproduce the composition of natural marine sediments. The mineral mixture consisted of 40% calcite, 30% quartz, and each 10% of the clay minerals illlite, kaolinite and montmorillonite. The pure diatom extract was then added to this mineral mixture (5%, 20%, 50%, 80% of diatom). Furthermore, measurements of the pure mineral endmember (0%) and the pure diatom extract (100%) were carried out. Equivalent mixtures including 3.5% NaCl were also considered to account for the sedimentary salt content. All results, independent of drying time prior to measurement and salt content, showed biogenic opal concentrations 20–30% lower than expected. Therefore, we suggest a possible temperature-dependent effect altering the structural composition of biogenic opal during the drying steps, or a yet unrecognized

influence of the nature of the tested material (natural marine, natural lacustrine or synthetic mineral mixture) that are worth investigating further to validate the FTIRS method.

Despite these deviations from expected values in the test sequence, comparison between measurement results from core PS2609-1 acquired with the FTIRS approach and with the wet chemical method at the Alfred Wegener Institute in Bremerhaven (AWI) (Müller and Schneider, 1993) yielded similar opal concentration values. Thus, although the absolute sedimentary biogenic silica concentrations and method inter-comparisons need to be treated carefully and more systematic testing is required, our analyses suggest that the FTIRS method provides robust and reproducible biogenic opal measurements.

Opal concentrations in two of the cores (DCR-1PC and COR-1bPC) were measured with FTIRS in Bern and three of the cores (PS2609-1, PS2606-6 and PS2603-3) were measured using the wet chemistry method at AWI in Bremerhaven.

6.3.2 Uranium and thorium measurements

The sediment samples for uranium (U) and thorium (Th) isotope analyses were prepared following the well-established method originally described by Anderson and Fleer (1982) and later adjusted by Choi et al. (2001), Pichat et al. (2004), and Lippold et al. (2009). Freeze-dried marine sediment samples of 150–200 mg were spiked (^{229}Th, ^{236}U) and fully digested in a mixture containing concentrated nitric acid (HNO_3, 3 ml), hydrochloric acid (HCl, 2 ml), and hydrofluoric acid (HF, 1 ml). After complete dissolution in a microwave digestion system under high pressure (maximum temperature 180°C), the samples were evaporated at low pressure (~250 mbar) and a maximum temperature of 110°C. Before separation of the elements, the samples were redissolved in 8M HNO_3. The U and Th fractions were separated by ion-exchange chromatography using Serva Dowex AG1-X8 resin (100–200 mesh). The columns were preconditioned with 8M HNO_3. The Th fraction was then eluted with 9M HCl and subsequently the U fraction was eluted with 1M HCl. The Th fraction was passed through the columns a second time to remove other elements, especially Ca, that could lead to interferences during the isotope measurements. With this repetition the Th fraction is pure enough for measurement, as it has been tested with ICP-OES in

2014 (Lippold et al., *unpublished*). The samples were evaporated to dryness with addition of a few drops of hydrogen peroxide (H_2O_2) to eliminate any organic residue. After redissolving the samples in 5 ml of 1M HNO_3, the samples were filtered (0.45 µm) and stored in centrifuge tubes until measurement. Each preparation batch included eight sediment samples, one procedural blank and one standard (UREM-11 Sarm 31, uranium ore with known concentrations of ^{238}U, ^{234}U, ^{230}Th, and ^{232}Th).

Approximately half of the samples of cores PS2609-1, PS2606-6, and PS2603-3 had been prepared earlier (by I. Stimac and S. Kretschmer at AWI) following a similar procedure, albeit with slightly less sediment material (50 mg) and higher temperatures during digestion (T_{max} = 210°C). The chromatographic separation and subsequent purification of the U and Th fractions were performed using UTEVA resin from Eichrom.

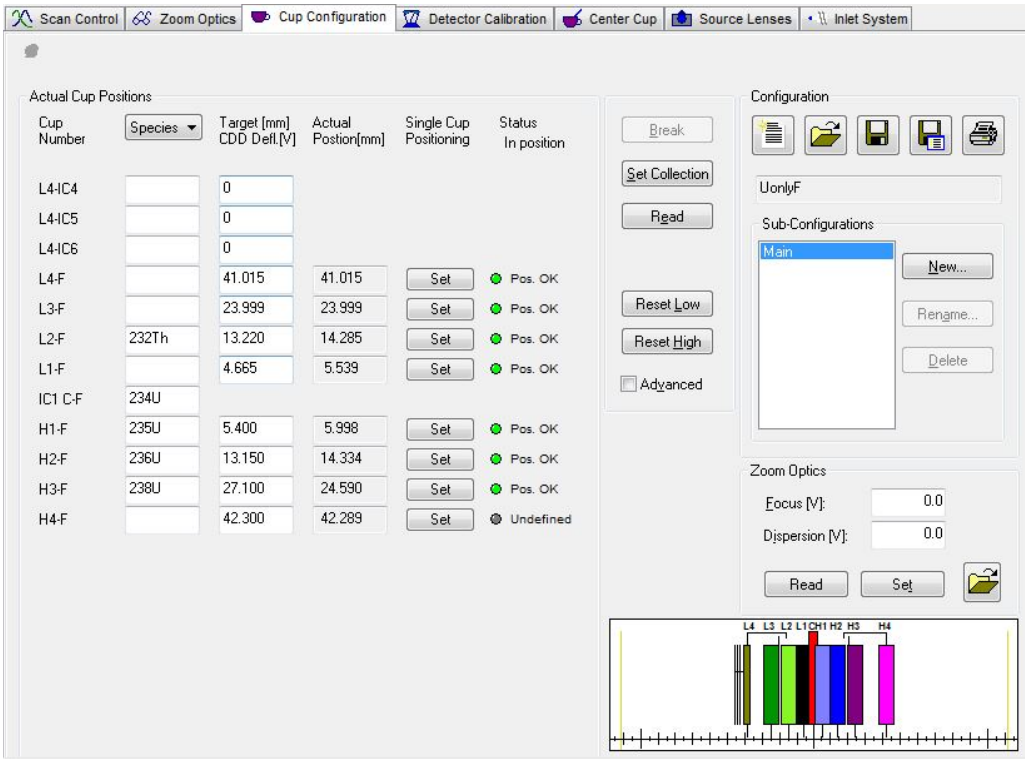

Figure 6.1: Cup configuration for U measurements. The center cup (IC1 C-F) is coupled to an ion counter to measure ^{234}U. Additional ion counters are not used for U measurements.

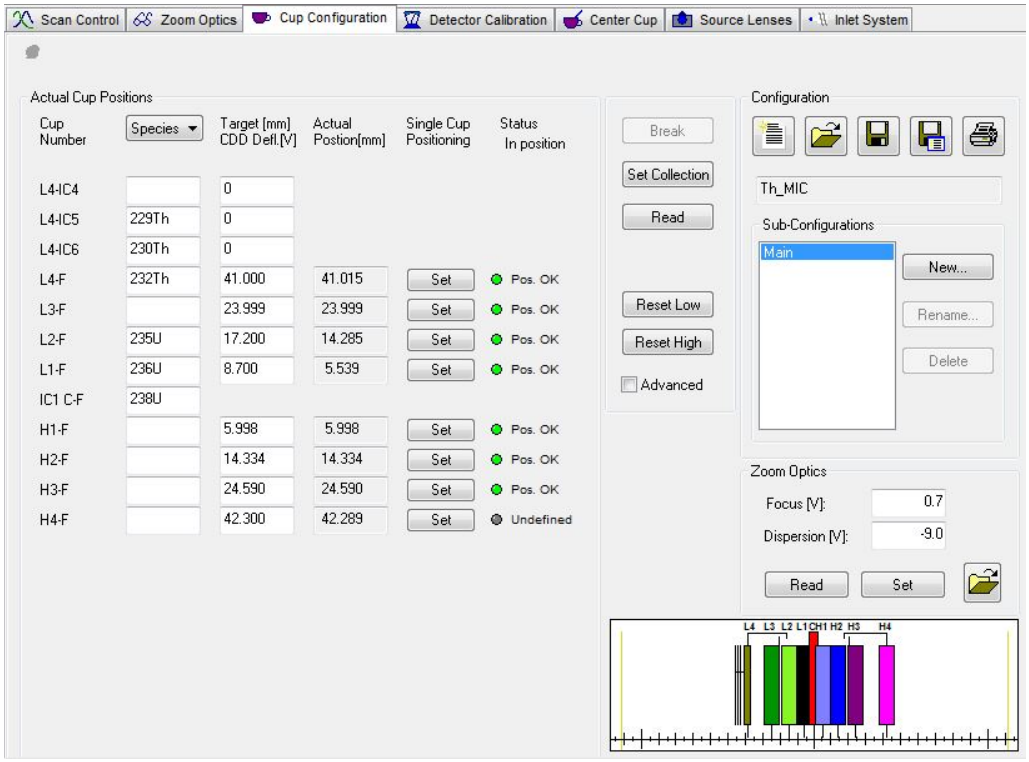

Figure 6.2: Cup configuration for Th measurements. The center cup (IC1 C-F) is set to ^{238}U. The ion counters L4-IC5 and L4-IC6 are attached to the cup L4-F.

The U and Th isotope compositions for DCR-1PC and COR-1bPC samples were measured on a multi-collector inductively coupled plasma mass spectrometer (MC-ICP-MS) with an APEX (DCR-1PC) and an ARIDUS (COR-1bPC) inlet system at the University of Bern (Figure 6.1 and 6.2 for cup configuration). The PS2609-1, PS2606-6, and PS2603-3 cores were measured on a single-collector ICP-MS with an APEX inlet system at AWI in Bremerhaven. The mass bias was corrected using the constant ratio of natural $^{238}U/^{235}U$ (=137.8) (Villa et al., 2016). For the MC-ICP-MS, the gain between the different cups, and the yield between the center cup and central ion counter, were calibrated every few days. For the Th measurements additionally the yield between the ion cup and the attached ion counters was assessed and corrected for by measuring a lab-internal standard solution with known ratios of all Th isotopes of interest (^{229}Th, ^{230}Th, ^{232}Th) every 10–12 hours. For the blank correction, an average of the procedural blank was subtracted for each of the PS cores. For DCR-1PC and COR-1bPC every sample had a preceding 1M HNO_3 acid blank that was subtracted from the sample measurement. The isotope measurements were corrected with the calibrated standard (UREM-11 Sarm 31, Table 6.1) and yielded a relative standard deviation of below 3.8% for ^{238}U and

below 3.5% for ^{234}U and less than 5.7% and 4.9% for ^{230}Th and ^{232}Th, respectively. The measurement differences between the two mass spectrometers were within these errors.

Table 6.1: Calibrated set values, measured average values and deviations thereof for the standard (UREM-11).

Isotope	^{238}U	^{234}U	^{232}Th	^{230}Th	^{238}U	^{234}U	^{232}Th	^{230}Th
set value (dpm/g)	43.67	43.83	2.55	43.85	43.67	43.83	2.55	43.85
	average measured value (dpm/g)				deviation from set value (%)			
DCR-1PC	41.7	42.8	2.29	38.0	95.5	97.6	89.7	86.8
COR-1bPC	41.8	42.6	2.20	35.7	95.8	97.2	86.3	81.4
PS2609-1	41.2	41.3	2.17	34.0	94.2	94.3	85.0	77.6
PS2606-6/ PS2603-3	42.5	42.4	2.19	35.2	97.2	96.7	85.9	80.3

6.3.3 Sortable silt measurements

For sortable silt analyses only the terrigenous fraction <63 µm is measured. Therefore, components of organic matter, carbonate and biogenic silica were removed (McCave et al., 1995). The preparation procedure had to be adjusted for diatom-rich sediment material. The biogenic siliceous fraction, especially diatom frustules, and to a lesser extent sponge spicules and radiolarian fragments, turned out to withstand the commonly used chemical dissolution steps to a substantial degree (McCave et al., 1995; Ohlendorf and Sturm, 2008; Roberts et al., 2017). Before establishing the final procedure described below, a set of tests were undertaken, mostly focusing on the complete dissolution of biogenic silica. Sodium carbonate (Na_2CO_3) and sodium hydroxide (NaOH) were tested at variable concentrations, reaction times and temperatures. The carbonate dissolution step was varied with hydrochloric acid and acetic acid at different concentrations. After extensive testing, we decided on a less aggressive chemical process in combination with physical removal of biogenic silica, to inhibit co-dissolution of siliciclastic grains. The final procedure for the samples of this study and the recommended approach to consistently remove biogenic opal fragments in opal-rich sediments is the following: 1 g of freeze-dried sediment was wet sieved through a 63 µm net into a 1 L beaker with deionized

water. The coarse fraction was dried separately at 40°C. For the fine fraction, after a one-week settling time the samples were transferred to centrifuge tubes in a disaggregating solution (0.2% Calgon, $(NaPO_3)_6$). Organic matter (at 50°C for ~12 h), carbonate (at 50°C for ~12 h), and biogenic silica (at 85°C for 2×0.5 h) were subsequently dissolved in a series of chemical steps using 10% H_2O_2, 1M acetic acid, and 20% NaOH, separated by multiple steps of rinsing with deionized water, centrifuging and vortexing. Remaining diatoms were physically removed by density separation using sodium polytungstate (SPT) at a density of 2.25 g/cm^3. The samples were kept in 0.2% Calgon to help the samples disperse until measurement using a Malvern Mastersizer 2000 laser diffractometer (Sperazza et al., 2004) at the Institute of Geography (GIUB) in Bern. Some sediment samples, especially in diatom-rich intervals, contained too little terrigenous material, so that the necessary obscuration for analysis could not be reached. If samples consist predominantly of diatoms, more than 1 g of sediment material may be used.

With laser diffractometry, the grain sizes are calculated by the level and angle of scattering of light energy of a specific wavelength induced by the grains in the solution. The Mastersizer utilizes the Mie theory for converting the scattering of light to grain sizes and reports the size-distributions as volume percentage for each size bin (Sperazza et al., 2004). The sizes are exported in a file and reported in 0.5 to 1 µm step size bins between 10 and 63 µm. For calculations of the mean size the geometric midpoint within each size-bin was used (McCave and Andrews, 2019).

Each preparation batch contained 37 samples and included three internal standards (marine sediment from the Indian Ocean, core catcher material from MD84-568 and MD84-542, by courtesy of Elisabeth Michel). Two of these standards yielded a procedural error of less than 2%, yet for the third standard the error was somewhat higher at 8.23%. To determine the analytical error, a poorly sorted glacial sediment collected in Sillikers (Bista et al., 2016) was measured and yielded a standard deviation of 1.37%.

A large part of the tests and the development of the final sample preparation procedure, including measurements and data evaluation, was conducted in the scope of an integrated and collaborative Master thesis led by Nicole Schmid at the University of Bern.

References

Anderson, R.F., Barker, S., Fleisher, M., Gersonde, R., Goldstein, S.L., Kuhn, G., Mortyn, P.G., Pahnke, K., Sachs, J.P., 2014. Biological response to millennial variability of dust and nutrient supply in the Subantarctic South Atlantic Ocean. Philos. Trans. R. Soc. A 372, 20130054. doi: 10.1098/rsta.2013.0054

Anderson, R.F., Fleer, A.P., 1982. Determination of Natural Actinides and Plutonium in Marine Particulate Material. Anal. Chem. 54, 1142–1147. doi: 10.1021/ac00244a030

Bista, D., Kienast, S.S., Hill, P.S., Kienast, M., 2016. Sediment sorting and focusing in the eastern equatorial Pacific. Mar. Geol. 382, 151–161. doi: 10.1016/j.margeo.2016.09.016

Choi, M.S., Francois, R., Sims, K., Bacon, M.P., Brown-Leger, S., Fleer, A.P., Ball, L., Schneider, D., Pichat, S., 2001. Rapid determination of ^{230}Th and ^{231}Pa in seawater by desolvated micro-nebulization Inductively Coupled Plasma magnetic sector mass spectrometry. Mar. Chem. 76, 99–112. doi: 10.1016/S0304-4203(01)00050-0

Crosta, X., Shukla, S.K., Ther, O., Ikehara, M., Yamane, M., Yokoyama, Y., 2020. Last Abundant Appearance Datum of *Hemidiscus karstenii* driven by climate change. Mar. Micropaleontol. 157. doi: 10.1016/j.marmicro.2020.101861

Geibert, W., Stimac, I., Rutgers van der Loeff, M.M., Kuhn, G., 2019. Dating Deep-Sea Sediments With ^{230}Th Excess Using a Constant Rate of Supply Model. Paleoceanogr. Paleoclimatology 34, 1895–1912. doi: 10.1029/2019PA003663

Hodell, D.A., Charles, C.D., Ninnemann, U.S., 2000. Comparison of interglacial stages in the South Atlantic sector of the Southern Ocean for the past 450 kyr: Implifications for Marine Isotope Stage (MIS) 11. Glob. Planet. Change 24, 7–26. doi: 10.1016/S0921-8181(99)00069-7

Ikehara, M., Katsuki, K., Yamane, M., Yokoyama, Y., Obrochta, S.P., Matsuzaki, T., Sato, H., Kusahara, K., (in prep.). Episodic enhancement of sea ice survivability in the glacial Southern Ocean driven by Antarctic warming.

Kuhn, G., 2003a. Documentation of sediment core PS2609-1. Alfred Wegener Institute - Polarstern core repository, PANGAEA. doi: 10.1594/PANGAEA.115378

Kuhn, G., 2003b. Documentation of sediment core PS2606-6. Alfred Wegener Institute - Polarstern core repository, PANGAEA. doi: 10.1594/PANGAEA.115376

Kuhn, G., 2003c. Documentation of sediment core PS2603-3. Alfred Wegener Institute - Polarstern core repository, PANGAEA. doi: 10.1594/PANGAEA.115375

Lambert, F., Bigler, M., Steffensen, J.P., Hutterli, M., Fischer, H., 2012. Centennial mineral dust variability in high-resolution ice core data from Dome C, Antarctica. Clim. Past 8, 609–623. doi: 10.5194/cp-8-609-2012

Lippold, J., Grützner, J., Winter, D., Lahaye, Y., Mangini, A., Christi, M., 2009. Does sedimentary ^{231}Pa/^{230}Th from the Bermuda Rise monitor past Atlantic Meridional Overturning Circulation? Geophys. Res. Lett. 36, L12601, 1–6. doi:

10.1029/2009GL038068

Lisiecki, L.E., Raymo, M.E., 2005. A Pliocene-Pleistocene stack of 57 globally distributed benthic $\delta^{18}O$ records. Paleoceanography 20, PA1003, 1–17. doi: 10.1029/2004PA001071

McCave, I.N., Andrews, J.T., 2019. Distinguishing current effects in sediments delivered to the ocean by ice. I. Principles, methods and examples. Quat. Sci. Rev. 212, 92–107. doi: 10.1016/j.quascirev.2019.03.031

McCave, I.N., Manighetti, B., Robinson, S.G., 1995. Sortable silt and fine sediment size/composition slicing: Parameters for palaeocurrent speed and palaeoceanography. Paleoceanography 10, 593–610. doi: 10.1029/94PA03039

Meyer-Jacob, C., Vogel, H., Boxberg, F., Rosén, P., Weber, M.E., Bindler, R., 2014. Independent measurement of biogenic silica in sediments by FTIR spectroscopy and PLS regression. J. Paleolimnol. 52, 245–255. doi: 10.1007/s10933-014-9791-5

Müller, P.J., Schneider, R., 1993. An automated leaching method for the determination of opal in sediments and particulate matter. Deep. Res. Part I 40, 3, 425–444. doi: 10.1016/0967-0637(93)90140-X

Ohlendorf, C., Sturm, M., 2008. A modified method for biogenic silica determination. J. Paleolimnol. 39, 137–142. doi: 10.1007/s10933-007-9100-7

Oiwane, H., Ikehara, M., Suganuma, Y., Miura, H., Nakamura, Y., Sato, T., Nogi, Y., Yamane, M., Yokoyama, Y., 2014. Sediment waves on the Conrad Rise, Southern Indian Ocean: Implications for the migration history of the Antarctic Circumpolar Current. Mar. Geol. 348, 27–36. doi: 10.1016/j.margeo.2013.10.008

Pichat, S., Sims, K.W.W., François, R., McManus, J.F., Leger, S.B., Albarède, F., 2004. Lower export production during glacial periods in the equatorial Pacific derived from $(^{231}Pa/^{230}Th)_{xs,0}$ measurements in deep-sea sediments. Paleoceanography 19, PA4023, 1–21. doi: 10.1029/2003PA000994

Roberts, J., McCave, I.N., McClymont, E.L., Kender, S., Hillenbrand, C.D., Matano, R., Hodell, D.A., Peck, V.L., 2017. Deglacial changes in flow and frontal structure through the Drake Passage. Earth Planet. Sci. Lett. 474, 397–408. doi: 10.1016/j.epsl.2017.07.004

Ronge, T.A., Prange, M., Mollenhauer, G., Ellinghausen, M., Kuhn, G., Tiedemann, R., 2020. Radiocarbon Evidence for the Contribution of the Southern Indian Ocean to the Evolution of Atmospheric CO_2 Over the Last 32,000 Years. Paleoceanogr. Paleoclimatology 35. doi: 10.1029/2019PA003733

Sachs, J.P., Anderson, R.F., 2003. Fidelity of alkenone paleotemperatures in southern Cape Basin sediment drifts. Paleoceanography 18, 1–19. doi: 10.1029/2002PA000862

Sperazza, M., Moore, J.N., Hendrix, M.S., 2004. High-Resolution Particle Size Analysis of Naturally Occurring Very Fine-Grained Sediment Through Laser Diffractometry. J. Sediment. Res. 74, 736–743. doi: 10.1306/031104740736

Studer, A.S., Sigman, D.M., Martínez-García, A., Benz, V., Winckler, G., Kuhn, G.,

Esper, O., Lamy, F., Jaccard, S.L., Wacker, L., Oleynik, S., Gersonde, R., Haug, G.H., 2015. Antarctic Zone nutrient conditions during the last two glacial cycles. Paleoceanography 30, 845–862. doi: 10.1002/2014PA002745

Thöle, L.M., Amsler, H.E., Moretti, S., Auderset, A., Gilgannon, J., Lippold, J., Vogel, H., Crosta, X., Mazaud, A., Michel, E., Martínez-García, A., Jaccard, S.L., 2019. Glacial-interglacial dust and export production records from the Southern Indian Ocean. Earth Planet. Sci. Lett. 525. doi: 10.1016/j.epsl.2019.115716

Villa, I.M., M.L. Bonardi, P. De Bièvre, N.E. Holden, P.R. Renne, 2016. IUPAC-IUGS status report on the half-lives of ^{238}U, ^{235}U and ^{234}U, Geochim. Cosmochim. Acta 172, 387–392. http://doi.org/10.1016/j.gca.2015.10.011

Vogel, H., Meyer-Jacob, C., Thöle, L., Lippold, J.A., Jaccard, S.L., 2016. Quantification of biogenic silica by means of Fourier transform infrared spectroscopy (FTIRS) in marine sediments. Limnol. Oceanogr. Methods 14, 828–838. doi: 10.1002/lom3.10129

Vogel, H., Rosén, P., Wagner, B., Melles, M., Persson, P., 2008. Fourier transform infrared spectroscopy, a new cost-effective tool for quantitative analysis of biogeochemical properties in long sediment records. J. Paleolimnol. 40, 689–702. doi: 10.1007/s10933-008-9193-7

Xiao, W., Esper, O., Gersonde, R., 2016. Last Glacial - Holocene climate variability in the Atlantic sector of the Southern Ocean. Quat. Sci. Rev. 135, 115–137. doi: 10.1016/j.quascirev.2016.01.023

Zielinski, U., Gersonde, R., 2002. Plio-Pleistocene diatom biostratigraphy from ODP Leg 177, Atlantic sector of the Southern Ocean. Mar. Micropaleontol. 45, 225–268. doi: 10.1016/S0377-8398(02)00031-2

List of Abbreviations

AABW:	Antarctic Bottom Water
AAIW:	Antarctic Intermediate Water
ACC:	Antarctic Circumpolar Current
ACR	Antarctic Cold Reversal
ALK:	alkalinity
AMOC:	Atlantic Meridional Overturning Circulation
ARC:	Agulhas Return Current
aU:	authigenic uranium
AZ:	Antarctic Zone
bSi:	biological opal
CDW:	Circumpolar Deep Water
COR:	Conrad Rise
CZ:	Continental Zone
DCR:	Del Caño Rise
DIC:	dissolved inorganic carbon
dpm/g:	disintegrations per minute per gram
EDC:	EPICA (European Project for Ice Core Drilling in Antarctica) Dome C
FTIRS:	Fourier transform infrared spectroscopy
GNAIW:	Glacial North Atlantic Intermediate Water
IDW:	Indian Deep Water
IODP:	International Ocean Discovery Program
IRD:	ice-rafted debris
LCDW:	Lower Circumpolar Deep Water
LGM:	Last Glacial Maximum
mbsl:	meters below sea level
MIS:	Marine Isotope Stage
MORB:	mid-ocean ridge basalt
NADW:	North Atlantic Deep Water
ODP:	Ocean Drilling Program
pCO_2:	partial pressure of carbon dioxide
PDW:	Pacific Deep Water
PF:	Polar Front

PFZ:	Polar Frontal Zone
ppm; ppmv:	parts per million; parts per million by volume
SACCF:	Southern Antarctic Circumpolar Current Front
SAF:	Subantarctic Front
SAM:	Southern Annular Mode
SAMW:	Subantarctic Mode Water
SAZ:	Subantarctic Zone
SBy:	Southern Boundary of the ACC
SHW:	southern hemisphere westerly winds
SO:	Southern Ocean
SS:	sortable silt
SST:	sea surface temperature
STF:	Subtropical Front
SWIR:	Southwest Indian Ridge
TERM:	Termination
UCDW:	Upper Circumpolar Deep Water
XRF:	X-ray fluorescence

Acknowledgements

I am grateful to have arrived at this point; I thank everybody who supported me throughout this learning process, who sparked my interest and curiosity for paleoceanography and geochemistry, opened doors to new opportunities, and who helped me to continue towards the completion of this PhD project.

I would like to express my gratitude to my supervisor Samuel L. Jaccard for his positivity and the opportunity to work on this research topic. Thank you for allowing me to participate in two expeditions to the Southern Ocean and for encouraging me to attend various national and international conferences.

I sincerely thank Minoru Ikehara for leading the scientific cruises on Hakuho-maru and for offering me a spot as an expedition member twice. I would like to thank all cruise members who contributed to the success of the expeditions and for the discussions, the input, and the overall inspiring experience.

I want to thank Gerhard Kuhn for organizing my two stays in Bremerhaven at the AWI, where I acquired an important part of the samples and data. A big thank you to Walter Geibert, Ingrid Stimac and also Sven Kretschmer for your help with the analyses and for fruitful discussions.

I want to acknowledge all the advice and help I got during the sample preparation, measurements, and laboratory work. I thank Daniela Fischer from GIUB who introduced Nicole and me to the Mastersizer and helped with the grain size measurements. I gratefully thank Julijana Krbanjevic and Priska Bähler for their valuable help with laboratory-related issues. Thanks to Igor Villa for introducing me to the world of Neptune. Thank you Martin Wille, I appreciate so much the countless times you offered your patience and expertise with the Neptune. Also Jörg Rickli, David Janssen, Alessandro Maltese, and Edel O'Sullivan, your experience was of great help.

I thank Lena Thöle deeply for her support during every step of the project. The majority of what I needed for my PhD I learnt from and with you; sample preparation, data evaluation, designing experiments, and carrying out measurements are the least to mention. I am grateful for our discussions about science and other important and not so important things in life. Looking back, even the most nerve-racking overnight measuring sessions were fun, when endured with you.

A big thank you goes to Nicole Schmid who in the scope of her Master thesis helped me tremendously with the sample preparation and evaluated the data for the sortable silt analyses. Your diligent work is greatly appreciated.

Annette Bretscher, I am so thankful for your openness and empathy. Thank you a lot for sharing your experiences, for listening and encouraging. Your final push was exactly what I needed.

Furthermore, I want to thank Verena Lanny, Julia Gottschalk, Peter Abbott, and Hendrik Vogel for your advice in the laboratory. Thanks to Elisabeth Michel, Diksha Bista, Stephanie Kienast, and Anja Studer for sending sediments for our internal standards. Thank you to Nicholas McCave, Oliver Esper, Xavier Crosta and many others at summer schools and conferences for their valuable input and contributions to this thesis.

Special thanks go to Elisabeth Michel who accepted to evaluate this thesis as external examiner and to Flavio Anselmetti for chairing the defense.

I thank the members of the institute and the Oeschger Centre for their support, especially Barbara Grose, Sarah Antenen, Sigrid Zimmermann, Marina Beutler, Ulrich Linden, Daniel Engimann, Thomas Siegenthaler, and Peter Stucki.

I thank my companions in the most beautiful office for the motivational conversations, shared frustrations, and relaxing moments: Anne, Nasim, Katja, Elena, Joana, Mirjam, and Michele. I would also like to thank many others at the institute for the great lunch and coffee breaks, for sharing ideas, interests, encouragements, sorrows, and hugs. Lena, Dave, Fabio, James, Jisuk, Catharina, Dimitri, Marius, Stefano, Philipp, Anne, Edel, Alannah, Alessandro, Elias, Arathy, Michael, and more; without you the PhD would have been much less enjoyable. Thank you to my friends around the globe for your friendship and connection, for sharing, for encouraging, and for the sense of belonging. And Lukas, of course I thank you. You have experienced the entire progression through my studies and my PhD life. You were a great steady support throughout, thank you.

And last but not least, I feel immense gratitude for my family, my parents Fumiko and Walter and my brother Max, who have always believed in me. Thank you for all the opportunities given, the great support, and for helping me prepare for my journey…

Declaration of consent

on the basis of Article 18 of the PromR Phil.-nat. 19

Name, First Name:	Amsler, Helen Eri
Registration Number:	06-914-345
Study program:	PhD (Phil.-nat.) in Climate Sciences Bachelor ☐ Master ☐ Dissertation ☐
Title of the thesis:	Paleoceanographic dynamics of the Southern Indian Ocean reconstructed from geochemical and sedimentological proxies across the last glacial cycle
Supervisor:	Prof. Dr. Samuel L. Jaccard

I declare herewith that this thesis is my own work and that I have not used any sources other than those stated. I have indicated the adoption of quotations as well as thoughts taken from other authors as such in the thesis. I am aware that the Senate pursuant to Article 36 paragraph 1 litera r of the University Act of September 5th, 1996 and Article 69 of the University Statute of June 7th, 2011 is authorized to revoke the doctoral degree awarded on the basis of this thesis.

For the purposes of evaluation and verification of compliance with the declaration of originality and the regulations governing plagiarism, I hereby grant the University of Bern the right to process my personal data and to perform the acts of use this requires, in particular, to reproduce the written thesis and to store it permanently in a database, and to use said database, or to make said database available, to enable comparison with theses submitted by others.

Place/Date

Signature

Curriculum Vitae

Helen Eri Amsler
Born on July 5th 1986 in Tokyo, Japan

EDUCATION:

2016 – 2020:	**PhD in Climate Sciences, University of Bern** Paleoceanography and Marine Biogeochemistry Group Thesis 'Paleoceanographic dynamics of the Southern Indian Ocean reconstructed from geochemical and sedimentological proxies across the last glacial cycle' (supervised by Prof. Dr. Samuel L. Jaccard)
2010 – 2012:	**Master of Science in Earth Sciences, ETH Zürich** Major Geology and Geochemistry Thesis 'Element distribution across different types of sedimentary contacts in the Nankai accretionary prism' (supervised by Prof. Dr. Michael Strasser)
2006 – 2009:	**Bachelor of Science in Earth Sciences, ETH Zürich** Thesis 'Variations in time and space of the tin concentration in lake sediments' (written in German, supervised by Dr. Adrian Gilli)
2005 – 2006:	**Maturität** Kantonsschule Wettingen, focus on Latin
1993 – 2005:	**Primary and middle school** Rudolf Steiner Schule, Schafisheim and Basel

PROFESSIONAL TRAINING

2016 – 2019:	Institute of Geological Sciences, University of Bern Teaching assistant
2013 – 2015:	Marine Works Japan Ltd., Yokohama, Japan Publications specialist, lab technician
2012 – 2013:	Geologie Jäckli AG; Sieber Cassina + Partner, Zürich Internships